To the Graduate Council:

I am submitting herewith a dissertation written by Mrunalini Dhamdhere entitled "Applications of In-Line Fiber Optic Raman Spectroscopy to Polymer Processes." I have examined the final copy of this dissertation for form and content and recommend that it be accepted in partial fulfillment of the requirements for the degree of Doctor of Philosophy, with a major in Chemical Engineering.

Marion G. Hansen, Major Professor

We have read this dissertation
And recommend its acceptance:

Accepted for the Council:

Associate Vice Chancellor and
Dean of The Graduate School

APPLICATIONS OF IN-LINE FIBER OPTIC RAMAN SPECTROSCOPY TO POLYMER PROCESSES

A Dissertation
Presented For The
Doctor of Philosophy
Degree

The University of Tennessee, Knoxville

Mrunalini Dhamdhere

May 2000

DEDICATION

आदरणीय ती . सौ . आई , ती . दादा

आणि

प्रिय जयदीप

यांना सप्रेम अर्पण

This work is dedicated to my parents and Jaydeep

ACKNOWLEDGEMENTS

I wish to thank my advisor, Dr. M. G. Hansen for his encouragement and ideas throughout this course of study. I also wish to thank the sponsors of this project, Measurement and Control Engineering Center. I would also like to express my gratitude towards the members of my committee, Dr. Robert Counce, Dr. Paul Frymier and Dr. Kevin Kit for their invaluable suggestions.

This endeavor would not have been complete without the love, understanding and sacrifice of my husband, Jaydeep. I would like to express my deepest gratitude to my parents, Anagha and Shireesh, for giving me opportunities in life and believing in me. Vikrant and Sheela have been very helpful in reminding me about deadlines at various times. Vikrant has always been a great brother and my best friend. My friends Suvrat, Ketan, Bhushan, Archana, Anita, Sachin, Parag, Nisha and colleagues Abdullah, Srinivas, Kislaya, Jigui have always provided stimulating discussion topics and great friendship.

ABSTRACT

Process monitoring is an essential part of ensuring the final product quality in a manufacturing process. In-line monitoring is developing at a fast pace as the method of choice as compared to the off-line monitoring techniques due to its advantages such as lower cost and lower waste. It also eliminates the sample preparation and handling concerns associated with the polymeric processes.

In this research, in-line monitoring techniques were developed for emulsion polymerization and extrusion processes using fiber-optic Raman spectroscopy. Varying product quality from batch to batch and the residual monomer content are important concerns in the emulsion polymerization reactions. The kinetics of the batch emulsion polymerization were studied for the methyl methacrylate (MMA) and vinyl acetate (VA) polymerization. The Raman spectroscopy was also used to monitor changes in the reaction rate due to varying comonomer content (AA) for copolymerization of 2-ethylhexyl acrylate (2-EHA) with acrylic acid (AA). For the extrusion processes, a thorough study of the poly(ethylene vinyl acetate) (EVA) random copolymers was performed. Rigorous multivariate analysis was used to develop robust calibration models for quantification of VA concentrations. Rheological properties, such as melt index (MI) and complex viscosity ($|\eta^*(\omega)|$) of the EVA and polypropylene (PP) samples were monitored in real time using polarized Raman spectroscopy.

TABLE OF CONTENTS

CHAPTER **PAGE**

INTRODUCTION **1**

BACKGROUND **4**

2.1 RAMAN SPECTROSCOPY 4

2.1.1 Origin of Raman Spectroscopy *5*

2.1.2 Selection Rules for Raman Spectra *8*

2.1.3 Instrumentation Used in Dispersive Raman Spectroscopy *12*

2.2 EMULSION POLYMERIZATION 17

2.2.1 Theory of Emulsion Polymerization *18*

2.2.2 Kinetics of homogenous free radical polymerization *23*

2.2.3 Effect of temperature on rate of polymerization *27*

APPLICATIONS OF RAMAN SPECTROSCOPY TO INDUSTRIAL PROCESSES **29**

3.1 INDUSTRIAL APPLICATION OF RAMAN SPECTROSCOPY 29

3.2 IN-LINE MONITORING OF POLYMERIZATION PROCESSES 33

3.3 IN-LINE MONITORING OF POLYMER EXTRUSION PROCESSES 39

REGRESSION METHODS 42

4.1 INTRODUCTION 42

4.2 PATTERN RECOGNITION METHODS 43

4.2.1 Hierarchical Cluster Analysis (HCA) 43

4.2.2 Principal Component analysis (PCA) 44

4.3 MULTIVARIATE CALIBRATION AND PREDICTION 47

4.3.1 Multiple Linear Regression (MLR) 47

4.3.2 Principal Component Regression (PCR) 48

4.3.3 Partial Least Squares (PLS) Analysis 49

4.3.4 Diagnostics of PCR and PLS 51

EXPERIMENTAL SETUP FOR IN-LINE MONITORING USING RAMAN SPECTROSCOPY 55

5.1 INTRODUCTION 55

5.2 MONITORING EMULSION POLYMERIZATION REACTIONS 55

5.2.1 THE BATCH REACTOR 55

5.2.2 THE RAMAN SPECTROMETER 56

5.2.3 SAMPLING SYSTEMS 62

IN-LINE MONITORING OF BATCH EMULSION POLYMERIZATION 66

6.1 EMULSION POLYMERIZATION OF DERIVATIVES OF ACRYLIC POLYMERS 66

6.2 MMA EMULSION POLYMERIZATION 66

6.3 VINYL ACETATE POLYMERIZATION 81

6.4 COPOLYMERIZATION OF 2-ETHYLHEXYL ACRYLATE WITH ACRYLIC ACID 90

6.4.1 Correlation of monomer conversion with in-line real time Raman spectra. 91

6.4.2 Prediction of monomer conversion from calibration reaction run..... 108

6.4.3 Monitoring difference in rates for 2-EHA/AA emulsion copolymerization reactions at different starting monomer ratios 115

6.4.4 Individual comonomer monitoring for 2-EHA and AA polymerization reactions using in-line Raman spectroscopy 125

6.4.4.1 Differentiation of 2-EHA and AA from Raman spectra of neat samples and emulsions 126

IN-LINE MONITORING OF POLYMER PROCESSING OPERATIONS USING RAMAN SPECTROSCOPY 136

7.1 INTRODUCTION 136

7.1 EXPERIMENTAL SET UP 137

7.2 IN-LINE MONITORING OF ETHYLENE VINYL ACETATE (EVA) COPOLYMERS 140

7.2.1 Monitoring of VA content in EVA samples 144

7.2.2 Monitoring rheological properties in EVA 158

7.3 CORRELATION OF COMPLEX VISCOSITY WITH THE RAMAN SPECTRA IN POLYPROPYLENE SAMPLES 171

7.4 DETERMINATION OF OCTENE CONTENT IN PE SAMPLES 179

7.5 RESULTS AND DISCUSSION 187

CONCLUSIONS AND FUTURE WORK 192

REFERENCES 196

VITA 202

LIST OF TABLES

Table		Page
6.1	Reaction recipe for methyl methacrylate emulsion polymerization	68
6.2	Reaction recipe for emulsion polymerization of vinyl acetate	84
6.3	Reaction recipe for emulsion polymerization of 2-EHA and AA	96
6.4	Percent variance explained by principal components	100
6.5	Physical properties of 2-EHA and AA	118
6.6	Reaction recipe for emulsion polymerization of 2-EHA and AA	120
6.7	Ratios of initial monomer concentration	121
6.8	Compositions of neat mixtures of 2-EHA and AA	127
6.9	Variance explained by each principal component for PCA performed on the spectra obtained from neat samples and emulsion	134
7.1	EVA sample set	145
7.2	Processing temperatures for EVA	146
7.3	EVA sample set for MI correlation	162
7.4	PCA variance results of 2750-3050 cm^{-1} region	167
7.5	Comparison of the measured and predicted *ln*(MI) values of the prediction set	170
7.6	Variance explained by the principal components of the **Y** matrix	177

7.7 Details of the PE samples with varying octene copolymer content 184

LIST OF FIGURES

Figure		Page
2.1	Comparison of energy levels for the normal Raman, resonance Raman, and fluorescence spectra	9
2.2	Raman spectrum of CCl_4 showing the Rayleigh, Stokes and Anti Stokes lines	10
2.3	Back scattering and right angle scattering geometry used in Raman spectroscopy	14
2.4	Simplified Representation of an Emulsion Polymerization Reaction System	20
2.5	Transport phenomena and reactions within a latex particle during emulsion polymerization	22
4.1	Possible behavior of RMSEP versus number of factors included in the model	53
5.1	Schematic of Raman Spectrometer and Emulsion polymerization reaction setup	57
5.2	Schematic drawing of HoloProbe Raman Spectrometer Light Path	59
5.3	Vibrational spectra on wavelength scale for various laser types	61
5.4	Schematic of 6 around 1 probe, showing excitation and collection end of the fiber	63
5.5	Optical configuration of fiber optic probe head	65
6.1	Chemical structures of typical acrylic monomers	67
6.2	Raman spectra collected for MMA polymerization at 25 ^{0}C	71
6.3	Baseline corrected C=C peak for MMA polymerization reaction plotted against the Raman shift (cm^{-1})	74

6.4	Maximum intensity of the baseline corrected C=C region vs. MMA conversion	75
6.5	Baseline corrected peaks in the Raman shift region 780-880 cm^{-1}	77
6.6	Three-dimensional representation of Raman spectra in the region 820-840 cm^{-1}	78
6.7	Three-dimensional representation of Raman spectra in the region 820-840 cm^{-1} (Orientation: 180^0 revolved as compared to figure 6.6)	79
6.8	First and second loadings obtained after performing PCA on the spectral data (Shown for reaction at 30 ^0C)	80
6.9	Scores plot for reactions at 25, 30 and 35 ^0C plotted against time.	82
6.10	In-line Raman spectra obtained for VA emulsion polymerization at 60 ^0C, monitored using filter based non immersion probe	85
6.11	In-line Raman spectra obtained for VA emulsion polymerization at 60 ^0C, monitored using filter based immersion probe	86
6.12	Real time monitoring of VA emulsion polymerization using the ratio of C=C (residual unreacted monomer) to C=O (internal standard) plotted against reaction time	88
6.13	Polymer glass transition temperature (T_g) ranges for various product applications	92
6.14	Chemical structures of 2-ethylhexyl acrylate and acrylic acid	93
6.15	Raman spectrum of neat 2-ethylhexyl acrylate (2-EHA) collected with filter based immersion probe	94
6.16	Raman spectrum of neat acrylic acid (AA) collected with filter based immersion probe	95

6.17	Real time Raman spectra depicting progress of emulsion polymerization of 2-EHA (90%) with AA (10%) at 60 ^{0}C, 200 rpm	98
6.18	Normalized intensity ($I_{(C=C)}/I_{(C=O)}$) against time (min)	99
6.19	Standard error of calibration (SEC) and cross validation (SEV)	102
6.20	Comparison of the measured and predicted conversion in calibration set, using two factor based model	103
6.21	Plot of the loading vector for the first principal component with Raman shift	104
6.22	PLS prediction results for real time Raman spectra recorded during emulsion copolymerization of 2-EHA with AA	106
6.23	Increase in the intensity of the laser line with time during emulsion copolymerization of 2-EHA and AA	107
6.24	Conversion based on 2-EHA and AA residual monomer content by gravimetric analysis, plotted against reaction time	110
6.25	Univariate least squares fit for prediction residual monomer content based on intensity changes	112
6.26	Comparison of the measured and predicted monomer conversion with time during emulsion copolymerization of 2-EHA with AA	114
6.27	Comparison of the measured and predicted monomer conversion during emulsion copolymerization of 2-EHA with AA	116
6.28	Monomer concentration profiles during the reactions with different concentrations of AA	122
6.29	Monomer concentration profiles during the polymerization of 2-EHA reactions with different concentrations of AA	124
6.30	Raman spectra of neat mixtures of 2-EHA and AA in a set of five samples of varying AA content	128

6.31	Raman spectra of neat 2-EHA/AA mixtures in 1600 to 1800 Raman shift region (C=C and C=O region)	129
6.32	In-Line Raman spectra obtained during emulsion polymerization of 2-EHA/AA	130
6.33	In-line Raman spectra during emulsion polymerization in the C=C and C=O region	131
6.34	First and second loadings obtained from PCA performed on Raman spectra of neat 2-EHA and AA samples	133
6.35	First and second loadings obtained from PCA performed on in-line Raman spectra of emulsions	135
7.1	Schematic of extruder and in-line monitoring using Raman spectroscopy	138
7.2	Schematic of the extruder flow cell	139
7.3	Chemical structures of ethylene, vinyl acetate and ethylene vinyl acetate (EVA) copolymer	141
7.4	Dynisco style Raman probe with movable inner barrel and fixed outer barrel	143
7.5	Overlaid Raman spectra of PE and EVA with 35.57% VA in plane polarized orientation	148
7.6	Overlaid Raman spectra of sample 16 in set I in plane and cross polarized orientation	149
7.7	Baseline corrected spectra in the C=O peak region (1710 to 1760 cm^{-1}), showing increasing band intensity with increasing VA content in EVA samples	151
7.8	Score plot for PC1 and PC2 for the EVA samples in set I and II (except sample 1 from set I)	152
7.9	Linear regression fit for intensity of C=O peak with known VA content in EVA samples	154
7.10	Comparison of measured and predicted values of VA content of samples from set I and II	155

7.11	Comparison of measured and predicted values of VA content of samples from set I and II	157
7.12	Schematic of ASTM standardized melt index (MI) measurement apparatus	160
7.13	Raman spectra of EVA samples in calibration set (2750-3050 cm^{-1} region) used to correlate the MI values of EVA samples	163
7.14	Hierarchical Cluster Analysis of EVA samples in the calibration set	165
7.15	Plot of standard error of validation vs. number of factors for PLS regression of Raman spectral intensity with melt index	168
7.16	Measured vs. predicted *ln*(MI) values for EVA samples	169
7.17	Schematic representation of experimental setup for rheological measurements using Rheometrics Dynamic Stress Rheometer	173
7.18	Typical behavior of G'(ω), G"(ω) and $\lvert\eta^*(\omega)\rvert$ as a function of ω	174
7.19	Complex viscosity response for PP samples over angular frequency range of 0.01 to 100 rad/sec	175
7.20	Plane and cross polarized Raman spectra of polypropylene samples in molten state	178
7.21	The first loadings obtained from the PCA analysis of the complex viscosity data of PP during extrusion	180
7.22	Comparison of predicted vs. actual scores for PP samples	181
7.23	Comparison of the measured complex viscosity (Symbol - solid line) and predicted complex viscosity (Symbol - o)	182
7.24	Structure of PE polymer with octene copolymer unit	185
7.25	Raman spectra of molten PE in plane and cross polarized orientation	186

7.26 Baseline corrected Raman spectra of molten PE in 2750 to 3000 cm^{-1} region depicting the CH_2 and CH_3 stretching peak 188

7.27 Normalized maximum intensity of the C-H stretching band plotted vs. octene content in the PE samples 189

NOMENCLATURE

Symbol	Description
α	Polarizability constant
β	Matrix of regression coefficient
$\lvert\eta^*(\omega)\rvert$	Complex viscosity, expressed as a function of ω
ω	Angular Frequency (rad/s)
ν	Vibrational state
AA	Acrylic acid
BS	Backscatter geometry of collection
E	Activation energy
EVA	Ethylene vinyl acetate copolymer
2-EHA	Ethylhexyl acrylate
I_0	Intensity of the first spectrum
I_t	Intensity of spectrum at time t
k	Rate constant for reaction in kinetic equation
LAS	Leave-a-sample cross validation approach
$M^{\bullet}$	Monomer radical
MI	Melt index

MIR	Mid-infrared
NIR	Near-infrared
PCA	Principal component analysis
PE	Polyethylene
PLS	Partial least square regression
PLS-1	PLS regression of one dependent variable
PLS-2	PLS regression of multiple **Y** data
PRESS	Predicted residual sum of sqaures
r	Correlation coefficient
R	Rate of reaction
RAS	Right angle geometry of collection
SEC	Standard error of calibration
SEP	Standard error of prediction
T	Scores matrix
t	Score vector, column of matrix **T**
U	Loadings matrix
u	Loading vector, column of matrix **U**
X	Matrix of Raman spectra
Y	Dependent variable vector

CHAPTER 1

INTRODUCTION

Polymers form an integral part of our daily life. Plastics have diverse applications in various markets. As these markets develop further at an alarming pace, there is a need to characterize the polymer manufacturing processes. There are various processes to carry out polymerization reactions, yielding polymers with varying properties. For applications such as pressure sensitive adhesives, paints etc., polymers in the form of latex are preferred. The method of choice for producing latex is emulsion polymerization. Due to environmental concerns, the use of solvents in all production processes is to be minimized (1). Emulsion polymerization is very advantageous for such applications, since it can be carried out in aqueous phase, thus minimizing the use of solvents. Since the majority of the ingredients are aqueous, heat transfer is facilitated in emulsion polymerization processes. The bulk production process can be carried out in batch, semi-batch or continuous mode of operation. For batch processes, the varying product quality from batch to batch is not preferred. Also, for polymerization reactions, it is difficult to determine the end time for the batch. Hence, various off-line techniques are in use to analyze the batches and thus determine the specific parameters associated with them. However, off-line methods are time consuming. Hence, there is need for developing on-line or in-line methods of analysis for batch processes.

In the last decade, fiber optic near-infrared (NIR) spectroscopy has proved to be a viable technique for rapid, non-destructive analysis. Raman spectroscopy is developing as a complimentary technique to NIR spectroscopy. Raman spectroscopy has distinct advantages over NIR spectroscopy (2). Water appears as a strong peak in the NIR spectroscopy, however, in Raman spectra water has a weak signal, thus facilitating study of aqueous systems (3). The development of optical fibers, charge coupled device (CCD) detectors, and lasers has allowed Raman spectroscopy to routinely characterize "real world" samples (4).

In this research, in-line monitoring of batch processes using Raman spectroscopy as the analytical tool was developed. The data obtained from Raman spectroscopy can be used to build multivariate calibration models. These models are used to predict the performance of a process. The ultimate use of this technology is in feedback control for the process. This minimizes the batch to batch variation. Also, abnormalities in the process could be detected early on and hence, loss of material can be minimized.

Another research aspect involves monitoring of a polymer extrusion process and on-line determination of rheological properties of polymers using Raman spectroscopy. This is a novel approach to monitor an extrusion process and yields information regarding rheological properties of the polymer such as the melt index and complex viscosity. Simultaneous monitoring of copolymer content is also

demonstrated. Polarized Raman spectroscopy is advantageous over isotropic Raman spectroscopy as it captures information that has strong, physical dependence on the molecular weight parameters of the polymer.

CHAPTER 2

BACKGROUND

2.1 Raman Spectroscopy

The Raman effect was discovered by Sir C. V. Raman in 1928. It is a phenomenon of light scattering and is observed as a change in frequency for a small percentage of the intensity in a monochromatic beam as a result of interaction with the sample material. The spectroscopic region in which the Raman effect is seen depends on the energy of the incident radiation and on the molecular energy levels. Raman spectroscopy was limited in its use until a decade ago because of the difficulties experienced in the experimental setup. The situation began to change with the introduction of continuous wave (CW) gas lasers, photomultiplier tubes, and photon counting equipment. Raman spectroscopy has seen an increase in the number of applications for several reasons. Raman spectra can be obtained on very small quantities of samples and without much sample preparation. Single crystals, single fibers, single grains of powder, and individual filaments from polymers can all be readily examined (5,6). The weak Raman scattering from water makes it an ideal tool for monitoring aqueous media.

The geometry used in experimental Raman spectroscopy facilitates the use of special cells, such as high temperature and/or pressure cells for in-situ spectroscopy in reactors. However, Raman spectroscopy is limited in its use due to a major drawback-fluorescence (6,7). Fluorescence is approximately 10^6 to 10^8 times stronger than

Raman scattering. Use of near infrared (NIR) excitation has proved to be effective in reducing this problem. NIR excitation has lower energy of excitation. Hence, the molecular transition to higher electronic level would not take place.

2.1.1 Origin of Raman Spectroscopy

Consider an incident photon of energy $h\nu_0$ interacting with a molecule having vibrational levels ν_1, ν_2, ν_3...etc. Most of the incident radiation is unchanged in energy. A small portion of the incident energy appears as $h(\nu_0-\nu_1)$, $h(\nu_0-\nu_2)$. This appears with a change in frequency as compared to the incident radiation. If the excited states ν_1, ν_2, ν_2 ...are close to the ground state, then at ordinary temperatures these levels will have a significant population determined by the Boltzmann distribution. The molecules in the vibrationally excited state can interact with the incident radiation and return to the ground state. This results in $h(\nu_0+\nu_1)$, $h(\nu_0+\nu_2)$ being observed. The lines observed at frequencies lower than that of the incident radiation are referred to as the Stokes lines and those at higher frequency as Anti-Stokes lines (8).

Light can be considered as an electromagnetic wave with an electric and a magnetic component. Consider that light with the electric component in xy plane is propagating in the z direction. When the light strikes a polarizable electron cloud, the electron cloud of the molecule starts oscillating, and thus it radiates energy in all

directions. This is known as light scattering. The electric field associated with the light wave fluctuates with time, at frequency ν_0, and can be represented as

$$E = E_o \cos 2\pi\nu_0 t \qquad \ldots(2.1)$$

where, E = time dependent intensity

E_0 = maximum amplitude, and

ν_0 = frequency

The dipole induced by the field is shown as

$$\boldsymbol{P} = \alpha E = \alpha E_0 \cos 2\pi\nu_0 t \qquad \ldots(2.2)$$

where α = polarizability (a constant of proportionality)

If the molecule is vibrating with frequency ν_m, the nuclear displacement q, can be written as

$$q = q_0 \cos 2\pi\nu_m t \qquad \ldots(2.3)$$

where, q_0 =vibrational amplitude

The polarizability, $\boldsymbol{P}$, is a second order symmetric tensor. In general the induced dipole is not in the same direction as the electric vector, and thus the polarizability terms can be written as follows (9):

$$\begin{aligned} \boldsymbol{P}_X &= \alpha_{XX}E_X + \alpha_{XY}E_Y + \alpha_{XZ}E_Z \\ \boldsymbol{P}_Y &= \alpha_{YX}E_X + \alpha_{YY}E_Y + \alpha_{YZ}E_Z \\ \boldsymbol{P}_Z &= \alpha_{ZX}E_X + \alpha_{ZY}E_Y + \alpha_{ZZ}E_Z \end{aligned} \qquad \ldots(2.4)$$

The quantities α_{XX} etc. are independent of the components of the electric vector, but are dependent on the orientation of the molecule relative to the space-fixed axes X, Y, Z. The intensity of the Raman scattered light is proportional to the square of the magnitude of $\boldsymbol{P}$.

For small amplitude of vibration, α can be written as a function of q.

$$\alpha = \alpha_0 + \left(\frac{\partial \alpha}{\partial q}\right)_0 q_0 + \ldots \qquad \ldots(2.5)$$

where, α_0 = polarizability in the equilibrium position,

$\left(\partial\alpha/\partial q\right)_0$ = Rate of change with respect to the change in q, evaluated at the equilibrium position.

The higher order terms can be neglected and hence, α can be considered as a linear function of q. Substituting equation (2.5) in equation (2.2) we get,

$$\boldsymbol{P} = \alpha_0 E_0 \cos 2\pi\nu_0 t + \left(\frac{\partial \alpha}{\partial q}\right)_0 q E_0 \cos 2\pi\nu_0 t \qquad \ldots(2.6)$$

Using equation (2.3) in equation (2.6),

$$\boldsymbol{P} = \alpha_0 E_0 \cos 2\pi\nu_0 t + \left(\frac{\partial \alpha}{\partial q}\right)_0 q_0 E_0 \cos 2\pi\nu_0 t \cdot \cos 2\pi\nu_m t \qquad \ldots(2.7)$$

Expanding the product cosine term gives,

$$\boldsymbol{P} = \alpha_0 E_0 \cos 2\pi\nu_0 t + \frac{1}{2}\left(\frac{\partial \alpha}{\partial q}\right)_0 q_0 E_0 [\cos\{2\pi(\nu_0 + \nu_m)t\} + \cos\{2\pi(\nu_0 - \nu_m)t\}] \ldots(2.8)$$

According to the classical theory, the first term represents an oscillating dipole that radiates light of frequency ν_0 (Rayleigh Scattering), the second term represents Raman scattering of frequencies ($\nu_0 + \nu_m$) and ($\nu_0 - \nu_m$), the Anti-Stokes and the Stokes lines respectively. Originally the population of molecules in the ground state is more than that in the higher vibrational states. Therefore, there are higher number of molecules being excited from the ground state to the higher vibrational state as compared to the number of molecules being excited from higher vibrational state to the ground state. Therefore it has generally been observed that the Stokes lines are always of higher intensity than the Anti-Stokes lines. Thus in Raman spectroscopy, vibrational frequency ν_m is measured as a shift from the incident beam frequency ν_0. A schematic of origin of Raman scatter is shown in figure 2.1. The figure also shows Resonance Raman and fluorescence origin on the molecular level. Example of Stokes, Rayleigh and Anti-Stokes lines is shown in figure 2.2 for CCl_4.

2.1.2 Selection Rules for Raman Spectra

Raman spectra of molecules are observed due to the various vibrations occurring in molecules. In diatomic molecules, the vibration occurs only along the chemical bond connecting the nuclei. In polyatomic molecules, all the nuclei can perform their own harmonic oscillations. Most of the complicated vibrations can be expressed as a superposition of a number of normal vibrations that are completely independent of each other. Not all vibrations are Raman or IR active. Selection rules

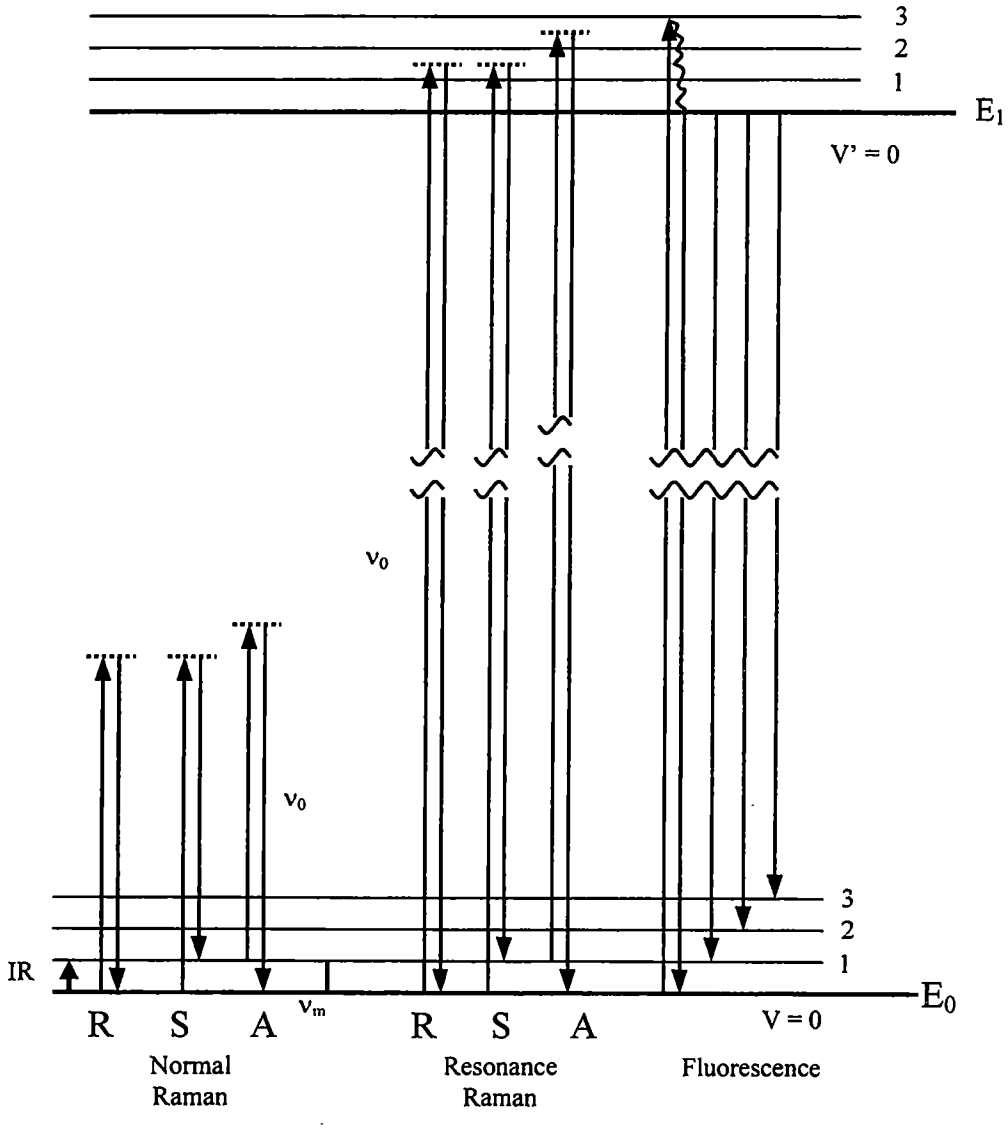


Figure 2.1: Comparison of energy levels for the normal Raman, resonance Raman, and fluorescence spectra
R = Raman, S = Stokes, A = Anti-Stokes
E_0 = Ground state, E_1 = Excited electronic state
V = Vibrational level
[Source: Ferraro, J. R. and Nakamoto, K. in "Introductory Raman Spectroscopy" (Academic Press Inc., San Diego, 1994)]

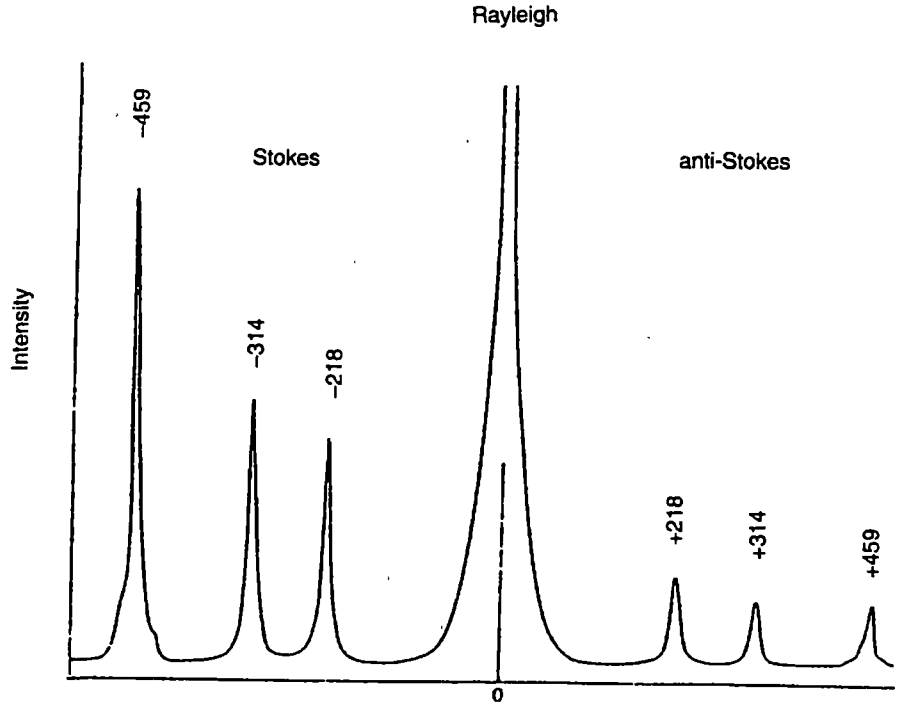


Figure 2.2: Raman spectrum of CCl_4 showing the Rayleigh, Stokes and Anti Stokes lines

[Source: Ferraro, J. R. and Nakamoto, K. in "Introductory Raman Spectroscopy" (Academic Press Inc., San Diego, 1994)]

based on the origin of both the spectroscopic techniques can be used as a guideline in determining whether a particular vibration is Raman or IR active. Some common observations about the Raman spectral intensities are stated here.

It has generally been observed that stretching vibrations associated with chemical bonds are more intense than deformation vibrations. Multiple stretching bonds give rise to intense stretching modes, e.g., a Raman band due to C=C vibration should be more intense than that due to a C-C vibration. Generally, the vibrations that do not distort the molecule, symmetric vibrations, are intense in the Raman spectrum. For example, C=C, P=S, S-S bonds etc. Whereas the vibrations that maximize the distortion are most intense in the IR spectrum. In general, totally symmetric and stretching vibrations are always Raman active and are intense. Vibrations are strong in Raman if the bond is covalent and strong in IR if the bond is ionic (O-H, N-H). For molecules with high symmetry both IR and Raman spectroscopy are needed to observe the vibrational modes. For molecules with a center of symmetry, no Raman active vibration is also IR active and vice versa. This is known as the "Mutual Exclusion rule" that applies to centrosymmetric molecules only.

It is very difficult to predict all the vibrations associated with a molecule using these rules and these rules should be used as a guideline only. Group theory calculations can be done to find out which terms in the transition moment integral are nonzero, but these calculations are usually very rigorous and time consuming (10). A

collection of several bonds and their characteristic wavelength regions where they appear has been published(11).

2.1.3 Instrumentation Used in Dispersive Raman Spectroscopy

A Raman Spectrometer consists of a light source, collection optics, a dispersing optical element, and a detection system (11). These components are discussed here.

Light Source:

The currently available light sources can be divided into two classes as pulsed lasers and continuous wave (CW) lasers. Most of the analytical work involves the use CW lasers whereas pulsed lasers are usually used for UV resonance Raman spectroscopy. Pulsed lasers find use in UV operation so as to get reasonable output powers in the UV range. The output power of the laser must be stable in order to eliminate the source of fluctuation noise from the spectrum. The types of lasers being used in analytical Raman spectrometry are Argon, Krypton, Nd/YAG, and diode lasers (12). These lasers are capable of delivering emission lines in the visible and near-infrared regions over a wide range of frequencies and at various powers.

Lenses and Filters:

Lenses and filters are the imaging optical elements. The laser is usually focused on the sample using a long focal length lens. The lens should be focused such

that there is a small spot size at the sample. This makes the collection of scattered light easier. In order to carry out polarized Raman spectroscopy, a linear polarizer is included in the train along with a filter for cutting out the laser line. Requirements for an effective laser filter include the capability of high transmission at and near the laser wavelength and very high rejection at other wavelengths. Thus, it is mostly a band pass interference filter. The illuminated area on the sample can be imaged onto the spectrometer slit with very little loss in collection efficiency.

Collection Optics:

The collection system is usually composed of two lenses. The first lens, which is of very short focal length, is used to collect the largest possible solid angle of the Raman scattering zone. The second lens is used to refocus the collected light onto the entrance slit of the monochromator, matching the focal length of the monochromator. This technique makes sure that the monochromator is neither overfilled nor underutilized. This two-lens system results in a magnification of the spot size at the slit. For various types of experiments, various collection geometries have been utilized such that the signal to noise ratio (S/N) is optimized. The 90^0 scattering geometry, called Right angle scattering (RAS), and 180^0 backscatter geometry (BS), are as shown in figure 2.3, and are the most popularly used. The 90^0 geometry minimizes the direct transmission of laser light into the collection optics and so reduces the burden on the laser light rejection components of the spectrograph. However, 90^0 geometry is difficult to align and focus, hence 180^0 geometry is usually preferred. For higher

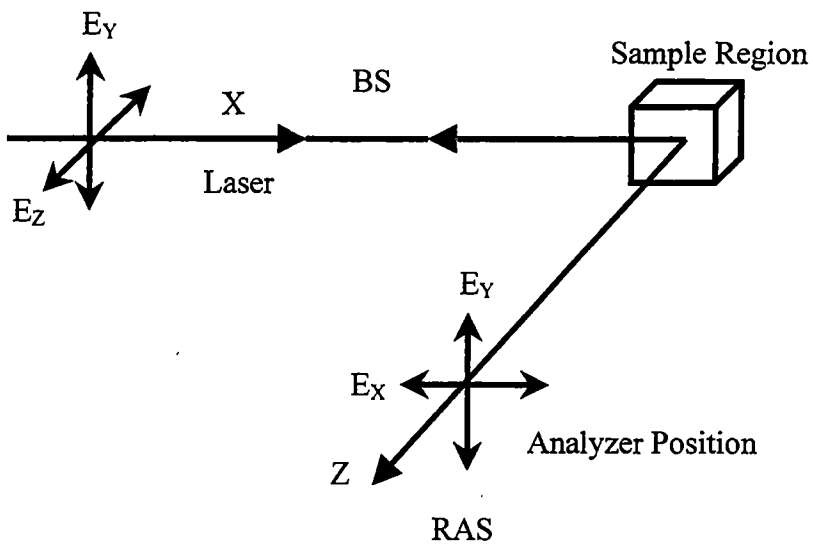


Figure 2.3: Back scattering and Right angle scattering Geometry

RAS: Right angle scattering (90^0)
BS: Backscattering (180^0)

collection efficiency, a camera lens can be used. Instead, if mirrors are used, typically lower efficiency is experienced. The use of fiber optics has been shown to be possible in remote monitoring (13). This system, if properly aligned, has high collection efficiency. In optical spectroscopy, optical fibers are used especially for the "on-line" investigation of remote samples. Silica fibers have good transmission properties in UV/VIS range, but their most potential use is in NIR range. Optical fibers, as attenuated total reflectance (ATR) crystals, are based on total reflection of radiation inside a material that has higher refractive index than its surroundings.

In polarized Raman spectroscopy the notation used for isotropic spectroscopy has to be modified. The direction of propagation of the excitation polarization and the direction of propagation of the collection path are noted along with the polarization of the excitation and collection (11). Thus, four combinations of the excitation and collection are possible in the backscatter geometry as shown in figure 2.3. For backscatter geometry, the direction of the propagation of excitation and collection is X, the polarization of the excitation and collection beam is either in the Y or Z direction. The arrangement denoted as X(YY)X and X(YZ)X were most frequently used in this research, denoted henceforth as the plane polarized and cross polarized geometry.

Monochromator:

The monochromator is the dispersing optical element and is needed to disperse collected light across the exit slit. In dispersive spectrometers, the Rayleigh radiation may produce stray radiation in the entire spectrum, the intensity of which may be higher than that of the Raman lines. Therefore, all types of spectrometers must have means to reduce the radiant power of the exciting radiation accompanying the Raman radiation. Dispersive spectrometers usually achieve this by employing double or triple monochromators. Each monochromator distributes stray radiation of about 10^{-5} of the power of the exciting radiation over the entire spectrum. Array detectors are being more commonly used. They are usually composed of a first stage double monochromator which acts as a bandpass filter. A bandpass filter is a diffraction grating that is used to transmit a narrow band of wavelength. It is followed by a third grating that acts as a normal monochromator and disperses the bandpass of the first stage onto surface of the array detector. Transmission losses could be a major concern with this arrangement.

Detection Systems:

Standard single channel detection system involves photon counting by photomultipliers. Another detection system is the multichannel system. This has an array detector coupled to it. One drawback of such a system is that the resolution/bandwidth trade-off. The introduction of Charge Coupled Devices (CCD) has further improved the multi-channel response.

2.2 Emulsion Polymerization

Emulsion polymerization is a heterogeneous reaction process in which unsaturated monomer(s) is dispersed in a continuous phase with the aid of an emulsifier system and polymerized with free-radical initiators. Emulsion polymerization is the predominant process for manufacturing polymers with large exothermic heats of reaction and low glass transition temperature, e.g., vinyl acetate, chloroprene, and various acrylates. It is also employed for the production of copolymers of butadiene with styrene and acrylonitrile etc. The final product is obtained in the form of a colloidal dispersion called *Latex*. The latex can be directly used as an emulsion without prior separation of the polymer from water and the other components (14).

Emulsion polymerization has several advantages. The physical state of the colloidal system makes it easy to control the process. The bulk of the ingredients is mostly water, thus the heat transfer and viscosity problems encountered in other polymerization processes, such as bulk and solution polymerization processes, are not significant in emulsion polymerization processes. Emulsion polymerization has one significant kinetic advantage as compared to other polymerization processes. For other polymerization processes, there is an inverse relationship between the polymerization rate and the polymer molecular weight. This places a restriction on the molecular weight control for the polymer. Large increase in the molecular weight can be brought about only by decreasing the rate of polymerization reaction. However, emulsion

polymerization is a unique process in which an increase in molecular weight of polymer can be obtained without decreasing the rate of reaction, as there is a linear relation between the polymerization rate and polymer molecular weight.

2.2.1 Theory of Emulsion Polymerization

The main components of an emulsion polymerization reaction are monomer, emulsifier, water-soluble initiator, and water (15). A chain transfer agent, such as mercaptan, can be added to have control over the molecular weight of the polymer formed. The ratio of water to monomer is usually in the range of 80/20 by weight, but can be varied as per the final desired application of the product. The monomer is selected such that it has very low water solubility. Thus a small fraction of monomer dissolves in the bulk phase and majority of the monomer is present in the form of monomer droplets. The initiator system can be a redox system, or a persulphate salt. The redox systems are advantageous in yielding desirable initiation rates at moderate to low temperatures (+50 ^{0}C to - 50 ^{0}C).

When the concentration of surfactant exceeds the critical micellar concentration (CMC), the surfactant forms aggregates of molecules called micelles. The bulk of emulsifier exists in this form, as the usual concentration of emulsifier is 2-3 times that of CMC. The number of micelles and their size depend on the amount of emulsifier as compared to that of the monomer. The monomer is dispersed in the form of monomer droplets. Droplet size is governed by the rate of agitation. The emulsifier molecules adsorbed on their surface stabilize these droplets. Size of micelles can be

20-100 Å at low emulsifier concentration and 1000-3000 Å at higher emulsifier concentration. The size of monomer droplets is about 10000 Å. The concentration of micelles is typically 10^{17}- 10^{18} per milliliter and there are 10^{10} – 10^{11} monomer droplets per milliliter. The initiator is present in water phase. A model for emulsion polymerization progress was developed by Harkins (16), and numerous references can be found on this theory (15). It explains the course of emulsion polymerization in three intervals. A simplified schematic is shown in figure 2.4.

Interval 1: The reaction mixture consists of water and monomer droplets. A very small amount of monomer is solubilized within the micelles and some is dissolved in the water. Reaction starts when the free radicals migrate into the monomer swollen micelles. This establishes a thermodynamic driving force that causes mass transfer from the monomer droplets through the water phase to the newly formed and growing polymer particles. The expanding particle surface provides new hydrophobic surface for emulsifier adsorption. Nucleation stops when the surface area of the previously formed particles is adequate to adsorb all the emulsifier. At this point the reaction sequence for interval 1 is complete. This is normally completed early in the course of the reaction and the conversion is about 2-10 % based on the monomer.

Interval 2: At the end of interval 1, about 90% of monomer is present in the form of monomer droplets. The monomer concentration in the polymer particles is thermodynamically limited because of the free energy required to expand the surface

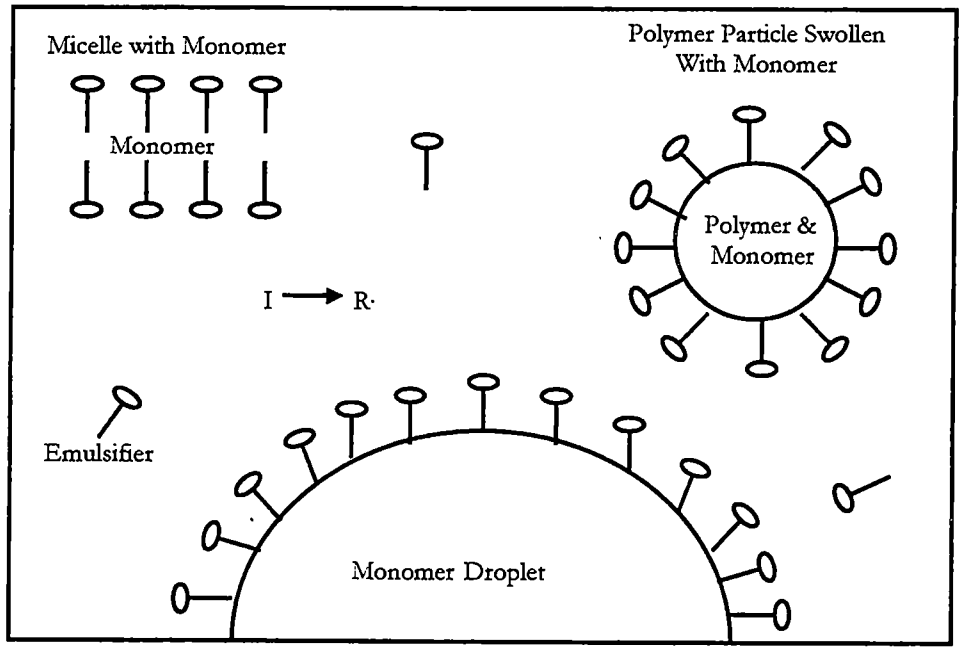


Figure 2.4: Simplified Representation of an Emulsion Polymerization Reaction System

[Source: Odian, G. "Principles of Polymerization" (John Wiley and Sons, Inc., New York, 1981)]

area of the colloidal particles. The reaction proceeds with polymerization in the particles. Monomer is supplied by diffusion from the shrinking monomer droplets. Interval 2 ends when monomer is depleted from the droplets. The degree of saturation of the particle surfaces by emulsifier is very low. The particle number remains constant as in interval 1.

Interval 3: Polymerization continues with higher polymer concentration at the reaction loci, thus more branching and cross-linking reactions are expected. The particle number remains the same as that in interval 1 and 2. The reaction can be stopped at the desired conversion by addition of inhibitor and quenching.

The Harkins mechanism of the three-interval reaction scheme accounts for most of the experimental data. This model has been widely used as a basis for examining the influence of various reaction and reactor parameters on the course of polymerization and the characteristics of the latex. Polymerization within small polymer particles is an important concept in Harkins mechanism as shown in figure 2.5. An individual polymer particle is seen in the diagram with various reaction and transport fluxes. The radical has a hydrophilic end group attached to it that might reduce the mobility of the chain. The size of the latex particle affects the overall rates of termination. The rate of reaction between free radicals is very fast, and it is significantly reduced by viscous and highly entangled environment. This is called as the Gel effect. Thus at high conversions, lower molecular weight polymer is formed.

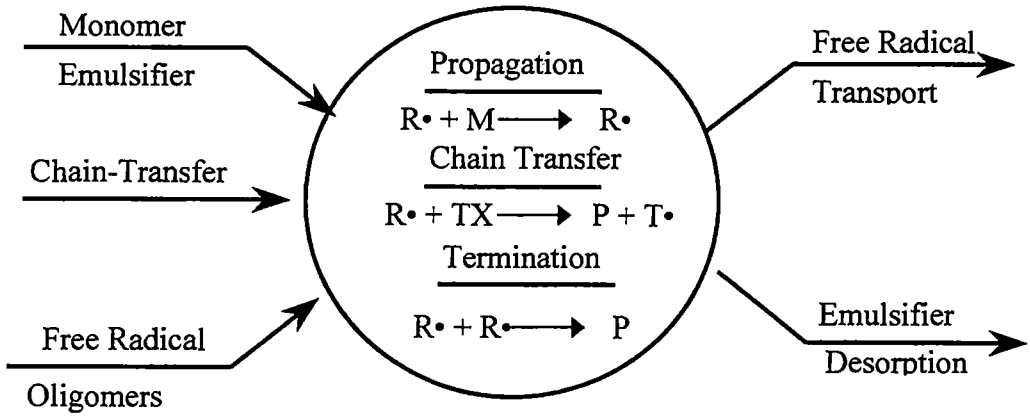


Figure 2.5: Transport phenomena and reactions within a latex particle during emulsion polymerization

$R^{\bullet}$ = macro radical, P = dead polymer

[Source: Poehlein, G. in "Encyclopedia of Polymer Science and Engineering" (John Wiley and Sons Inc., New York, 1996)]

In Smith-Ewart theory (17), the main locus for particle nucleation is the surfactant micelles. The number of particles, N, is given by the following expression:

$$N = k\left(\frac{\rho}{\mu}\right)^{0.4}(a_s S)^{0.6} \qquad \ldots(2.9)$$

where, ρ is the rate of radical generation, μ is the rate of particle volume growth, a_s is the area occupied by a surfactant molecule, and S is the total amount of surfactant in the micelles. The value of k is between 0.37 and 0.53 depending on the assumptions made regarding the relative efficiencies of radical capture by micelles versus polymer particles (14).

Commercial emulsion polymerization can be carried out in continuous, semi-continuous and batch mode. In this research, batch emulsion reactions are carried out and monitored in-line using Raman spectroscopy.

2.2.2 Kinetics of homogenous free radical polymerization

Free radical polymerization is the most widely practiced method of chain polymerization. It is widely used for the production of polymers from olefinic monomers of general structure $CH_2=CR_1R_2$, where R_1 and R_2 are the substituent molecules. Free radical polymerization can be divided into three stages: initiation, propagation and termination. The chemistry of emulsion polymerization can be expressed using equations (2.10) to (2.15).

Initiation:

$$I \xrightarrow{k_i} xR^{\bullet} \qquad \ldots(2.10)$$

$$R^{\bullet} + M \xrightarrow{k_1} RM_1^{\bullet} \qquad \ldots(2.11)$$

Propagation:

$$RM_n^{\bullet} + M \xrightarrow{k_p} RM_{n+1}^{\bullet} \qquad \ldots(2.12)$$

Termination:

$$RM_n^{\bullet} + RM_p^{\bullet} \xrightarrow{k_{tc}} (RM_n - M_pR) \qquad \ldots(2.13)$$

$$RM_n^{\bullet} + RM_p^{\bullet} \xrightarrow{k_{td}} RM_n + RM_p \qquad \ldots(2.14)$$

Chain Transfer:

$$RM_n^{\bullet} + (T-A) \xrightarrow{k_{tr}TA} (RM_n - T) + \dot{A} \qquad \ldots(2.15)$$

where, x = number of primary free radicals R formed from one molecule of initiator I

M = monomer molecule, or monomer unit in polymer chain

RM_p = propagating chain radicals with degree of polymerization p

RM_n = terminated (dead) polymer chain with degree of polymerization n

(T-A) = species undergoing chain transfer

• denotes a radical

k_i, k_1, k_p, k_{tc}, k_{td}, k_{trTA} = rate coefficients for initiation, propagation, termination by combination, chain transfer to species TA respectively.

Rate of polymerization:

$$R_p = -\frac{d[M]}{dt} = k_1[R^\bullet][M] + k_p[M^\bullet][M] \qquad \ldots(2.16)$$

where, k_1 = rate coefficient for reaction of primary free radicals with monomer,

$[R^\bullet]$ = concentration of primary free radicals

$[M^\bullet]$ = total concentration of free radicals $= \sum_{i=1}^{\infty}[M_i^\bullet]$

At the beginning of the reaction, the amount of the monomer consumed is negligible as compared to the propagation stage. Hence, R_p can be simplified.

$$R_p = k_p[M^\bullet][M] \qquad \ldots(2.17)$$

In order to use this equation effectively, the quantity [M$^\bullet$] needs to be defined in terms of easily accessible quantities. Hence, steady state approximation should be used. Assuming that the chain transfer reactions are followed by rapid initiation, then chain transfer would have no effect on [M$^\bullet$] and the rate of change of [M$^\bullet$] with time can be given by equation (2.18).

$$\frac{d[M^\bullet]}{dt} = R_i - 2k_{tc}[M^\bullet]^2 - 2k_{td}[M^\bullet]^2 \qquad \ldots(2.18)$$

where, R_i = rate of formation of chain radicals,

k_{tc} = rate coefficient for termination by combination,

k_{td} = rate coefficient for termination by disproportionation.

Combining the coefficients k_{tc} and k_{td}, the equation can be simplified to

$$\frac{d[M^{\bullet}]}{dt} = R_i - 2k_t[M^{\bullet}]^2 \qquad \ldots(2.19)$$

where, k_t = overall coefficient for rate of termination.

At the start of polymerization, the rate of formation of radicals greatly exceeds the rate of termination of radicals. Hence, [M$^{\bullet}$] increases rapidly and so the rate of loss of radicals by termination increases. Thus, a value of [M$^{\bullet}$] is attained at which the termination rate exactly equals the rate of radical formation. The net change in [M$^{\bullet}$] is zero and the reaction is said to be under steady state condition. In practice, the free radical polymerization reactions operate under steady state conditions, except at the beginning of the reaction (18). Hence, an assumption that d[M$^{\bullet}$]/dt = 0 can be satisfactorily made to yield

$$[M^{\bullet}] = \left(\frac{R_i}{2k_t}\right)^{0.5} \qquad \ldots(2.20)$$

Therefore, the rate of propagation in equation (2.17) can be expressed as

$$R_p = k_p\left(\frac{R_i}{2k_t}\right)^{0.5}[M] \qquad \ldots(2.21)$$

Degree of polymerization:

The number-average degree of polymerization, x_n, of the polymer produced in a chain polymerization is given by

$$x_n = \frac{\text{Moles monomer consumed in unit time}}{\text{Moles of polymer formed in unit time}} \qquad \ldots(2.22)$$

2.2.3 Effect of temperature on rate of polymerization

There are several individual rate coefficients that contribute to the overall rate coefficient in kinetic rate expression. These individual rate coefficients are considered separately in determining the effect of temperature on the rate of reaction.

In general, the Arrehenius equation is expressed as

$$k = Ae^{(-E_a/RT)} \qquad \ldots(2.23)$$

where, A = exponential factor

E_a = Activation energy

The pre-exponential factor, A, is a measure at which collisions occur irrespective of their energy. The activation energy, E_a, is the minimum energy that the reactants must have in order to form products. The fraction of collisions with a kinetic energy in excess of energy E_a, is given as $exp(-E_a/RT)$. Hence, this exponential term indicates the fraction of collisions that have enough energy to lead to a reaction between the reactants (19).

Application of Arrhenius equation to the rate coefficient equations, equations (2.16) and (2.22) with the assumption that the pre-exponential factors are temperature independent, lead to the following equations:

$$\frac{d(\ln R_p)}{dT} = \frac{(2E_p + E_d) - E_t}{2RT^2} \qquad \ldots(2.24)$$

$$\frac{d[\ln(x_n)_0]}{dT} = \frac{2E_p - (E_d + E_t)}{2RT^2} \qquad \ldots(2.25)$$

$$\frac{d \ln C_{TA}}{dT} = \frac{E_{trTA} - E_p}{RT^2} \qquad \ldots(2.26)$$

where, R_p = rate of propagation,

x_n = degree of polymerization,

C_{TA} = transfer constant for chain transfer to the species TA,

E_d = Activation energy for initiator dissociation,

E_p = Activation energy for propagation,

E_t = Activation energy for termination,

E_{TA} = Activation energy for chain transfer to species TA.

These equations indicate that R_p will increase continuously as the reaction temperature increases. The degree of polymerization, x_n will decrease continuously as the reaction temperature increases. Also, at higher temperatures, the term C_{TA} will increase. Thus, values of x_n will be further reduced at increasing temperature.

CHAPTER 3

APPLICATIONS OF RAMAN SPECTROSCOPY TO INDUSTRIAL PROCESSES

3.1 Industrial Application of Raman spectroscopy

Raman spectroscopy has been used for studying various polymer properties. The use of this technique is also evaluated for remote monitoring using optical fibers. The application of Raman spectroscopy to chemical analysis has been studied (20). Quantitative analysis is feasible through the use of a direct relationship between the intensity of Raman signal and the specific or molar intensity of the line.

$$I_R = JC \qquad \ldots(3.1)$$

where, I_R is the Raman intensity, J is the specific or molar intensity of the line and C is the concentration of the scattering molecules in moles per liter. This equation is similar to the more familiar Beer-Lambert's law for absorption spectrophotometry. I_R is given as follows

$$I_R \propto [\text{(Sample area) / (standard area)}] \qquad \ldots(3.2)$$

An excellent review by Lyon *et al.* (21) covers various aspects of techniques and literature about Raman spectroscopy. Hendra *et al.* (22) have demonstrated the use of optical fibers in Raman spectroscopy that resulted in the development of a flexible fiber optic remote sampling system. Optical fibers are well developed for use in the NIR region. This can be put to use in various industrial applications, and in varying conditions. Variation in the collection angle, variation with fiber height from the

sample, and different geometries and their effect on the intensity of collected light was studied by these workers. It was shown that the use of six collection fibers around one excitation fiber was very compatible with a wide range of samples and use in hostile environments.

In-situ Raman measurements during synthesis of a conducting polymer were done by Chong *et al.* (23). A heterogeneous, strongly absorbing sample hexacyanoferrate (III) and -(II) that changed its physical state during the course of measurements was studied. The monitoring system was reliable, and non-invasive.

Application of Raman spectroscopy to the study of polymers and polymerization processes is an area of vast research interest. Application of Raman spectroscopy in determination of structure of polymers has been reviewed by Koenig (5). Infrared spectroscopy has been reported to be advantageous for identifying the polar substituents on the macromolecular chain, whereas Raman spectroscopy is helpful in characterizing the homonuclear polymer backbone. Thus, Raman spectroscopy is more useful for polymers with a carbon-carbon backbone linkage. Studies of natural polymers such as natural rubber, cis-1,4-polyisoprene, have been severely hampered by fluorescence. FT-Raman techniques have been successfully utilized to get spectrum of 'out-of-the-tree' rubber (24).

Raman spectroscopy is also being used to follow the polymerization process and provide information on the extent of polymerization and structural information on the end product of a batch reaction. Raman spectroscopy is ideally suited for study of monomers with C=C, as this band has a strong intensity in stretching mode. The intensity of the monomer decreases as the polymerization proceeds. Thus, monitoring the intensity with time and comparison with the initial intensity would give an idea about the conversion of monomer to polymer in a polymerization reaction (25). Raman spectroscopic study of paints and coatings has also been carried out. The end product as well as the polymerization and curing reaction has been studied. The paint systems studied by Ellis *et al.* are based on acrylates and the loss in intensity of the ν(C=C) stretching was used quantitatively to follow the polymerization process (26). Raman spectroscopy has also been used for real-time determination of the percent cure of epoxide polymers and composites with multivariate techniques (27). A probe design was developed for real-time monitoring of polymer curing and multivariate analysis to interpret the data and determine percent cure. The predicted percent cure of laboratory epoxy samples was within 0.52%, and that for the industrial samples was within 0.82%. These results show the robustness of prediction using the multivariate calibration model.

Tribology is a science of friction, lubrication and wear of materials. Fundamental understanding of the nature of friction and wear has economic consequences. Raman spectroscopy has emerged as a very useful technique for the

study of problems in polymer tribology. Poly(ether ether ketone) (PEEK) is used as a bearing material due to its high toughness, and fatigue resistance. Raman spectroscopy can be conveniently used for the estimation of nature of thermal changes induced in PEEK (28). The spectroscopic data is used for comparison with data obtained from sliding friction test and other thermal experiments.

Use of remote Raman spectroscopy for process control has been demonstrated by Marteau *et al.* (29). Raman spectroscopy was used for control of a C_8 aromatic separation process based on moving-bed chromatography. The real-time drawings of the internal concentration profiles, the purity of para-xylene and the loss of para-xylene in the raffinate stream allowed control of the unit.

Raman spectroscopy with fiber optic sampling has gained importance during the last decade owing to development of cheap and reliable lasers, especially near infrared (NIR) diode lasers. The commercial development of low-noise, high quantum efficiency, silicon charge-coupled device (CCD) arrays has taken Raman spectroscopy into a new era. The CCD can be used to detect radiation from 40,000 to 9500 cm^{-1}. Advances in Raman spectroscopy and improvement in radiation coupling efficiency are reviewed by Lewis and Griffiths (4).

3.2 In-Line Monitoring of Polymerization Processes

Emulsion polymerization is an industrially important process for the manufacture of bulk polymers such as poly(vinyl acetate), poly(methyl methacrylate) etc. Several techniques have been explored for monitoring this important process in-line. Similarly, the reactions can also be carried out using solution polymerization process. Raman spectroscopy has been used to investigate the kinetics of free-radical polymerization of methyl methacrylate in toluene, initiated using azobisisobutyronitrile (AIBN) at 70^0 C (30). During the polymerization process, the C=C bond is opened, and this change was monitored using the decrease in intensity of C=C bond at 1640 cm^{-1}. Raman spectra were recorded using the standard 90^0 configuration using DILOR Z-24 single channel triple monochromator with a photomultiplier and a photon counting chain. The excitation source used was 90.3 argon ion laser with 514.5 nm excitation radiation and incident power 30 mW. The solvent peak due to toluene in the region 1550 to 1620 cm^{-1} Raman shift was used to normalize the spectra. The time dependence of conversion during polymerization matches well with the intensity decrease of C=O and C=C. This paper successfully demonstrates the use of Raman spectroscopy in solution polymerization. Wang and Vickers have studied monitoring of emulsion polymerization of styrene using fiber optic Raman spectroscopy (31). The disappearance of styrene band at 1631 cm^{-1} was monitored. Another band at 1601 cm^{-1} that was common to styrene monomer and polymer was used as a pseudo internal standard. The reaction was carried out at 70^0 C. It was monitored using argon laser with 514.5 nm excitation. The laser power at the

sample was 140 mW. The reaction mixture is opaque during the course of the reaction. This opacity is caused due to light scattering, initially by monomer droplets and then by the particles of dispersed polymer. The authors claim that there is no change in efficiency of Raman sampling with increasing opacity. As an independent check, the reaction was also monitored using a UV probe. The results obtained with both the analyses matched well.

Numerous workers have studied modeling the emulsion polymerization reactions, in either batch or continuous mode. Poehlein has reviewed the emulsion polymerization kinetics (32). He has suggested a continuous system instead of the commercial batch reactions for latex manufacture. The kinetic parameters have been evaluated with the aid of a continuous stirred tank reactor (CSTR).

On-line gas chromatography and densimetry have been utilized by Noel *et al.* to monitor partial conversions of methyl acrylate and vinyl acetate in emulsion polymerization (33). On-line densimetry results in overall weight conversion and on-line gas chromatography results in overall ratios of residual monomer. Combination of these two techniques has been shown to give partial conversion without the need of an internal standard. Estimation of copolymer composition by on-line headspace analysis in batch emulsion polymerization has been investigated by Alonso *et al.* (34). Frequent sampling from the batch emulsion polymerization system was used to provide fast headspace analysis of reactor vapor space. The system is applied for

styrene and acrylonitrile copolymer. Values of reactivity ratios and equilibrium parameters are used in the calculations. On-line conversion monitoring can also be carried out through the use of ultrasound (35). An on-line sensor for estimating conversion from measurements of ultrasound propagation velocity in emulsion polymerization has been developed. Performance of a sensor was tested by comparison with off-line gravimetric measurements of conversions under various operating conditions. Homopolymerizations of methyl methacrylate and vinyl acetate were studied for various monomer/water ratio and initiator concentration. Preliminary experiments were run in order to develop the model parameters and then the conversion value is calculated from the measured sound propagation velocity using the model developed previously. Some inaccuracies were observed at low conversion due to the presence of droplets and hence the sensor exhibited weak sensitivity.

Clarkson *et al.* have monitored polymerization processes for styrene and methyl methacrylate monomers at a range of temperatures (36). The effects of oxygen on the process were also studied. Symmetric stretching band of the vinyl moiety at 1640 cm^{-1} was used to monitor the progress of the reaction. The depletion of the monomers was followed to approximately 80-90%. The fractional conversion was calculated using the following equation:

$$X=([M]_0 -[M])/[M]_0 \qquad \ldots(3.3)$$

where, $[M]_0$ is the initial monomer concentration and [M] is the monomer concentration at time *t*. Several reactions were monitored over a range of

temperatures. The difference in reaction rates due to temperature could be clearly observed. The problem faced by the authors was of polymer insolubility that in turn produced erratic and non-reproducible data.

Gulari *et al.* have studied Raman and FT-IR monitoring of bulk polymerization of methyl methacrylate and styrene (37). Conversion was followed in real time by measuring the integrated intensity of the Raman band due to C=C. A new band at 1545 cm^{-1} was observed during azobisisobutyronitrile (AIBN) initiated polymerization at 60^0 C. This band was observed only during the gel effect and thus is attributed to a reactive free radical intermediate stabilized by conjugation and detectable due to resonance Raman enhancement. No internal calibration standard was used in this study. The activation energies and the initial rates of polymerization determined from spectroscopic data were in good agreement with the classical data for styrene polymerization.

Wang *et. al.* have studied feasibility of using dispersive Raman spectroscopy for quantitative monitoring of styrene (38). They compared the Raman measurements with the UV measurements and found them to be essentially the same. Fourier transform Raman spectroscopy has also been used for monitoring latex systems. An excellent review by Horlick describes use of FT Raman spectroscopy for various polymer process monitoring applications (39). Claybourn *et al.* have investigated emulsion polymerization of methyl methacrylate, butyl acrylate and allyl methacrylate

monomers in water as a continuous phase (2). They used Nd/YAG laser operating in the NIR region at 1064 cm^{-1}. A seed emulsion was used to reduce any probability of re-initiation of new crops of particles during the emulsion polymerization process and this allows control of the final latex particle size and distribution. Samples were periodically extracted during the reaction and inhibited to avoid any further conversion of the monomer. The ratio of C=O to CH bending band was plotted against percent polymer in latex and remained almost constant as both these species do not take part in the reaction. This is an important result for the emulsion polymerization monitoring. Thus, if the spectral region up to a Raman shift in the C=O stretching region can be assumed to be invariant, then the C=C band of the acrylic monomers can be followed with process time over a wide range of solids and using C=O band as an internal standard. Authors have illustrated the use of this technique and reproducible results have been obtained for monitoring C=C band.

Polymers produced by emulsion polymerization processes find many applications in the industry. The latex can be directly put to use in applications such as paints, pressure sensitive adhesives (PSA). Many monomers can be used in the manufacture of PSA, but acrylic monomers find a special use in production of PSA. Polyacrylates of a certain monomer composition are inherently pressure sensitive without any additional compounding. Properties of polyacrylates that set them apart from other PSA are that they are saturated and are resistant to oxidation. It is transparent, colorless, and does not yellow upon exposure to sunlight. Polymerization

of acrylics is relatively easy and does not require high temperature or pressure. The basis of pressure sensitive acrylic adhesives is acrylic esters that yield soft and tacky polymers of low glass transition temperature (T_g) (1). In order to possess a low modulus of elasticity and an acceptable tack, the polymer must have a sufficiently low T_g. Commonly available monomers are 2-Ethylhexyl Acrylate (2-EHA) with T_g of –70 ^{0}C and *n*-butyl acrylate with T_g of –54 ^{0}C. The lower the glass transition temperature, the higher is the tack. Functional groups on the adhesive polymer backbone are useful as sites for intermolecular cross-linking. Mayo and Reegan (40) have reported their findings on the effect of copolymerizing methyl methacrylate with acrylic acid, acrylamide, and methacrylic acid. The peel adhesion of these copolymers increases with increasing copolymer content. Acrylic acid was found to be the most effective comonomer. In some comonomers, the peel adhesion decreases at higher percentage due to increase in crystallinity.

Chatzi *et al.* (41) have used a midrange infrared (MIR) optical fiber probe for the on-line monitoring of 2-EHA /styrene emulsion copolymerization. They have discussed one major drawback of using NIR region as the presence of broad, overlapping and non-specific absorption peaks. Hence, empirical multivariate sensor calibration models have to be developed in order to work in the NIR region. Most NIR absorptions are overtones and combinations of the fundamental MIR molecular vibration bands. The spectrophotometer developed in the MIR region had signal to noise ratio greater than 4000. Total monomer conversion was monitored during

polymerization using conventional gravimetry and thermogravimetric analysis (TGA). Characteristic absorption bands are used for individual comonomer identification. A band due to skeletal ring breathing vibration at 1630 cm^{-1} for styrene and C-O stretching vibration of the saturated ester group at 1190 cm^{-1} for 2-EHA are used. The corresponding vibrations of the two monomeric structural units in the produced copolymer appear at 1600 and 1155 cm^{-1}, respectively, and are indicative of the overall comonomer composition. An excellent agreement between the predicted monomer conversion and TGA results has been reported. IR spectra and compositional analysis of styrene/2-EHA copolymers is reported by Chatzi *et al.* (42).

3.3 In-Line Monitoring of Polymer Extrusion Processes

A second aspect of this research involves the in-line determination of copolymer content and rheological properties during extrusion processes. Such efforts have been carried out previously by Shimoyama *et al.* (43). They used FT-Raman spectroscopy to measure 12 different grades of ethylene/vinyl acetate (VA) copolymers with varying VA content in 7 to 44 % range. Chemometric analyses, especially principal component analysis (PCA) was carried out after normalization of the Raman spectra. A review paper by Lavine describes various aspects and uses of chemometric techniques (44). Principal components (PC) discriminate in the various grades based upon the bands due to C=O stretching and O=C-O bending modes of VA and those assigned to C-C stretching modes of ethylene units. Partial least squares regression (PLS) model was used to predict the VA content in EVA with correlation

coefficient and standard error of prediction of 0.997 and 0.95% wt. %, respectively. NIR spectroscopy was used by Khettry and Hansen (45) to carry out real time analysis of EVA random copolymers during extrusion. Chemometric analysis was done on the data thus obtained and prediction of totally unknown samples from an entirely different source could be carried out. In-line fiber optic monitoring was also shown to be feasible for monitoring rheological properties of EVA copolymers by Vedula and Hansen (46), and Hansen and Vedula (46,47). This work describes a methodology to estimate rheological properties as dynamic linear viscoelastic material functions from the NIR spectra of EVA copolymers. Quantitative calibration models were built for in-line prediction.

Rohe *et. al.* have studied the in-line monitoring of polymer extrusion using NIR spectroscopy to provide a monitoring and control technique for processes (48). A sensor with optical quartz components was developed such that it could be adapted to various extruders for in-line measurements. Multivariate analysis was used for PE/PP blend studies and the deviation between measured and predicted polymer composition was calculated to be about 2%. Real time measurements of chemical composition in polymer processes was studied by McPeters *et. al.* (49). Fiber optic NIR spectroscopy was used to extract chemical information with minimum delay times without having to physically remove the sample from the process. Polymer blends and terpolymer systems were studied. The in-line analysis for blend levels in the polymer blend had a standard error of 0.78 %. The authors have also noted that limitations to the setup

included long term drift due to changes in the spectrometer, fiber optics and the difficulty of checking the calibration offline without making a molten polymer.

CHAPTER 4

REGRESSION METHODS

4.1 Introduction

Chemical plants are becoming more heavily instrumented and the data are recorded more frequently. This data overload needs to be handled by proper usage of this measurement data. Such data usually contains a great deal of correlated and/or redundant information along with the process noise that gets recorded into the measurement. The essential information is buried in the way various variables are related to the process measurement of interest and their correlation with each other. This information could be extracted from the data using mathematical techniques of regression. Regression techniques are used to develop correlation between the dependent variable (**Y**) with the independent variable (**X**). The mathematical complexity of the model and the degree to which it is realistic depends on the amount of information available about the process being studied. Calibration is the process of constructing a model to relate the output of a measurement to known properties of the sample. Prediction is the process of using that model to predict the properties of an unknown sample given the measurement. If a single measurement is related to the concentration of a single chemical component, the calibration is called univariate calibration. Multivariate calibration is the process of relating multiple responses from an instrument to one or more properties of the sample. In this chapter, several exploratory pattern recognition methods; univariate, multivariate calibration and prediction methods will be discussed.

4.2 Pattern Recognition Methods

Pattern recognition techniques include Hierarchical Cluster Analysis (HCA), Principal Component analysis (PCA). These exploratory data analysis techniques are used to compute and graphically analyze the display of patterns of association in the independent variables of multivariate data sets (50). These algorithms reduce large data sets to useful graphical information that provides insight into the correlation among the variables.

4.2.1 Hierarchical Cluster Analysis (HCA)

HCA presents data in such a manner to emphasize the natural groupings among samples or variables. In this analysis, the distances between pairs of samples (or variables) are calculated and compared. Thus, similar samples will be presented closer to each other whereas; dissimilar samples will be separated by a large distance between them. HCA groups data into clusters having similar attributes. HCA presents results from high dimensional row space in the form of a dendogram in two dimensions. The dendogram reveals clustering of samples. If HCA is performed on samples, the resulting dendogram yields information about similar samples. For analysis of variables, the dendogram shows the variables that are closely related and affect the measurement in a similar manner. Several methods, such as single and centroid linking, Euclidean and Mahalanobis distance, are used to calculate the distances between clusters.

The single link approach links clusters based on the distance between the nearest neighbors contained in each of the clusters. In centroid link approach, the dendogram shows the distance between centroids of the clusters. The centroid method measures the distance between the centers of the clusters rather than the distances from the edges of the cluster as in single link (51). Hence, it results in a better measure of the distance between well separated clusters. However, the centroid method is sensitive to outliers because these unusual points adversely influence the calculation of the centroid of a cluster.

4.2.2 Principal Component analysis (PCA)

The data from a chemical process is present in the form of numerous measurement variables. PCA is a mathematical manipulation technique for such data matrix where the goal is to represent the variation present in many variables using a smaller number of "factors" or principal components (PC) (52). A factor is a combination of several variables that describe major trends in the data set. Thus, a new row space is constructed in which the samples are plotted using factors as the newly defined axes rather than the original variables. Thus, PCA reveals the true multivariate nature of the data in relatively small number of dimensions.

Preprocessing the data prior to PCA is very important. Using preprocessing the data is transformed into the most suitable form for analysis. There are many ways to scale or weigh the data. The most common methods of standardization are mean

centering and autoscaling. In mean centering, the mean of the variable vector is subtracted from all the elements of the vector. The effect of mean centering is the removal of the mean sample vector from all the sample vectors in the data set (53). Mean centering accounts for the intercept term in the regression model. Autoscaling is obtained by dividing each variable vector by its standard deviation. Thus, each variable gets scaled to the same variance. This is a common scaling method when the variables are measured in different units. Standardization allows the subtle variations to play the same role in the analysis as the large variations.

Mathematically, PCA relies upon an eigenvector decomposition of the covariance or correlation matrix of the process variables. It decomposes the matrix **X**, where the rows correspond to samples and the columns correspond to variables, as the sum of the outer product of vectors t_i and p_i plus a residual matrix **E**:

$$\mathbf{X} = t_1 p_1^T + t_2 p_2^T + \ldots + t_n p_n^T + E \qquad \ldots(4.1)$$

$$\mathbf{X} = \mathbf{TP} + \mathbf{E} \qquad \ldots(4.2)$$

where, n = number of rows,

m = number of columns

T = scores matrix

P = Loadings matrix

The matrix **X** has to be mean-centered and autoscaled before PCA is carried out. The t_i are known as scores and the p_i are known as loadings. Scores contain information on how the samples relate to each other whereas; the loadings contain

information on how the variables are related to each other. The scores form an orthogonal set and the loadings form an orthonormal set.

Generally it is found that the data can be adequately explained with far fewer factors than original number of variables since PCA reduces the dimensionality of the data. Thus, the data compression can be addressed by monitoring a fewer number of scores and loadings (54). PCA has a tendency to group variables with similar characteristics into the same PC, hence, it also gives an idea about the way in which the variables covary.

The number of PC's to be included in the analysis is an important consideration. The PCs are arranged orthogonally, in decreasing order, along the direction of maximum variance of the data. Thus, PCs explain important information in the data until there is no preferred orientation in the remaining data (55). From this point onwards the next PCs explain the noise in the data. The number of PCs is a subjective decision. However, a rule of thumb can be stated here. When the incremental variance explained by consecutive PCs is less than about 5 % then the next PCs account for noise in the data. The optimum number of PCs to include is the number of PCs that gives the clearest break point in the total residual variance plot.

4.3 Multivariate Calibration and Prediction

Calibration is the process of constructing a mathematical model to relate the output of a measurement to the properties of the sample. Calibration is mostly followed by prediction that is a process of predicting properties of an unknown sample using the calibration model. Multivariate regression methods are discussed in this section.

4.3.1 Multiple Linear Regression (MLR)

MLR is a classical method that combines a set of several **X** variables in linear combinations that correlate as closely as possible to the corresponding y values. The process can be expressed as:

$$y = b_0 + b_1x_1 + b_2x_2 + \ldots + b_nx_x + f \qquad \ldots(4.3)$$

which can also be expressed as

$$y = \mathbf{X}b + f \qquad \ldots(4.4)$$

where, y = dependent variable column

X = independent variable data matrix

b = regression coefficient

f = error

The regression coefficient b is found using least squares estimate such that $f^T f$ is the smallest possible. Therefore,

$$\hat{b} = (\mathbf{X}^T\mathbf{X})^{-1}\mathbf{X}^T y \qquad \ldots(4.5)$$

Inversion of matrix b might cause problems due to collinearity. Collinearity is the linear interrelation between the **X** variables. When collinearity exists in the data, the inversion means a division by zero, and hence MLR would fail in such cases.

4.3.2 Principal Component Regression (PCR)

Principal component regression is a multivariate analysis method that combines the PCA and MLR techniques respectively. The scores vectors from PCA are used to carry out MLR using the dependent column. Thus, PCR takes care of the collinearity in the data. PCR consists of two distinct processes, PCA followed by MLR. The scores matrix **T** is used to carry out MLR. The number of PCs to be used in the PCA model is decided on the variance explained by the respective PCs. If too many components are used, then the advantage of data reduction gained by PCA is lost. If too less numbers of PCs are used, then the data is not adequately expressed. PCR makes use of the inverse calibration approach where it is possible to calibrate for the desired components while implicitly modeling for other sources of variation. Estimation of an inverse calibration model involves the inversion of a typically unstable matrix. Both PLS and PCR solve this problem by using linear combinations of variables.

The data matrix **X** is decomposed as

$$\mathbf{X} = \mathbf{USV}^{\mathrm{T}} \qquad \ldots(4.6)$$

where, U = matrix of row space eigenvectors

S = matrix of singular values

V = matrix of column space eigenvectors

The regression step similar to equation (4.3) is carried out using the decomposition of matrix X.

$$y = (\mathbf{USV}^{\mathrm{T}})b + f \qquad \ldots(4.7)$$

Therefore, the solution becomes

$$b = \mathbf{VS}^{-1}\mathbf{U}^{\mathrm{T}}y \qquad \ldots(4.8)$$

Prediction of y from a new data set is carried out as

$$y_{new} = \mathbf{X}_{new}b = \mathbf{X}_{new}\mathbf{VS}^{-1}\mathbf{U}^{\mathrm{T}}y \qquad \ldots(4.9)$$

4.3.3 Partial Least Squares (PLS) Analysis

PLS is a regression technique developed to address shortcomings of other standard regression techniques when applied to a data set with highly collinear variables and noise present in the **X** and **Y** data sets (54). PLS is also called as projections onto latent structures. Similar to PCR, it decomposes data into a smaller score space T. The difference between PCR and PLS lies in the way they relate to the **Y** data. In PLS, both the **X** and **Y** data are decomposed into scores and loadings matrices, T and U respectively. These orthogonal matrices are generated in such a way as to maximize the covariance between the scores for the **X** and **Y** data. PLS attempts to find a different set of orthogonal representation for the **X** data to give better predictions of the **Y** data.

Mathematically, **X** matrix is decomposed as follows:

$$\mathbf{X} = \mathbf{T}\mathbf{P}^{\mathrm{T}} + \mathbf{E} \qquad \ldots(4.10)$$

and the **Y** data is decomposed as

$$\mathbf{Y} = \mathbf{U}\mathbf{Q}^{\mathrm{T}} + \mathbf{E} \qquad \ldots(4.11)$$

When the first pass is made, the scores and loading vectors, t_1, p_1, u_1 and q_1 are found along with the residual matrices. These residual matrices are used to continue the procedure and find t_2, p_2, u_2 and q_2. This procedure is continued until the residuals contain no useful information. There exists a relation between the scores of the **X** and **Y** matrix as

$$u_i = b_i t_i + r_i \qquad \ldots(4.12)$$

PLS may underfit or overfit the data. By underfitting, not enough loadings are used, and the model fails to capture some of the information. By overfitting, too many loadings are used, and the model tends to fit some of the noise. Both cases produce suboptimal results. Hence, validation of the model should be done to avoid these problems. Cross validation is an important method of validation in which the data is divided into different groups. A PLS model is built using all but one of the groups and this model is then used to predict the group that was left out. This procedure is repeated until each group is left out once. The number of optimum components is chosen from this information (56).

4.3.4 Diagnostics of PCR and PLS

There are several tools that are used to investigate various aspects of the data set, the model and the variables. The primary objective of the model diagnostic is to determine the optimum rank of the model. The sample and variable diagnostics are used to study the relationships between the samples and variables respectively. They are also used to identify the presence of unusual samples and variables.

Percent Variance Plot:

It is a compilation of the amount of variance explained plotted versus the number of factors. This plot helps to determine the number of relevant factors, also called the rank of the data. In the case of a well-behaved data and an appropriate number of factors, the amount of variance unexplained in the data is indicative of the known errors present in the data set. A problem is indicated if most of the measurement variance is explained with appropriate number of factors and a considerable amount of data variance still remains unexplained.

Root Mean Square Error of Prediction (RMSEP):

Prediction error is an important diagnostic for the model since the models built using the calibration data are used to predict values for unknown samples in future. RMSEP is defined as

$$RMSEP = \sqrt{\frac{\sum_{i=1}^{n}(y_i - \hat{y}_i)^2}{n}} \qquad \ldots(4.13)$$

where y_i = measured value of the variable

$\hat{y}_i$ = predicted value of the variable

n = number of prediction samples.

RMSEP is a single value that quantifies the magnitude of the measurement residuals for the validation samples for a given number of factors included in the model. The ideal RMSEP plot decreases as the number of factors added to the model increases. Figure 4.1 shows the common behavior trends of RMSEP plots. The optimum number of factors is chosen at the minimum or where RMSEP levels off as shown in figure 4.1.

Predicted vs. Measured Value Plot:

In this plot, the predicted values for the model are plotted versus the known measured values. This plot gives an idea about the goodness of the predicted values using the model. A modeling problem is indicated when a systematic pattern can be observed away from the ideal line. Ideally, the points should vary randomly about a line of slope one and intercept zero. Similarly, a plot of (y_i - $\hat{y}_i$) residuals vs. $\hat{y}_i$ can also be plotted. It gives similar information as the predicted vs. measured value plot.

Loadings Plot:

Loadings can be used to help determine the optimal number of factors to consider for the model. For spectroscopic data, the point at which the loading displays

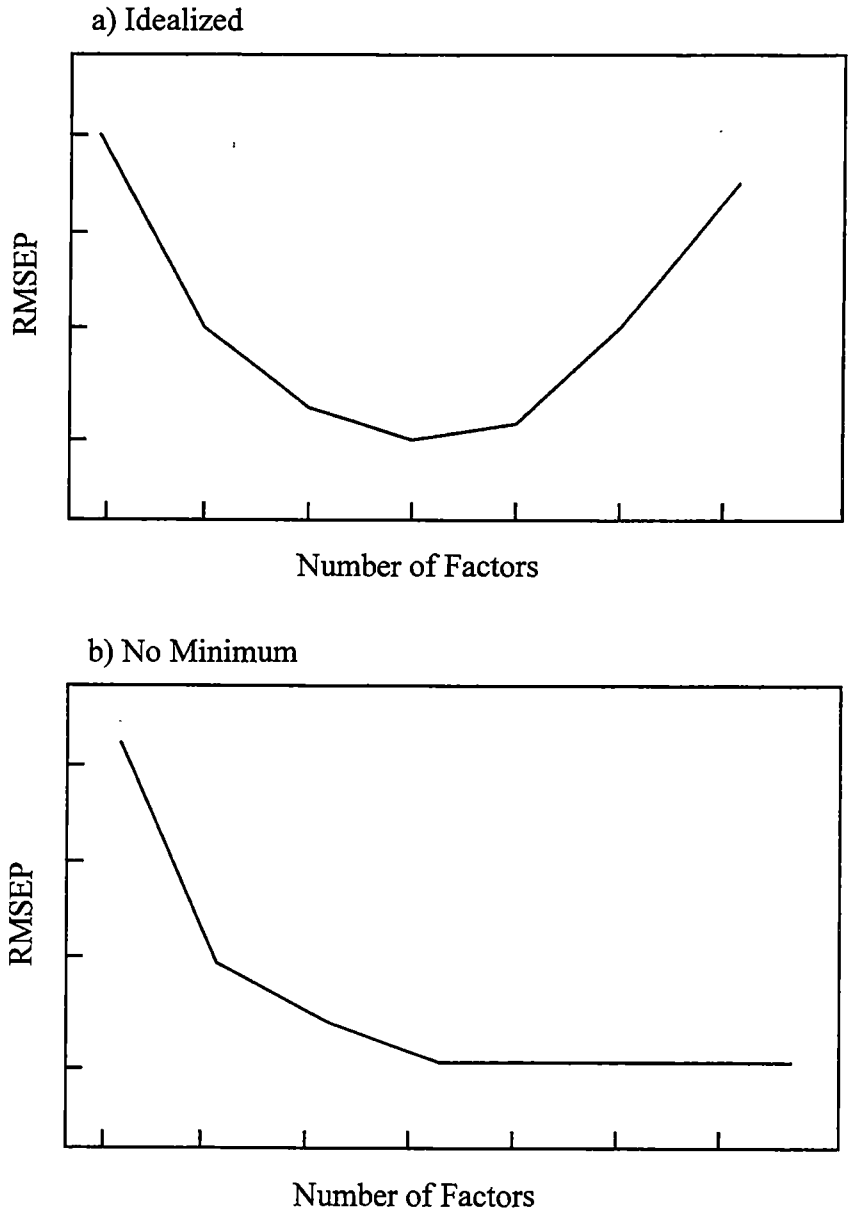


Figure 4.1: Possible behavior of RMSEP versus number of factors included in the model, (a) Idealized behavior, (b) Behavior more typically observed
[Source: Beebe, K. R., Pell, R. J., Seasholtz, M. B. in Chemometrics: A Practical Guide (John Wiley and Sons Inc., New York, 1998)]

a random behavior indicates the maximum number of factors to consider. Loadings can also be used as a variable diagnostic. They represent the relative contribution of the variables in the model. For well-behaved data, the features of the loading vectors are similar to the preprocessed data.

CHAPTER 5

EXPERIMENTAL SETUP FOR IN-LINE MONITORING USING RAMAN SPECTROSCOPY

5.1 Introduction

The need for in-line monitoring of processes in industry is tremendous and has been discussed before. In this research, instrumentation and experimental set up for a laboratory scale equipment is developed. In-line monitoring techniques have been applied to monitoring emulsion batch polymerization processes and extrusion processes.

5.2 Monitoring Emulsion Polymerization Reactions

The principle that underlines the development of in-line monitoring technique for emulsion polymerization reactions is the ability of Raman spectroscopy to monitor changes in the concentration of species of interest with time. The experimental setup consists of reactor, Raman spectrometer and probe, and a personal computer (PC).

5.2.1 The batch reactor

The polymerization reactions are conducted in a one-liter capacity batch reactor. The reactor is equipped with a cooling jacket through which cooling water is circulated to maintain constant reaction temperature. The temperature of water circulating through the bath is controlled by an automated water bath from NESLAB Instruments Inc. The bath controls the temperature within ±0.01 ^{0}C. The reaction setup is maintained under nitrogen atmosphere by bubbling nitrogen through the reaction

contents. This is important for free radical polymerization reaction as contact of the reaction contents with oxygen drastically reduces the ability of free radicals to initiate the reaction. Thus, care has to be taken to avoid contact of oxygen to the reaction mixture. A schematic of experimental set up is shown in figure 5.1.

5.2.2 The Raman Spectrometer

The reaction is monitored using a Kaiser Optical Systems Inc. HoloProbe® Raman spectrometer. This spectrometer unit consists of the base unit and monitoring probes. The HoloProbe consists of a base unit that connects to a fiber optic probe and a computer system. The base unit contains the laser, the spectrograph, the 2-D array detector (CCD).

Light Path Description:

The light from the laser source is coupled into an optical fiber with 50 μm core diameter. These optical fibers can be used over a distance of hundreds of meters to carry the light without much loss of light. Silica Raman generated in the fiber is filtered out at the probehead and the laser light is focused onto the sample. Backscattered light from the sample is filtered to remove the light at the laser wavelength and then sent to the spectrograph in the base unit through a 100 μm core diameter fiber optic cable. The spectrograph removes any residual laser light and disperses the Raman light into two tracks that are imaged onto the charge coupled device (CCD) detector. The CCD detector measures the intensity of the Raman

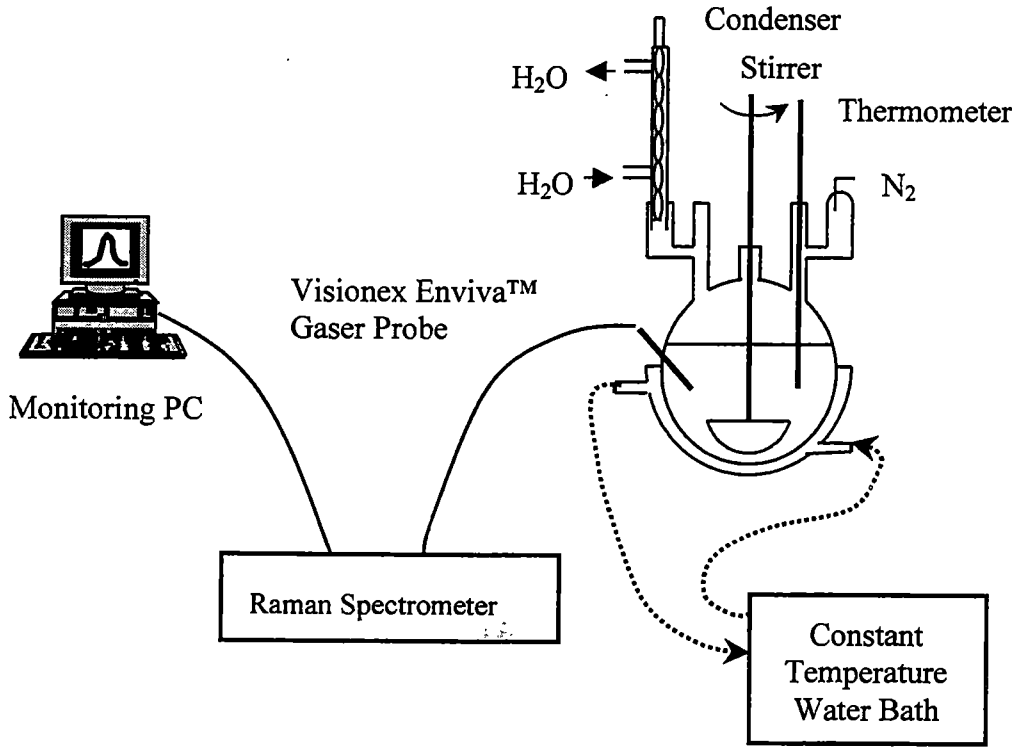


Figure 5.1: Schematic of Raman Spectrometer and Emulsion polymerization reaction setup

scattered light. It is a rectangular two dimensional array of independent, integrating detectors on a silicon chip. The individual detectors, called Pixels, collect light and store it in a potential well under the photo-active surface of the pixel. The spatial and axial resolution of the spectrograph is determined by the detector pixel size. The HoloPlex® transmission grating disperses and divides the undispersed Raman light into a low wavenumber shift stripe and a high wavenumber shift stripe on the CCD detector. Thus, the grating nearly doubles the spectral coverage without reducing its spectral resolution.

A simplified schematic of the HoloProbe® spectrometer is given in figure 5.2. The laser light is carried through a fiber optic coupler via the optical fiber cables to the probe head (FPH). The probe head contains optics to filter the laser light before it illuminates the sample. As the laser light travels towards the sample, a large amount of Raman signal and sometimes fluorescence is generated and efficiently collected by the fiber. It is thus necessary to separate the laser light from the background so that the fiber background does not overwhelm the Raman signal. Light backscattered by sample is collimated by PL4 and passes through a pair of notch filters in the probe head. The Raman light enters the spectrograph from the fiber optic cable. The light is collimated by camera lens L2 and is then sent through a holographic notch filter (NF) and an electronic shutter (SH). Transmitted light is focused onto the 50 μm wise spectrograph entrance slit (SL) by a camera lens L3. Light from the slit is collimated

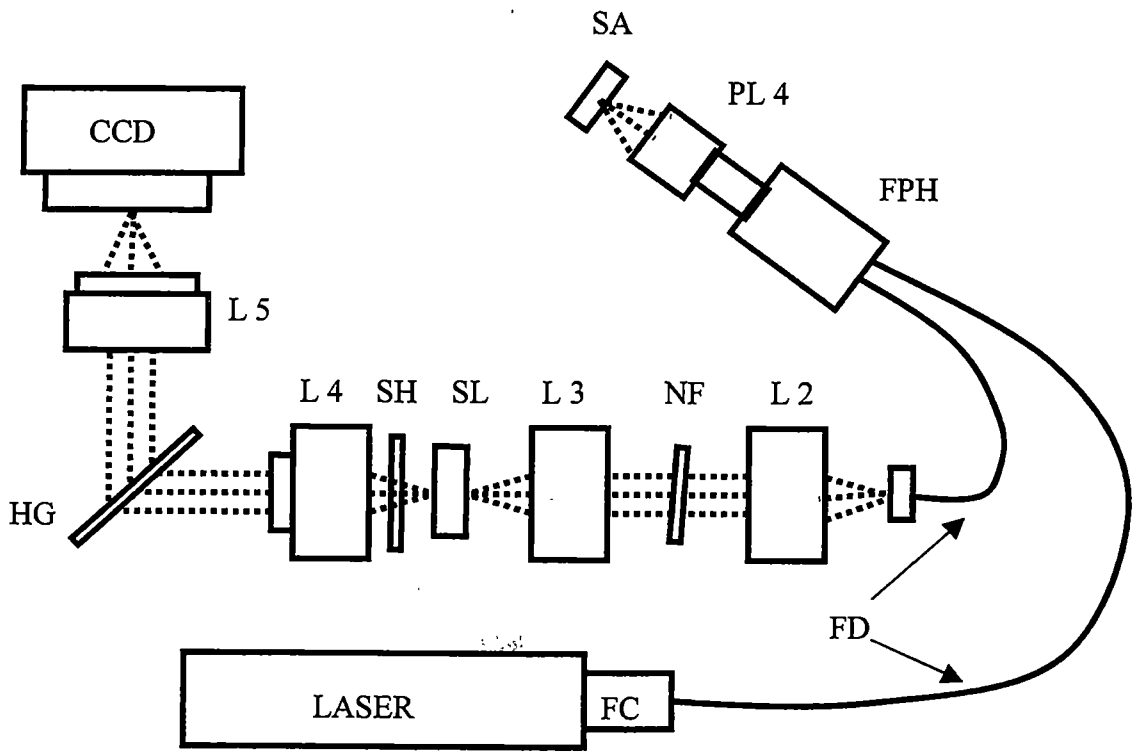


Figure 5.2: Schematic drawing of HoloProbe Raman Spectrometer Light Path
[**FC**: Fiber optic coupler, **FO**: Fiber optic cable, **FPH**: fiber optic probe head, **PL4**: Probe head focus and collection lens, **SA**: sample, **L2**: Pre-filter collimating lens, **NF**: Holographic Notch-filter, **SH**: Shutter, **L3**: Pre-filter focusing lens, **SL**: Spectrograph entrance slit, **L4**: Spectrograph collimating lens, **HG**: HoloPlex Grating, **L5**: Spectrograph focusing]

by lens L4 and then sent to the HoloPlex transmission grating (HG). Diffracted light from the grating is imaged onto the detector by camera lens L5.

Laser Wavelength:

In Raman spectroscopy, the interaction of the incident light with the vibrating molecule leads to a frequency shift of the scattered light with respect to the incident frequency. Thus, Raman spectrum is obtained by measuring the intensity of the scattered photons as a function of the frequency difference. Hence, the breadth of a Raman spectrum on the wavelength scale depends on the excitation wavelength (57).

Figure 5.3 shows the vibrational spectra on wavelength scale for various laser types. The wavelength ranges for Raman spectra are shown as bars relative to the excitation at 514 nm (argon), 632 nm (HeNe), 752 nm (Krypton), 1064 nm (Nd:YAG). The Rayleigh line of these spectra (0 cm^{-1} Raman shift) Is at the left end of each bar and the Stokes shift of 3600 cm^{-1} is on the right end of the bar. All the spectra have the same length on the wavenumber scale (0-3600 cm^{-1}). For example, the bar indicating the range of the IR spectrum covers wavenumber range from 3600 cm^{-1} (2.77 μm) to 2500 cm^{-1} (4 μm).

With excitation in the NIR range, the sample fluorescence is greatly reduced. Thermal degradation of the samples and background emission are reduced as the absorption processes are minimized in the NIR range. NIR diode lasers are

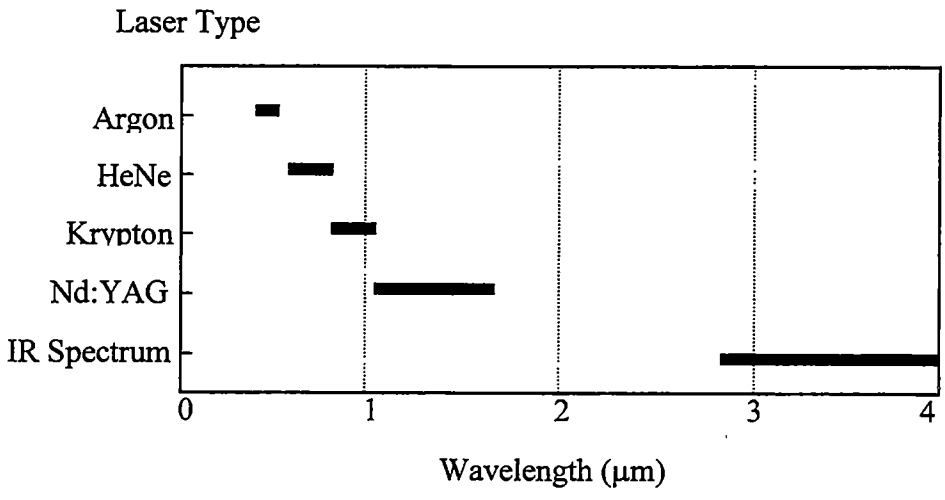


Figure 5.3: Raman Vibrational spectra on wavelength scale for various laser types
[Source: Hergeth, W. D. in "Polymeric Dispersions: Principles and Applications" ed. Jose. M. Asua (NATO ASI series Applied Sciences, vol 335]

commercially available in low power requirement rating and thus allow the Raman spectrometer to be compact and portable. They have a longer lifetime compared to the NIR gas lasers (12).

5.2.3 Sampling Systems

Optical fiber probes are widely used as sampling system. They are compact, usable in the laboratory environment or for remote sampling. They provide stable, reproducible signals from solids, liquids and gases. There are two types of probe designs widely used in monitoring applications. The concentric "n around 1" fiber bundle type probe and the filtered probe (4,58). Figure 5.4 shows the concentric fiber bundle probe (59). An immersion probe obtained from Visionex® Inc. that has such "7 around 1" design was used for monitoring. The central fiber delivers light to the sample and the surrounding fibers collect Raman scatter. The laser beam is focused into the delivery fiber with a microscope objective or other short focal length lens. For better coupling to the spectrograph entrance slit, the output ends of the collection fibers are arranged in a linear array, as shown in figure 5.4. Probes with multi fiber design gather more light as compared to a single excitation and collection fiber probe because a single fiber collects only about 10-15 % as much light. The optical fibers are themselves a source of background signal. As the light travels down the fiber length, fluorescence from the fiber cladding and from the cement holding the components together is generated. These signals are incident on the sample as light emerges from the probe tip. They are reflected from the sample and get collected along with the

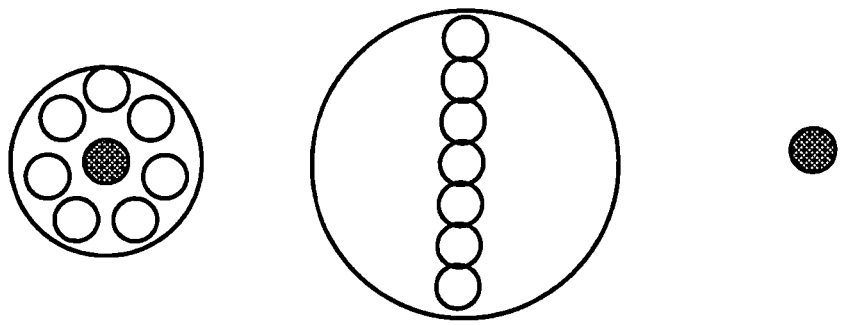


Figure 5.4: Schematic of 7 around 1 probe, showing excitation and collection end of the fiber

Raman spectrum of the sample. The reflected laser light also generates more background signal as it travels through the collection fibers. The background noise may obscure a weak Raman signal. Distortions due to inherent spectrum of fiber material could be suppressed by minimizing direct reflections of excitation laser beam into probe end (13).

In order to avoid these problems, filter based probes are used. They use a lens to focus filtered laser light from the tip end of the excitation fiber onto the sample. Similarly, the collected light is also filtered before the Raman signal information of interest is collected using the collection fibers. In Kaiser Optical Systems Inc. HoloProbe Probe head, the light emerging from the delivery fiber is collimated and presented to a holographic transmission grating which diffracts the laser light to a spatial filter. The collected Raman signal along with the Rayleigh scatter and reflected laser radiation, is passed through a pair of notch filters. These filters remove reflected laser light and avoid any fiber background generation as the collected Raman light travels to the spectrograph. A schematic of the probe head is shown in figure 5.5.

The Visionex and Kaiser Raman probe are both used for in-line monitoring of batch emulsion polymerization. The Kaiser probe head has various lens and probe fixtures such that it could be either immersed in the reaction mixture or it can be used to monitor the reaction progress from outside the reactor. The Visionex probe was used to collect data in immersed fashion.

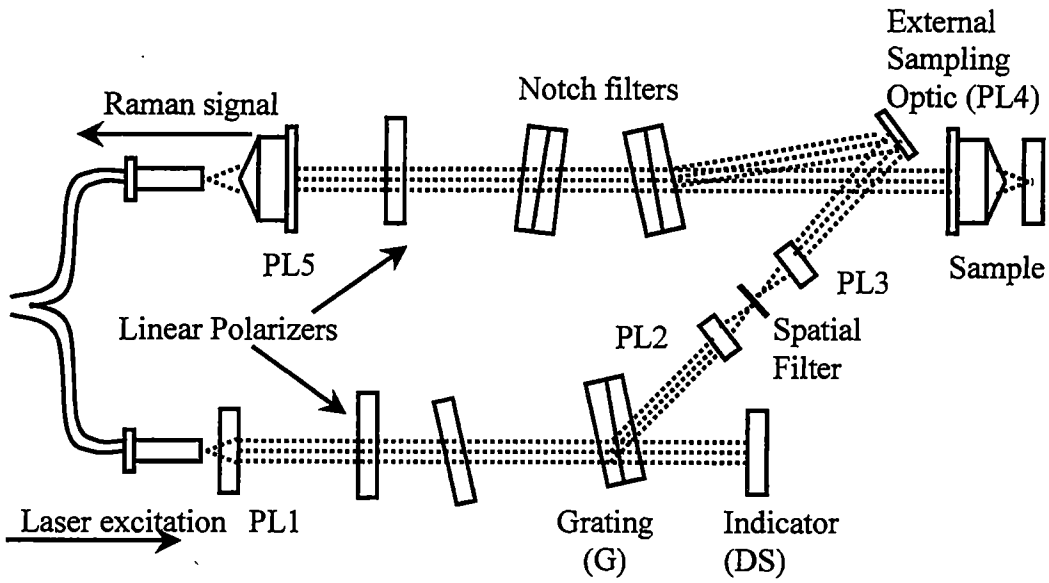


Figure 5.5: Optical configuration of fiber optic probe head
[PL1 through PL5: lenses, PA: power adjustment control, G: grating, DS: diffuse screen indicator, probe head shutter, SF: spatial filter, M: turning mirror, BC: beam combiner, NF: notch filter, PB: block of linear polarizers]

CHAPTER 6

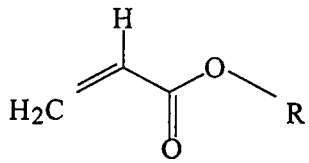
IN-LINE MONITORING OF BATCH EMULSION POLYMERIZATION

6.1 Emulsion polymerization of derivatives of acrylic polymers

Emulsion polymers derived from the acrylic monomers constitute a diverse and versatile range of polymers used for many diverse applications. Figure 6.1 shows the chemical structures of typical acrylic molecules used in emulsion polymerization. The acrylic and styrene-acrylic compositions account for nearly 30% of commercial emulsion polymers. These monomers have an excellent ability to copolymerize with other members in the family. Thus, polymers can be manufactured with various compositions that have varied physical properties such as glass transition temperature and solubility characteristics of the resulting polymer. Polymers in this family also display versatility in particle morphology design. Relatively homogenous polymer compositions as well as a variety of core-shell morphologies have been produced. Methyl methacrylate (MMA) homopolymerization, vinyl acetate (VA) homopolymerization, and 2-ethylhexyl acrylate (2-EHA) copolymerization with acrylic acid (AA) as the functional monomer have been studied in this research.

6.2 MMA emulsion polymerization

MMA polymerization reactions were carried out using the reaction recipe as given in Table 6.1. The Fe (II) heptahydrate along with potassium persulfate ($K_2S_2O_8$)



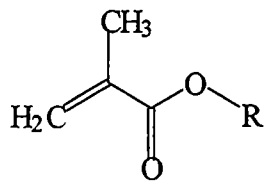


Figure 6.1: Chemical structures of acrylic monomers

R = H (acrylic or methacrylic acid)
R = methyl, ethyl, butyl, hydroxyethyl, etc. alkyl groups

Table 6.1: Reaction recipe for methyl methacrylate emulsion polymerization

Ingredient	Amount
Methyl methacrylate	111.82 gm
Water	672.00 gm
Emulsifier (Sodium Lauryl Sulfate)	49.00 gm
Fe (II) sulfate heptahydrate	0.0294 gm
Potassium persulfate	3.0184 gm
Sodium metabisulfite ($Na_2S_2O_5$)	6.713 gm
Total	842.57 gm

forms a strong redox initiator system. A prime advantage of redox systems is that radical production occurs at reasonable rates over a very wide range of temperatures, including initiation at moderate temperatures of 0-50 ^{0}C or lower (14). This allows a greater freedom of choice of the polymerization temperature than is possible with the thermal homolysis of initiators.

$$K_2S_2O_8^{2-} + Fe^{2+} \rightarrow Fe^{3+} + SO_4^{2-} + SO_4^{-} \quad \ldots(6.1)$$

MMA polymerization reactions were carried out at three different temperatures, viz. 25 ^{0}C, 30 ^{0}C, and 35 ^{0}C. The monomer is dispersed using mechanical force, i.e., using agitation. During the reactions, the reaction mixture was continuously stirred at 200 rpm. The reactor was initially charged with water and emulsifier. The monomer was charged once the reaction contents attained the desired temperature. The contents were held at reaction temperature using a water bath and nitrogen was bubbled in the mixture for approximately 15-20 minutes. The reaction time was noted when the initiator was added to the mixture and the collections of in-line Raman spectra were simultaneously started. Each Raman spectrum was collected for 15 seconds and average of two consecutive scans was recorded. This is important to avoid any contamination in the spectral information due to stray light that might enter the collection optics. The laser wavelength was 785 nm. The spectra were collected every 1.5 minutes.

During the progress of the reaction, samples were withdrawn and inhibited using 2% (w/w) 3-tert-Butyl-4-hydroxy-5-methyl-phenyl sulfide solution in acetone.

The inhibitor destroys any free radicals remaining in the reaction sample and thus terminates the reaction. In order to quench the reaction, the samples were also stored in ice.

The samples were analyzed for monomer conversion based on total polymer content using gravimetric analysis. Approximately 3-4 mL aliquot were transferred from the sample vial into an aluminum dish and weighed. The contents of the dish were then dried at constant temperature of 80 ^{0}C to constant weight for about 24 hours. The % solids and conversion were calculated using formulae in equation (6.2) and (6.3).

$$\% \text{ Solids} = \frac{(\text{Weight of dried sample and dish - weight of empty dish})}{(\text{Weight of sample and dish - weight of empty dish})} \times 100 \quad \ldots(6.2)$$

$$x = \frac{\left(\frac{\% \text{ solids}}{100}\right) - \text{wt. fraction initiator - wt. fraction emulsifier}}{(\text{wt. fraction of monomer initially})} \quad \ldots(6.3)$$

Figure 6.2 shows the progress of the polymerization reaction with time. All the spectra show the same overall nature. However, there is a change in intensity of some of the Raman bands due to the chemical changes taking place during the reaction. Figure 6.2 shows the Raman bands due to C=C and $=CH_2$ species present in the monomer. The filter based non-immersion probe from Kaiser Optical Inc. was used

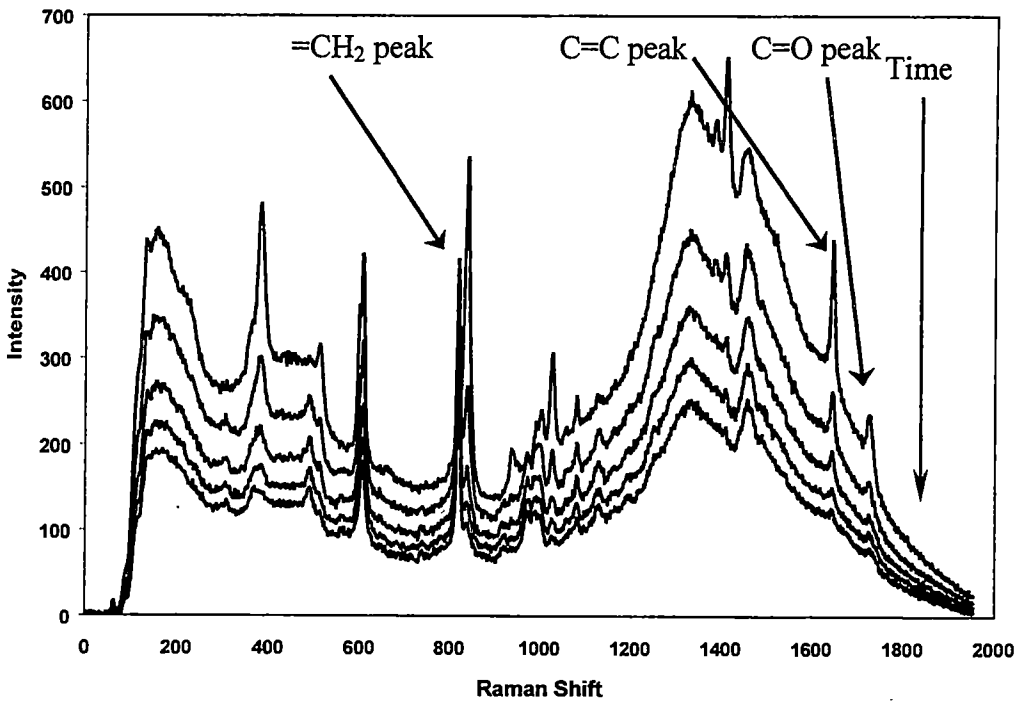


Figure 6.2: Raman spectra collected for MMA polymerization at 25 ^{0}C

for monitoring this reaction. The probe was positioned outside the glass jacket of the reactor. The focus of the probe was adjusted to be inside the glass reactor by adjusting the distance of the probe from the reactor wall using a micrometer screw stage. As the light passes through the glass wall of the jacket and the reactor in its excitation and collection path, the light is scattered by glass. This light also gets collected along with the Raman signal of interest. The interference due to the glass reactor walls is observed in the Raman spectra in Raman shift region 1000-1800 cm^{-1} in the form of a raised background. The peaks of interest are in the Raman shift region 1600 to 1800 cm^{-1}. The peak at 1640 cm^{-1} is due to >C=C< present in the MMA monomer. Polymerization reaction breaks the π bond and converts it into a σ bond in the polymer product. Hence, the amount of >C=C< in the reaction mixture decreases, causing a visible decrease in the >C=C< peak intensity in the spectra collected later during the reaction.

Under similar experimental conditions, MMA polymerization reactions were carried out at 30 ^{0}C and 35 ^{0}C and Raman spectra were recorded. The spectra were analyzed to observe and quantify the effect of the temperature on the reaction progress. It is important to be able to detect and quantify the difference in reaction rate at different temperatures using Raman spectroscopy. This has direct utilization in the polymer manufacturing plant as Raman spectroscopy can be employed to detect the variation of the batch reaction from its set point or calibrated reaction path.

Results and discussion:

The spectra recorded with reaction progress were processed before mathematical information was extracted. The spectra were recorded in HoloProbe format (*.hol). The Kaiser Optical Systems Inc. software has ability to convert the spectra into GRMAS32 (*.spc) format which is more easily processed. MATLAB was used as the mathematical processing environment. The spectra were arranged into a matrix with time and Raman shift information as the independent variables.

There are several regions of interest in the spectra. The peak due to >C=C< stretching appears at about 1640 cm^{-1} and that due to C=O appears around 1730 cm^{-1}. There are peaks in the region 820-860 cm^{-1} that also change as the concentration of reactants in the reaction mixture changes. The peak at 820 cm^{-1} appears in increasing intensity as the reaction proceeds, and the peak at 840 cm^{-1} decreases very rapidly as the concentration of monomer in the reaction mixture depletes. The peak at 840 cm^{-1} has been attributed to the $=CH_2$ in the monomer species (60-62). These regions in the spectral matrix **X** were analyzed individually for information regarding the progress of the reaction. The region between 1600-1660 cm^{-1} was baseline corrected using a user-defined program developed in MATLAB®. Figure 6.3 shows the baseline corrected region plotted with the Raman shift (cm^{-1}) scale. In figure 6.4 the maximum intensity of the baseline corrected region is plotted with the MMA conversion. The regression coefficient, r^2, which is measure of the goodness of fit, is 0.95. This graph shows that there is a good correlation between the observed Raman intensity of the C=C peak and

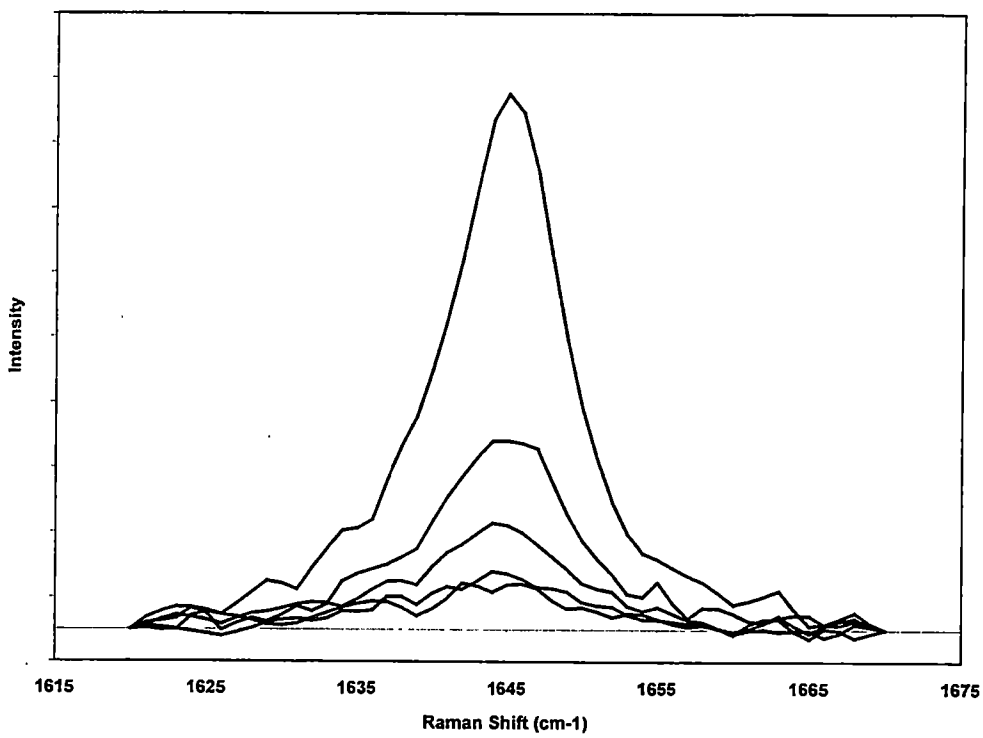


Figure 6.3: Baseline corrected C=C peak for MMA polymerization reaction plotted against the Raman shift (cm^{-1})

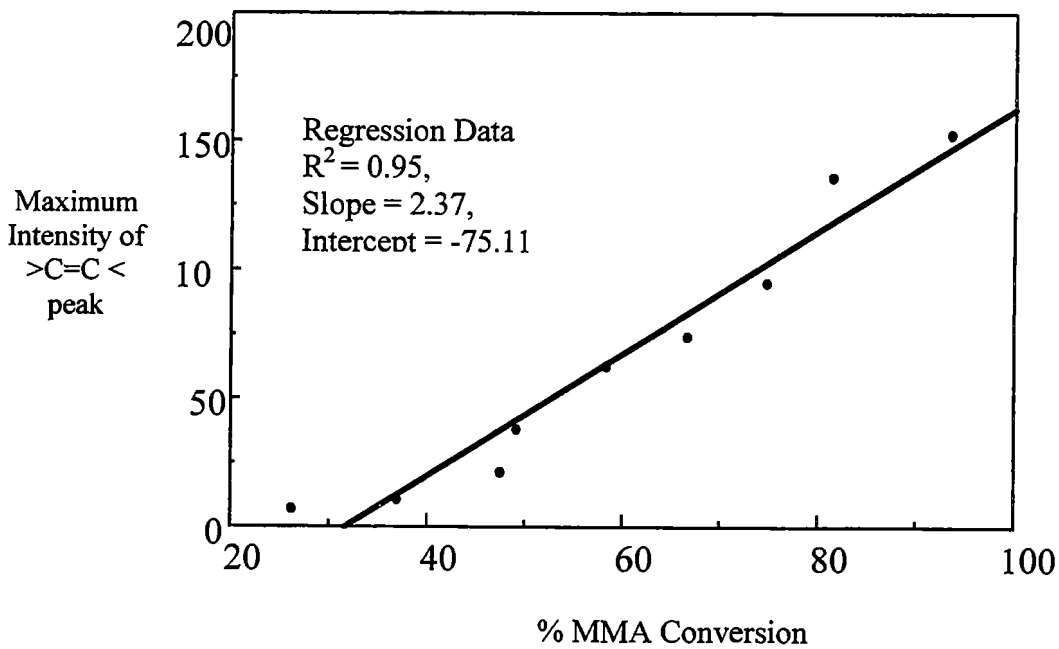


Figure 6.4: Maximum intensity of the baseline corrected C=C region vs. MMA conversion

the concentration of C=C in the reaction mixture. Figure 6.5 depicts the baseline corrected spectral region in 780 through 880 cm^{-1} Raman shift. The monomer peak at 840 cm^{-1} that decreases in intensity with time can be clearly seen here along with the 820 cm^{-1} peak that increases as the reaction proceeds. However, exact band assignment of this peak has not been defined (61). Figures 6.6 and 6.7 depict the three-dimensional view of the peaks at 820 and 840 cm^{-1} with time.

Principal Component Analysis (PCA):

Mathematical description and background of PCA has been described in chapter 4 on regression methods. Here, PCA was used a chemometric tool to distinguish between the subtle differences in the rates of the three MMA polymerization reactions at 25, 30 and 35 ^0C. The spectral region between 790 to 870 cm^{-1} was chosen to perform the data analysis. The **X** matrix containing the spectra with respect to time was mean centered and then subjected to PCA. The resulting loadings and scores plots were analyzed. Loading values are viewed as the weights associated with each independent variable, and thus they describe the relative importance of the independent variables. The loadings obtained from PCA are as shown in figure 6.8. The loading plot shows the relative importance of the peaks at 820 and 840 cm^{-1}. The first principal component (PC) explains information in the region of the peak around 840 cm^{-1} whereas the second PC explains information in the region around peak at 820 cm^{-1}. Scores plot are sample diagnostics and are used as a tool that aids in qualitative interpretation of the multivariate data. The values of score

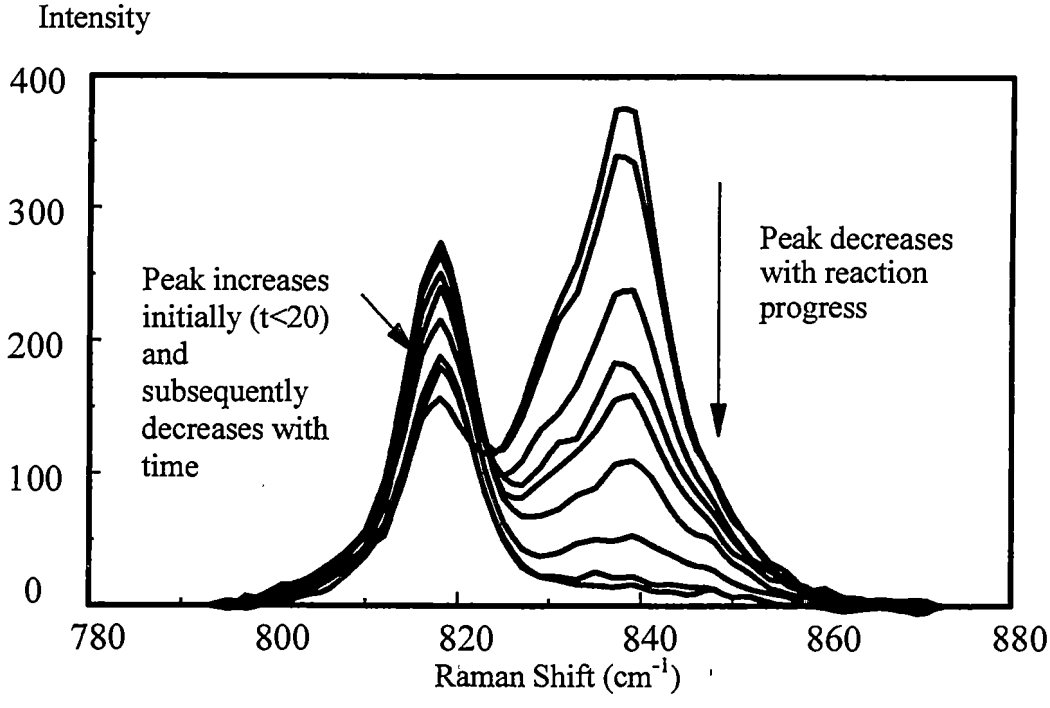


Figure 6.5: Baseline corrected peaks in the Raman shift region 780-880 cm^{-1}. The peak at 820 cm^{-1} increases in intensity, and the peak at 840 cm^{-1} decreases in intensity with increasing monomer conversion.

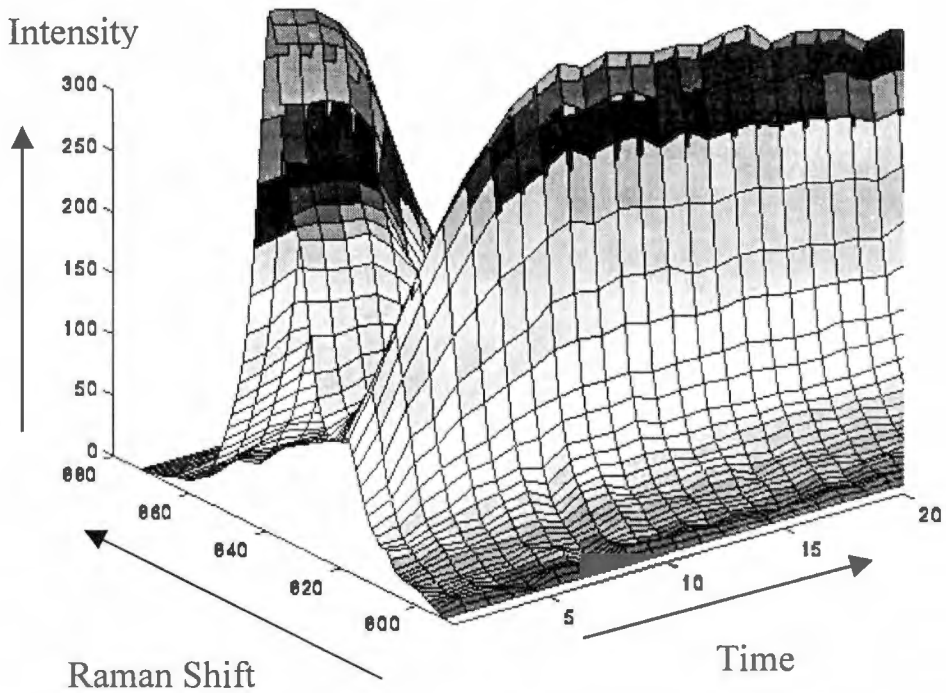


Figure 6.6: Three-dimensional representation of Raman spectra in the region 820-840 cm^{-1}

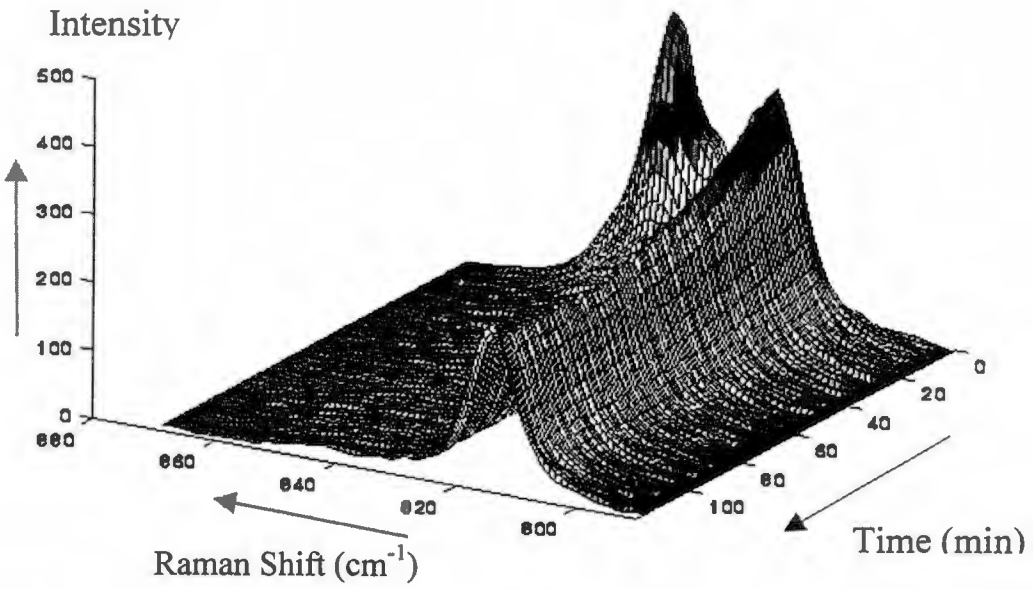


Figure 6.7: Three-dimensional representation of Raman spectra in the region 820-840 cm^{-1} (Orientation: 180^0 revolved as compared to figure 6.6)

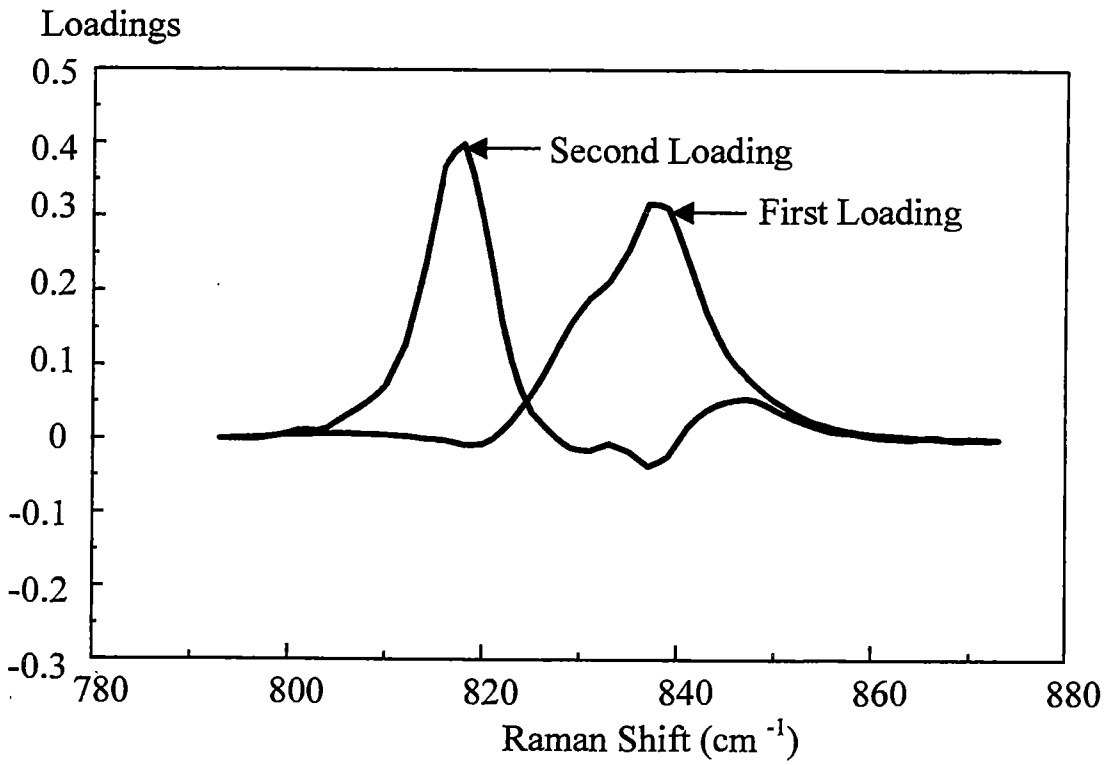


Figure 6.8: First and second loadings obtained after performing PCA on the spectral data (Shown for reaction at 30 ^{0}C)

vectors are "magnitudes" of the vectors resulting from matrix decomposition. Thus, the score values characterize the relationship between various samples included in the data matrix **X**. PCA was carried out on the data obtained from all the three reactions, and the resulting first scores are plotted in figure 6.9. The scores plot for the reactions at 25, 30 and 35 ^{0}C are well distinguished from each other. The scores plot for the reaction at 25 ^{0}C indicates that the polymerization reaction at this temperature proceeds relatively slower than the reactions at 30 and 35 ^{0}C. The reactions also begin and end faster as the temperature rises. Thus, for the reactions at 30 and 35 ^{0}C, the scores plots show a steeper decrease in the intensity as compared to the score plot for the reaction at 25 ^{0}C. The results seen here are in agreement with the Arrehenius equation discussed in section 2.2.3.

6.3 Vinyl Acetate Polymerization

Vinyl copolymers are one of the largest selling class of binders for coatings applications. Emulsion copolymers of vinyl acetate are increasingly used for exterior as well as interior architectural coatings, and in adhesives. Their use in these markets arises from the advantageous combination of good durability and wide availability at low cost.

Work has been published on the emulsion polymerization of vinyl acetate (VA) using a non-ionic emulsifier (63,64). Most of the investigators have used non-ionic detergents that do not form micelles. In this research, emulsion polymerization

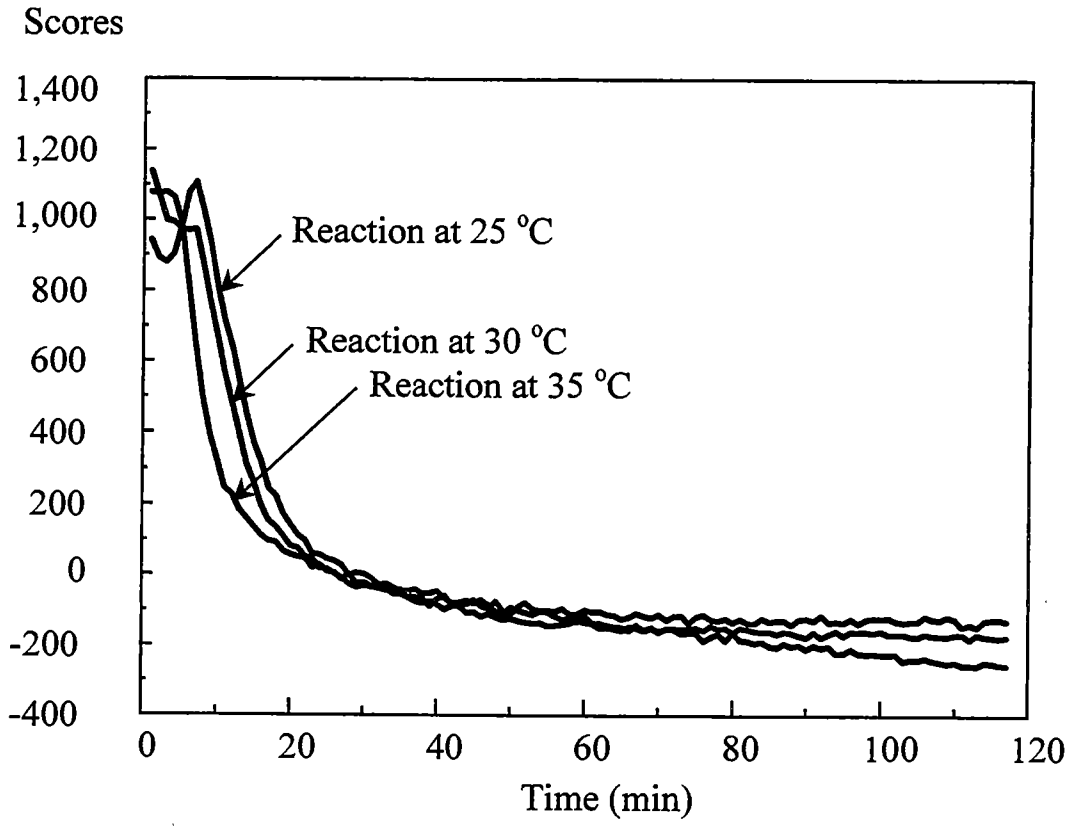


Figure 6.9: Scores plot for reactions at 25, 30 and 35 ^{0}C plotted against time.

of vinyl acetate monomer was carried out in presence of emulsifier, according to the recipe as shown in Table 6.2.

The emulsion polymerization reactions were monitored in real time using Raman spectroscopy. The filter based non-immersion probe was used for monitoring the reactions along with filter based immersion probe ("filters in the tip" technology) (65). The spectra collected during a polymerization reaction of VA using filter based immersion probe are shown in figure 6.10. Figure 6.11 shows the spectra collected in real time using the filter based immersion probe. The spectra collected using the filter based immersion probe have lesser signal to noise ratio as compared to those collected by the filter based non-immersion probe.

The effect of temperature on the VA emulsion polymerization was studied at two different temperatures, 60 ^{0}C and 65 ^{0}C. The Raman spectra were recorded using 785 nm laser for 15 seconds and as an average of two spectra was recorded. The reaction was conducted under inert atmosphere generated by circulating nitrogen through the contents of the reactor. The dispersion of the monomer in aqueous system was maintained by using mechanical agitation at 200 rpm.

The Raman spectra obtained in real time during the reaction were mathematically treated in a similar manner as described in detail in section 6.2. In previous work by Claybourne *et al.* (1994) (2), the real time monitoring of emulsion

Table 6.2: Reaction recipe for emulsion polymerization of vinyl acetate

Ingredient	**Amount**
Vinyl Acetate	210.00 gm
Water	630.00 gm
Emulsifier	4.20 gm
Potassium persulfate	0.14 gm
Total	844.34 gm

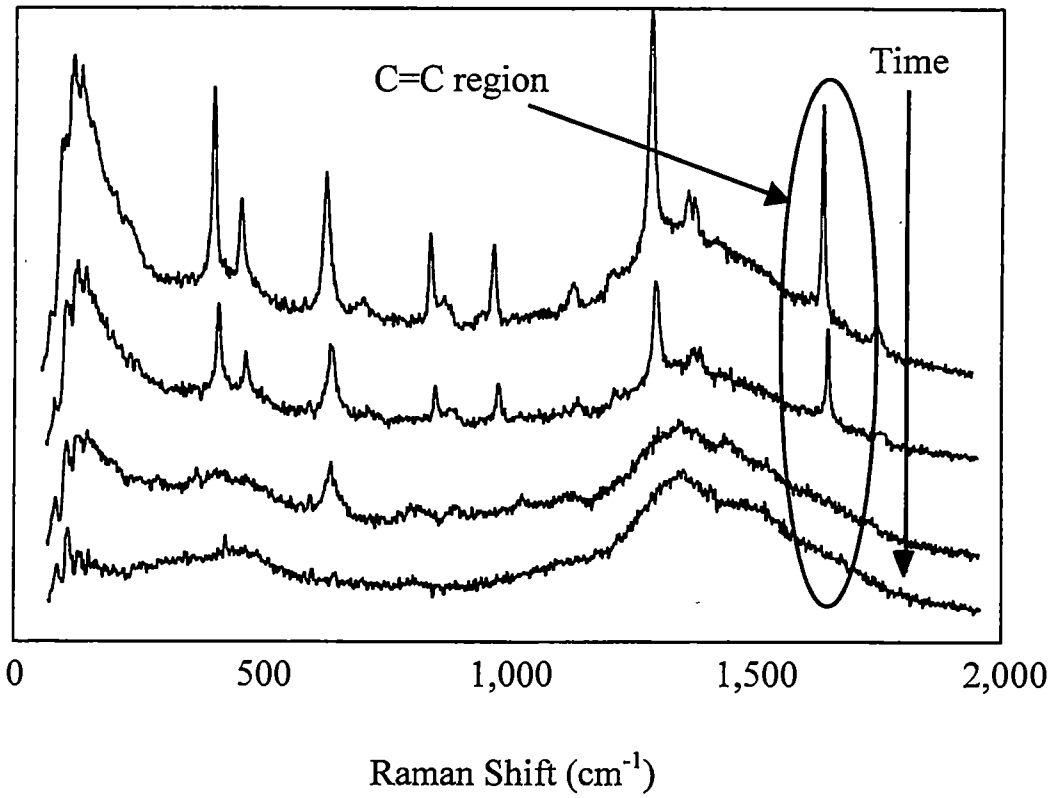


Figure 6.10: In-line Raman spectra obtained for VA emulsion polymerization at 60 ^{0}C, monitored using filter based non immersion probe.

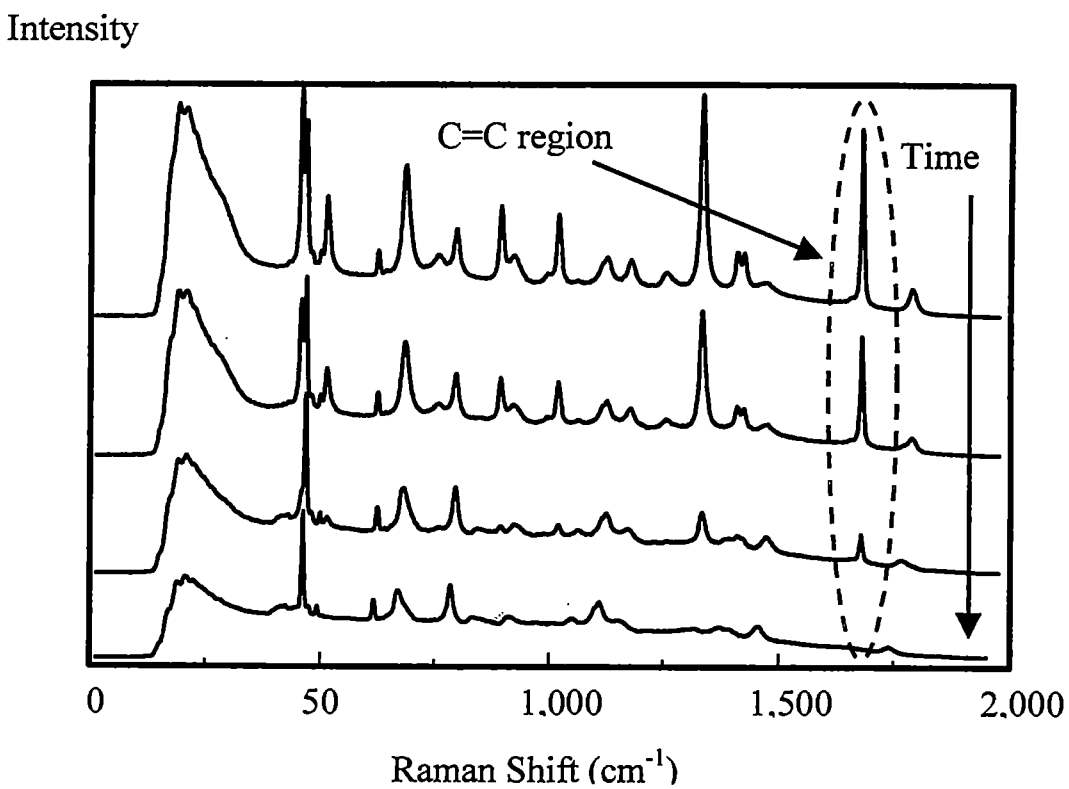


Figure 6.11: In-line Raman spectra obtained for VA emulsion polymerization at 60 ^{0}C, monitored using filter based immersion probe.

polymerization of methyl methacrylate, butyl acrylate and allyl methacrylate monomers in water as a continuous phase has been investigated using the ratio of C=C peak in the Raman spectrum to the C=O peak. It is noted that if the spectral region up to a Raman shift in the C=O stretching region can be assumed to be invariant, then the C=C band of the acrylic monomers can be followed along reaction over a wide range of solids and using C=O band as an internal standard. Figure 6.12 shows the plot of baseline corrected (C=C/C=O) with reaction time. This technique of monitoring the reaction monomer profile with respect to an internal standard clearly brings out the differences in the rate of propagation at different temperatures. As seen in figure 6.12, the reactions at 60 and 65 ^{0}C, have the same level of monomer C=C ratio with the internal standard C=O peak. As the reaction kicks off, the reaction at higher temperature enters the propagation stage earlier than the one at lower temperature. This is an industrially invaluable finding as it clearly demonstrates the ability of Raman spectroscopy to detect the changes in rate of polymerization with temperature. The success of Raman spectroscopy in harsh industrial environment is critically dependent upon the ability of the instrumentation and probes to withstand the continuous use.

Experimental limitations for MMA and VA polymerization:

The real time in-line monitoring of the emulsion polymerization reactions was carried out in a laboratory batch set up. The excitation and collection signals were collected through the reactor glass wall. Thus, a source of noise is introduced when the

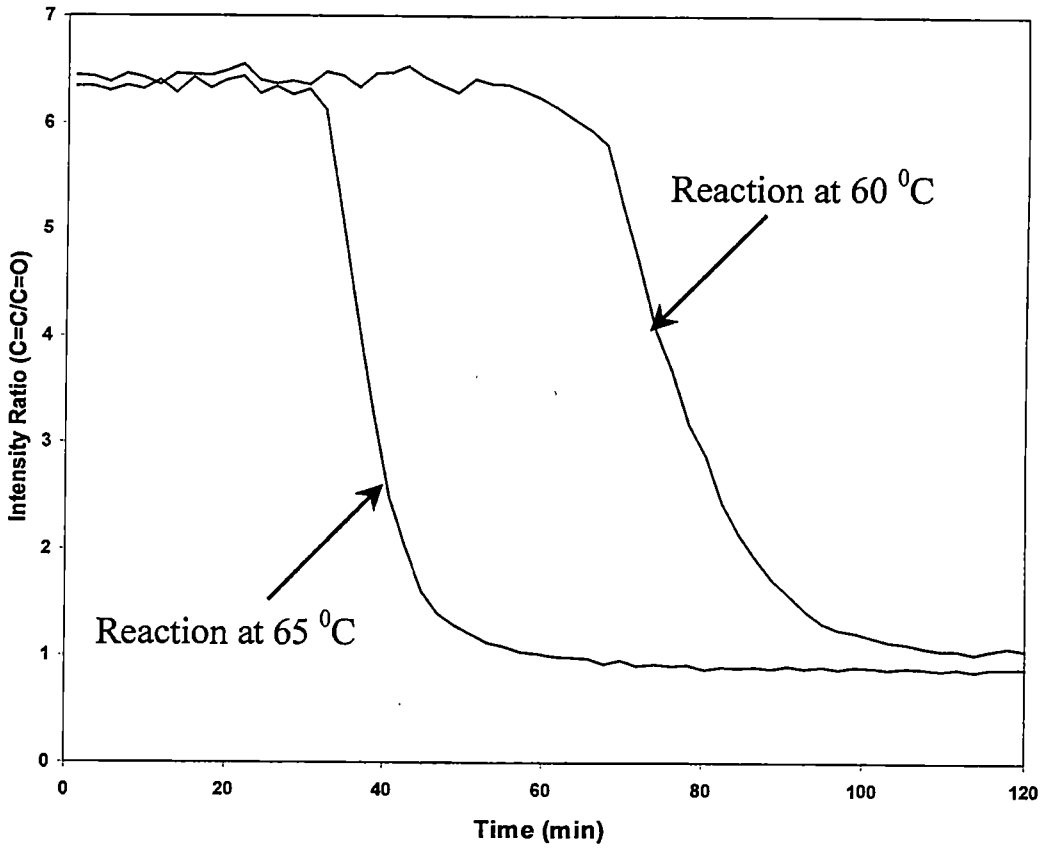


Figure 6.12: Real time monitoring of VA emulsion polymerization using the ratio of C=C (residual unreacted monomer) to C=O (internal standard) plotted against reaction time

non-immersion type of probe is used for reaction monitoring. In terms of noise reduction, the immersion type of probe yields superior results than the non-immersion probe. However, use of an immersion type of probe is an intrusion in an otherwise homogeneous emulsion system. If the latex stability is not sufficient, then coagulum could be formed on the tip of the immersion probe. Coagulum can form during and after polymerization, and is undesirable in either case. One source of coagulum formation is polymerization in monomer droplets, which takes place when free radicals enter the droplets (66). The polymer resulting from the bulk polymerization of the monomer in the droplets eventually becomes a coagulum. Polymerization in monomer droplets may occur for highly water soluble monomer. Coagulum formation may result when the stabilization provided by the emulsifier in the system is not adequate for polymer droplets. As the monomer droplets get depleted through the normal process of supplying monomer to growing latex particles via diffusion through the aqueous phase, the polymer concentration in the droplets which have been hit by free radicals increases. Ultimately, these particles become large swollen polymer particles of low colloidal stability and act as nuclei for further coagulum formation.

Raman spectroscopy has been reported as an excellent technique for monitoring analytes in the percent range, however the results published in literature are not reproducible in many cases (67). Generally, laboratory analytical instrumentation is very accurate in the parts per million (ppm) range and versatile but also expensive and delicate. Therefore, if it is to be applied industrially, the cost per

measurement must be minimized and the instrument must be rugged to withstand the operating conditions.

In Raman spectroscopy, the excitation wavelength of the laser ranges anywhere from the ultraviolet to the NIR region. Raman signal is to be collected efficiently from the sample scatter. The Rayleigh scatter also simultaneously takes place and is orders of magnitude stronger in intensity than the Raman scatter. Hence, the probes used for Raman signal collection have to be equipped with filters to cut off the signal from Rayleigh light otherwise the Raman information could get masked.

6.4 Copolymerization of 2-ethylhexyl acrylate with acrylic acid

Acrylic emulsion polymers find use in the industry for various applications under the broad category of non-woven fabric binders. This class of emulsions includes pressure sensitive adhesives, paper coatings, and industrial coatings. The end uses include its use as architectural coatings (paints), floor polishes etc. High volume commercial production of these acrylic emulsion polymers provides economic access to a continuous range of copolymers of glass transition temperature (T_g) ranging from -80 ^{0}C to over 100 ^{0}C, and with solubility characteristics ranging from highly oil soluble to highly polar and solvent resistant emulsions. Thus acrylic emulsions find end uses based on their T_g. Very soft (low T_g) emulsions are used as pressure sensitive adhesives, other film forming tough binders are used for latex paints and hard compositions are used for floor polishes. Various applications of acrylic emulsions

classified according to the T_g are shown in figure 6.13. Higher acrylates, such as 2-EHA find application as pressure sensitive adhesives (PSA). These acrylic adhesives are generally composed of two monomers that are copolymerized. One of the monomers that is present in excess (about 80-98 % of the total weight of the two monomers), is hydrophobic and its carbon number ranges from 4-10 carbon atoms. (68). The second monomer, incorporated during copolymerization is a reinforcing monomer, present in 2-20 % of the total weight of monomers. It usually contains 1-3 carbon atoms in the alkyl group. The chemical structures of 2-EHA and acrylic acid are shown in figure 6.14. Figure 6.15 shows the Raman spectrum of 2-EHA and figure 6.16 shows that for AA. With this in mind, the polymerization system of 2-EHA copolymerization with acrylic acid was studied using Raman spectroscopy.

6.4.1 Correlation of monomer conversion with in-line real time Raman spectra

Emulsion polymerization reactions of 2-EHA and AA were carried out using recipe in Table 6.3. The total monomer concentration was maintained at about 10% of the total latex amount, thus accounting to 10% solids in the finished latex. Reactions were carried out at 60 ^{0}C and varying monomer ratio of the two monomers (90/10 and 80/20 2-EHA and AA). The stirrer speed was maintained constant at 200 rpm. Raman spectra were collected in real time with 15 seconds accumulation time and the spectra were recorded as average of 2 collections. The laser wavelength was 785 nm. The reaction time was recorded throughout the experimental run and 2-5 ml aliquots were withdrawn from the reactor at regular intervals. The sample latex was then inhibited

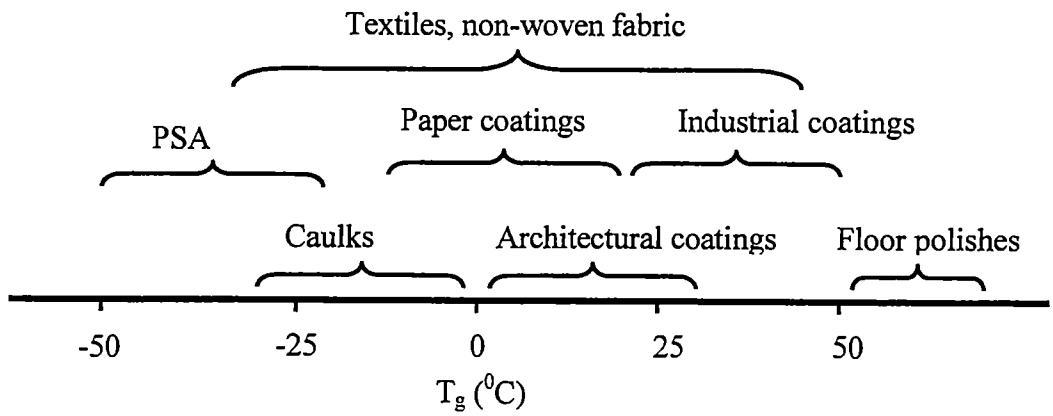
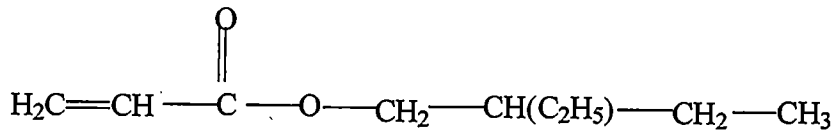


Figure 6.13: Polymer glass transition temperature (T_g) ranges for various product applications
[Source: Lowell, P. A., El-Aasser, M. S. in "Emulsion Polymerization and Emulsion Polymers" (John Wiley and Sons Inc., New York, 1997)]

(A) 2-Ethylhexyl acrylate



(B) Acrylic acid

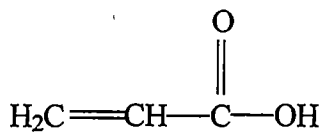


Figure 6.14: Chemical structures of 2-ethylhexyl acrylate and acrylic acid

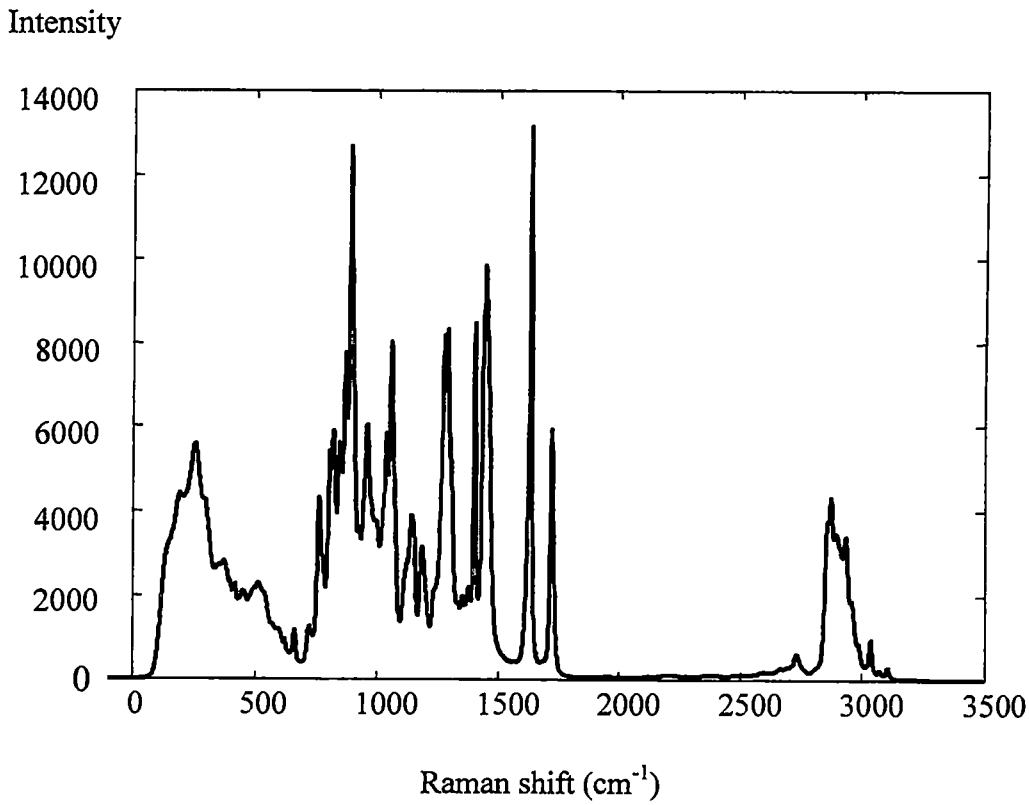


Figure 6.15: Raman spectrum of neat 2-ethylhexyl acrylate (2-EHA) collected with filter based immersion probe

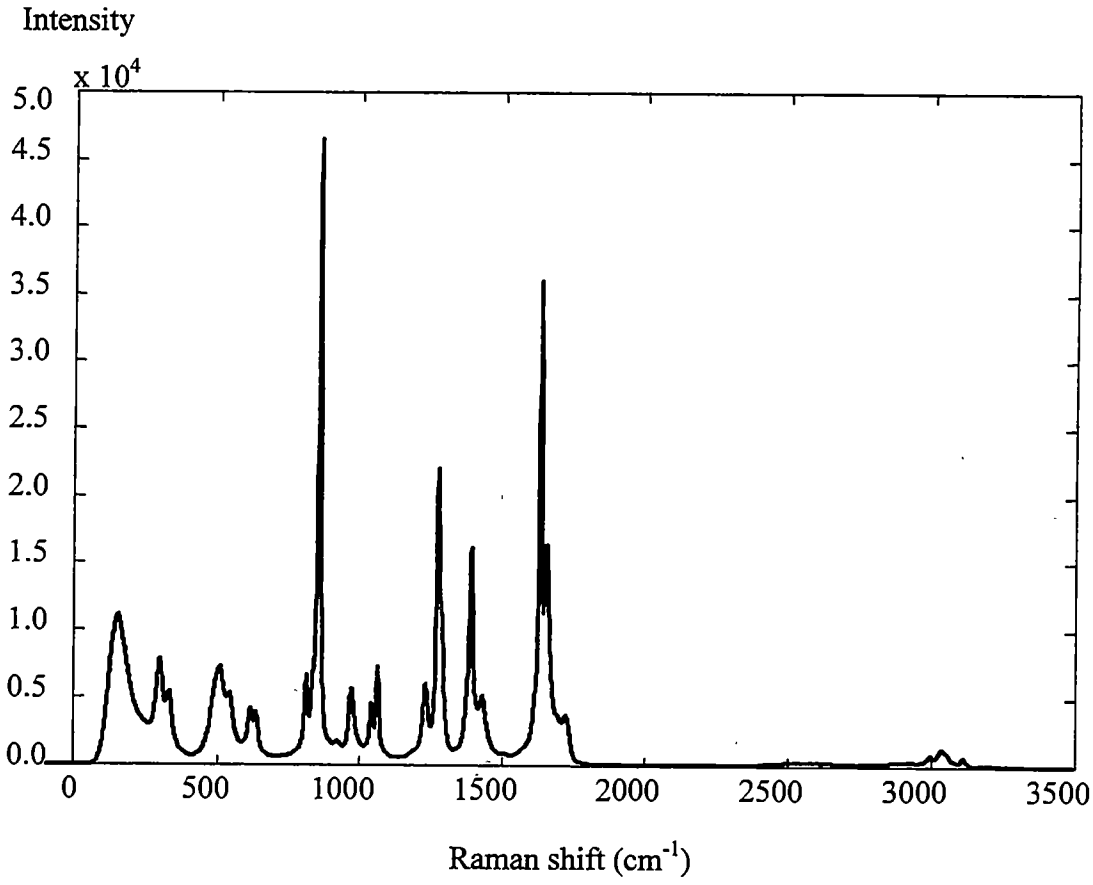


Figure 6.16: Raman spectrum of neat acrylic acid (AA) collected with filter based immersion probe

Table 6.3: Reaction recipe for emulsion polymerization of 2-EHA and AA

Ingredient	**Parts by weight**	**Weight**
2-Ethylhexyl acrylate	90	68.85 gm
Acrylic acid	10	7.65 gm
n-dodecyl mercaptan	0.2	0.15 gm
Water	900	688.50 gm
Emulsifier	0.3	0.255 gm
Potassium persulfate	0.3	0.23 gm
Total	~1000	766.15 gm

with 2% hydroquinone solution in water and stored in ice. Combination of the inhibitor and cold storage completely inhibited the reaction. These samples were analyzed for the conversion based on total monomer content using gravimetric technique. The conversion based on both the monomers taken together was calculated using equations 6.2 and 6.3. Figure 6.17 shows the real time spectra obtained during the progress of the reaction. The Raman peak at 1640 cm^{-1} is due to the >C=C< present in the monomer. It is important to note that this peak appears due to the total monomer content in the reaction mixture. Thus, this peak has contribution from residual >C=C< in 2-EHA and AA at any time during the reaction. As the reaction proceeds, the monomers polymerize. Thus, the Raman peak due to the monomer decreases in intensity with time. For the monitoring of emulsions using Raman spectroscopy, an internal standard method was chosen. The Raman peak due to C=O was chosen as the internal standard.

Results and discussion:

The spectra were arranged into a matrix and the wavenumber range of 1600 to 1700 cm^{-1} due to C=C was analyzed to correlate with the amount of residual monomer in the reaction mixture. The data was baseline corrected and the intensity of the peak maximum at 1632 cm^{-1} is plotted against time in figure 6.18. PCA was performed for this wavenumber region. Table 6.4 gives the variance explained by each of the PC. The first PC accounts for 98.82% of the data variance. The second PC accounts for

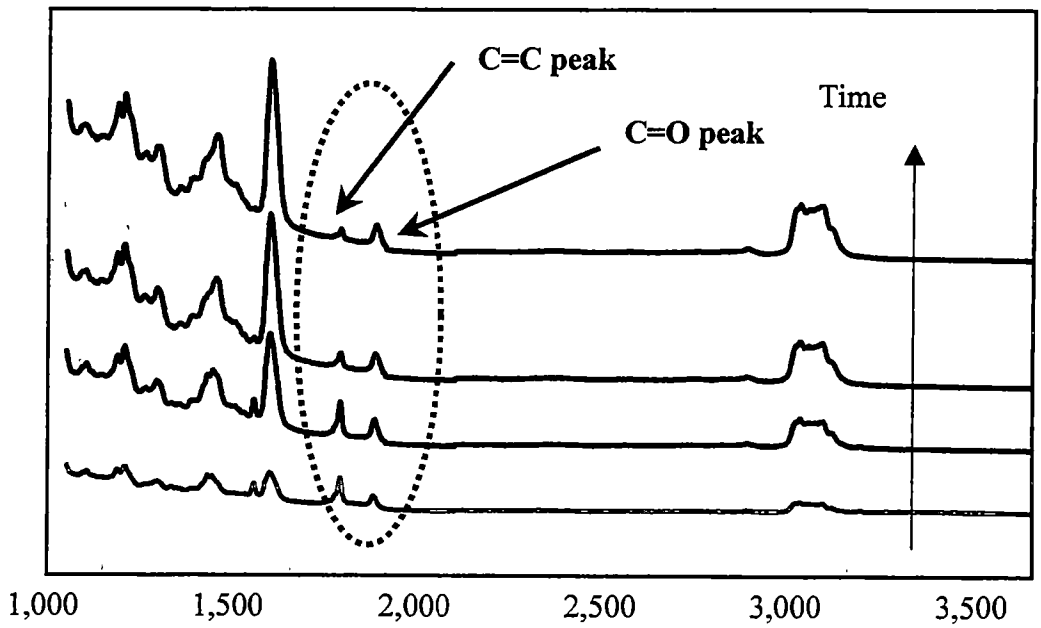


Figure 6.17: Real time Raman spectra depicting progress of emulsion polymerization of 2-EHA (90%) with AA (10%) at 60 ^{0}C, 200 rpm.

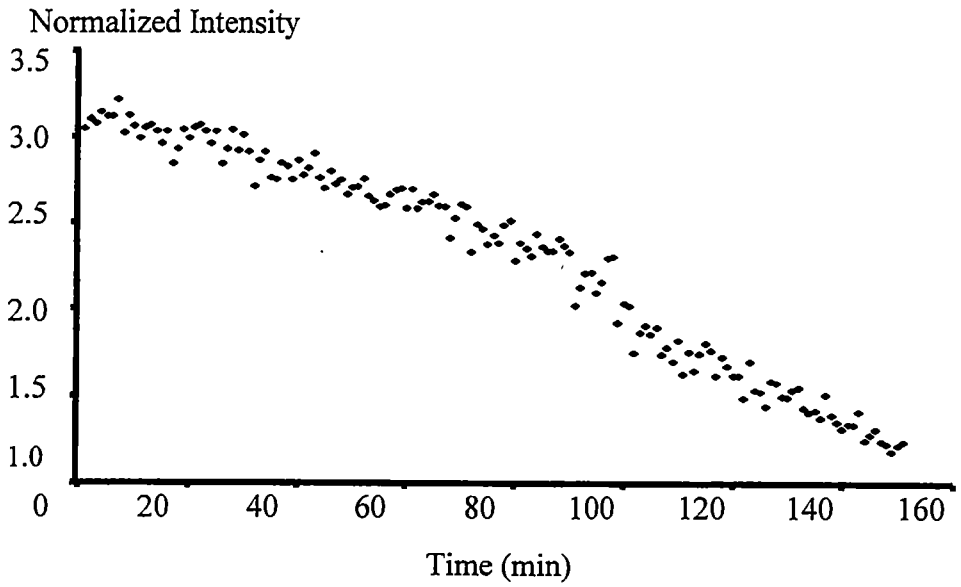


Figure 6.18: Normalized intensity ($I_{(C=C)}/I_{(C=O)}$) against time (min)

Table 6.4: Percent variance explained by principal components

Principal Component	Cumulative % variance explained
1	98.82
2	99.42

0.80% data variance. This clearly indicates that the first PC adequately explains the information contained in the data set.

In order to build a PLS model the baseline corrected spectral region in 1600 to 1750 cm^{-1} Raman shift was used. These peaks were individually baseline corrected. The peak due to C=C was normalized using the maximum intensity of the peak at 1730 cm^{-1} due to C=O. From the resultant matrix, the spectra corresponding to the time when the samples were withdrawn were separated. This matrix was used as the **X** data matrix to build a predictive PLS model. The data was mean centered. Mean centering involved subtracting the mean of each of the columns in the **X** and **Y** matrices from the data points (69). For building the calibration model, leave-a-sample (LAS) cross validation technique was used. Details of such analyses were described in chapter 4 on regression techniques. The optimal number of principal components was decided by evaluating the standard error of calibration chart as shown in figure 6.19. The SEC with two factors was found to be 9.31. Thus, two principal components were used for building the PLS model. Figure 6.20 shows the comparison of predictions and measured values for samples in the calibration set, with a calibration model based on two factors. This plot shows that the sample prediction for total conversion value agrees well with the actual conversion calculated using the gravimetric analysis. A qualitative interpretation is obtained from analysis of the first and second loading vectors. In figure 6.21, the first loading vector is plotted against the Raman shift. The first loading mimics the profile of the normalized Raman spectrum. The information

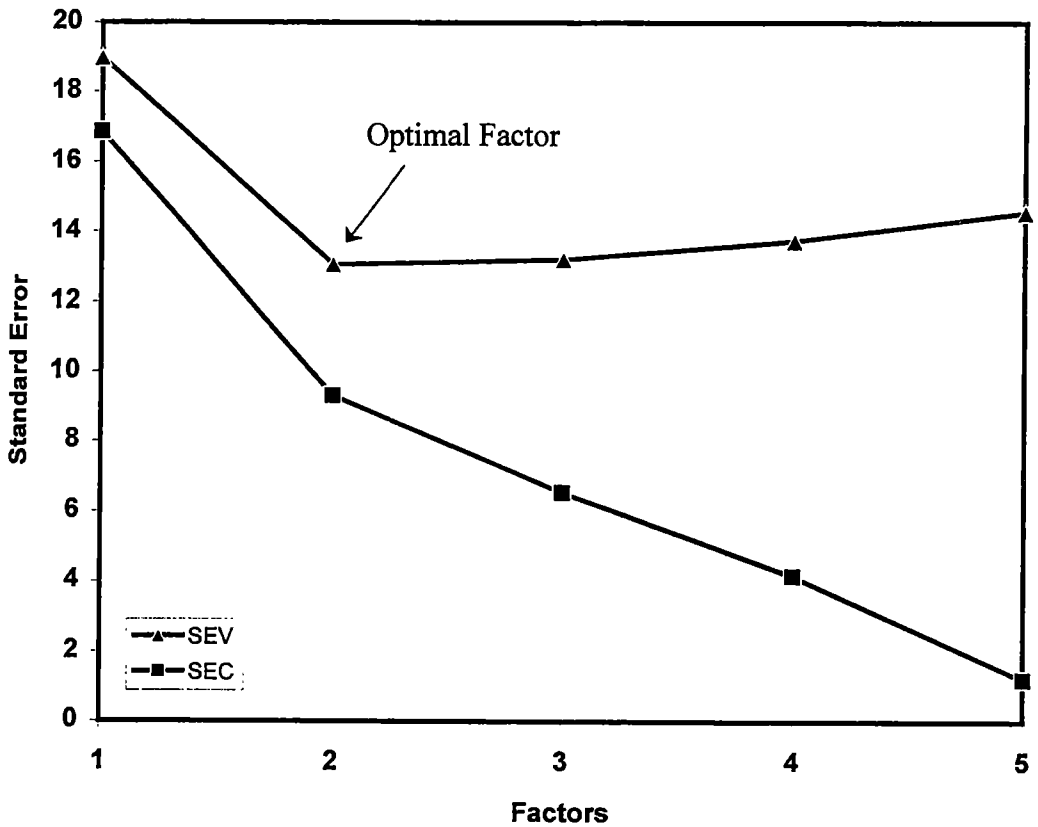


Figure 6.19: Standard error of calibration (SEC) and cross validation (SEV)

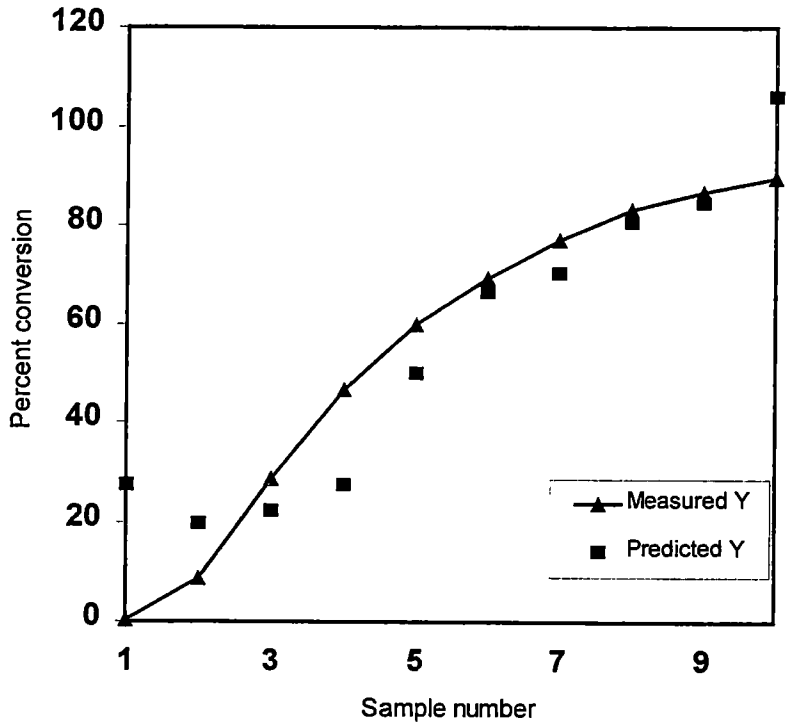


Figure 6.20: Comparison of the measured and predicted conversion in calibration set, using two factor based model.

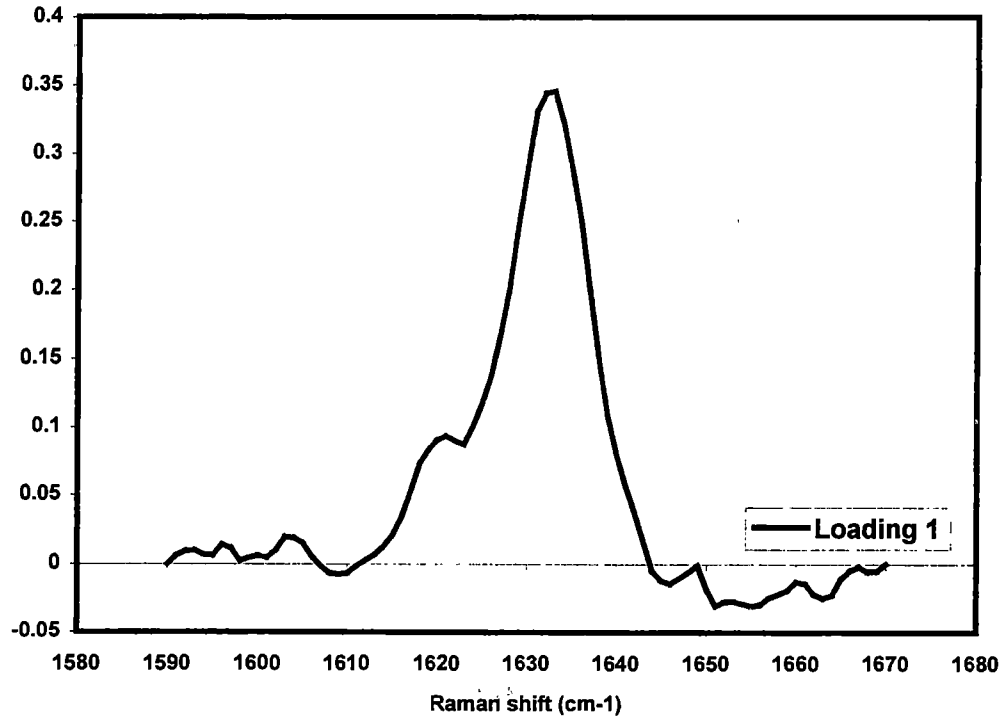


Figure 6.21: Plot of the loading vector for the first principal component with Raman shift.

about the monomer content is the dominant feature in the Raman spectrum in this region. Therefore, it is expected that the first PC contains information about the monomer content. Thus, the first loading vector explains the strong contribution of monomer content variation. This model was used for predicting the conversion for all time values during the reaction using the real time Raman spectra.

An external prediction set was formed using the spectra that were collected during the emulsion polymerization reaction. The spectra that were not included in the calibration set were only used in the prediction set. The spectra were subjected to mathematical processing similar to that of the calibration set. The calibration model developed was used for prediction of conversion with time. The results of prediction are plotted in figure 6.22. The standard error of validation (SEV) was 13.06 %.

Observations and Conclusions:

In all the spectra collected in real time using immersion type Raman probe, the laser Rayleigh line at 0 cm^{-1} was seen. This is caused by inadequacy of the filters in the probe to cut off the laser line. Therefore, some of the laser light appears in the spectrum. However, as the reaction progresses, the scattering of the incident laser light increases. Therefore, the intensity of the laser line at 0 cm^{-1} increases tremendously with consecutive spectra and finally the detector saturation was observed. This can be seen from the spectra in figure 6.23. During the mathematical processing and subsequent treatment of the data, the initial part of the Raman spectra was cut off. This

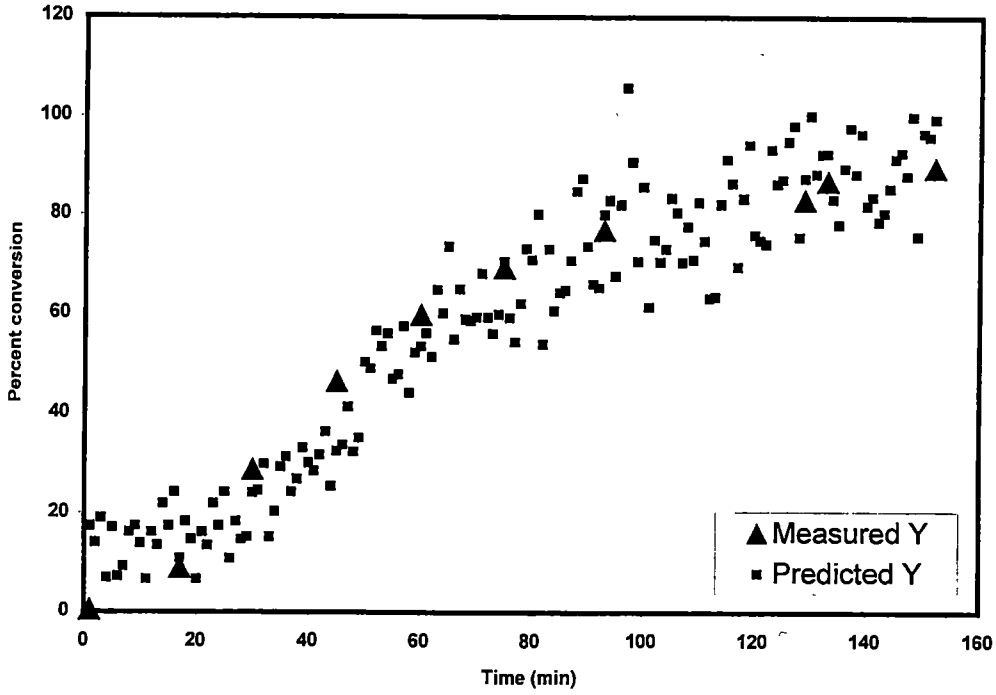


Figure 6.22: PLS prediction results for real time Raman spectra recorded during emulsion copolymerization of 2-EHA with AA

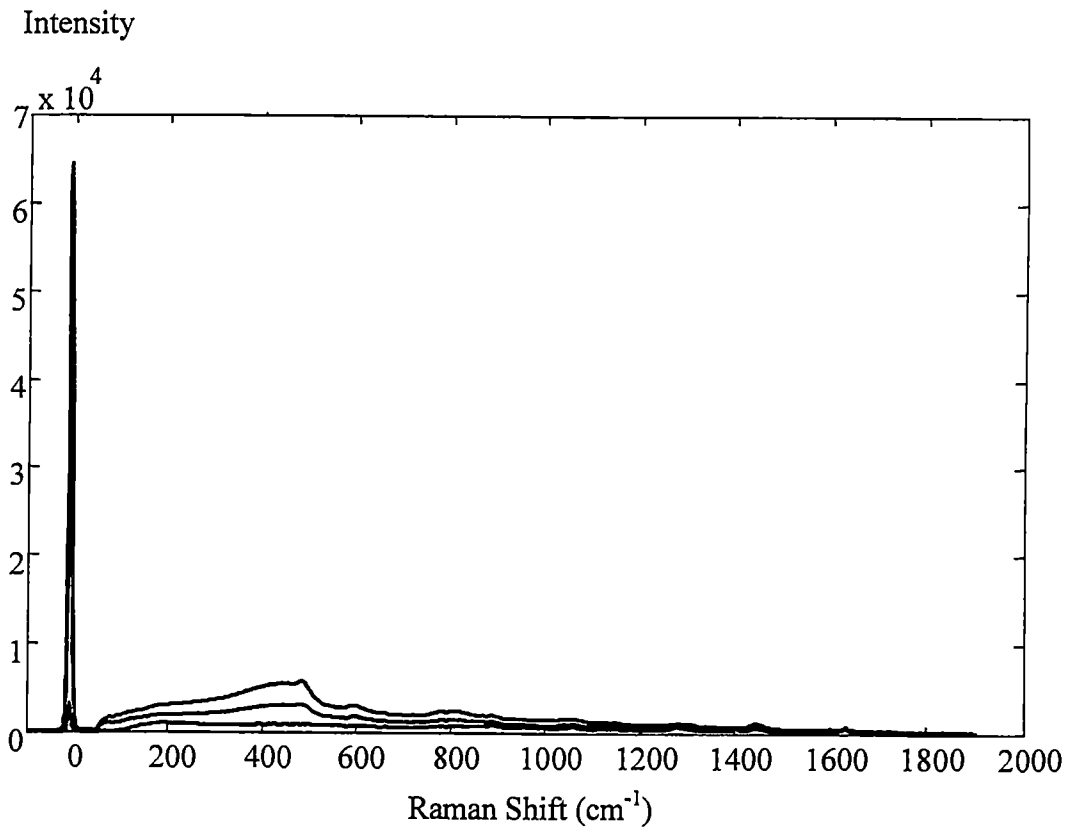


Figure 6.23: Increase in the intensity of the laser line with time during emulsion copolymerization of 2-EHA and AA

method of data treatment and analysis does not affect the calibration or prediction of the residual monomer conversion. However, the observation of the laser line is a visual disadvantage for monitoring of the reaction.

The above study has demonstrated that the application of in-line fiber optic Raman spectroscopy can be extended to monitoring emulsion polymerization reactions in terms of the total residual monomer content. The standard error of or validation prediction is dependent upon the ability of the Raman probe to "see" the monomer. This is dependent upon the opacity of the reaction contents. It was observed that the reaction mixture was transparent in appearance at the beginning of the reaction. As the polymerization proceeds, the opacity of the mixture increases. Thus, light scattering takes place, which affects the amount of Raman signal generated and collected. The polymer formed in this reaction, copolymer of 2-EHA with AA, has very low T_g. Hence, it has a tendency to stick to the Raman immersion probe if the emulsion becomes unstable. Polymer coagulum globules are observed in the reactor and on the probe tip. This influenced the prediction values for real time emulsion copolymerization monitoring of 2-EHA and AA. Hence, later experiments were carried out at higher emulsifier content to increase the stabilization of the polymer.

6.4.2 Prediction of monomer conversion from calibration reaction run

The ultimate use of Raman spectroscopy as an in-line reaction monitoring tool is based on its utility to monitor emulsion polymerization reactions of unknown

chemical composition. For application of in-line Raman spectroscopy at the production facility, a calibration model is needed. This calibration model could be utilized to predict the conversion profile of an emulsion reaction carried out under similar set of conditions. Use of Raman spectroscopy for such applications is demonstrated in this section.

Emulsion copolymerization reactions were carried out with recipe as given in table 6.3. The emulsifier concentration was increased threefold in order to make the emulsion stable thus reducing the risk of emulsion sticking to the immersion probe. The experimental procedure was followed as described in section 6.4.1. The samples were withdrawn from the reaction mixture and analyzed separately using gravimetric analysis. Figure 6.24 shows the conversion of the monomers as calculated by gravimetric analysis plotted with reaction time. The real time Raman spectra were collected using a filter based immersion probe.

Results and Discussion:

Raman spectra were arranged into a matrix and the peak in the region 1600 and 1680 cm^{-1} due to C=C were selected and baseline corrected. The peak intensity of all the baseline corrected spectra was normalized with respect to the intensity of peak in this region from first spectrum at t=0. Thus, the spectra are indicative of the conversion of the monomers at any time. The conversion was calculated according to the formula in equation 6.4. The intensity of the first spectrum corresponds to the

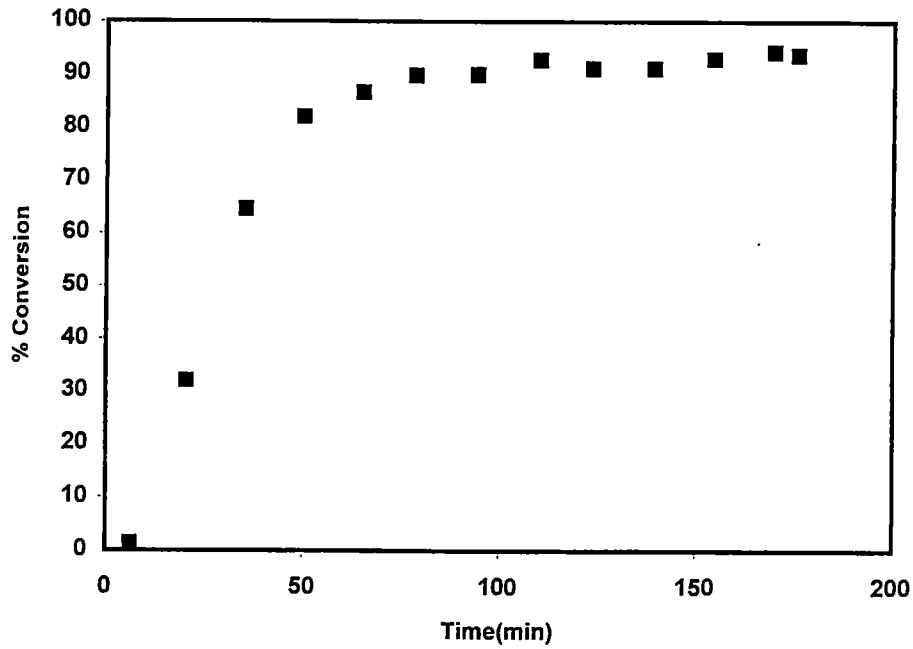


Figure 6.24: Conversion based on 2-EHA and AA residual monomer content by gravimetric analysis, plotted against reaction time

beginning of the reaction at t=0. Based on I_0, the conversion is calculated using the intensity variation in C=C peak with time.

$$\text{Conversion } \mathbf{X} (\%) = \frac{I_0 - I_t}{I_0} \times 100 \qquad \ldots(6.4)$$

where, I_0 = Intensity of the peak at 1640 cm^{-1} in the first spectrum at t=0 (baseline corrected)

I_t = Intensity of the peak at time t in the real time spectra during the reaction progress (baseline corrected)

A least square univariate fit was developed and model was used to predict the conversion for another reaction carried out under similar reaction conditions. Figure 6.25 shows the results of this analysis. The monomer content calculated using gravimetric analysis is plotted against the conversion value obtained from formula in equation 6.4. The correlation coefficient for the model was 99.5%; thus indicating a good degree of correlation between the normalized spectral intensity and the conversion of the monomers based on gravimetric analysis. The least squares univariate model proposed a linear fit between the normalized spectral intensity with the conversion obtained from gravimetric analysis.

$$y = 0.9793\,x + 4.9576 \qquad \ldots(6.5)$$

where, y = conversion obtained from normalized C=C, using equation 6.5,

x = Monomer conversion at any time during the reaction using gravimetric analysis.

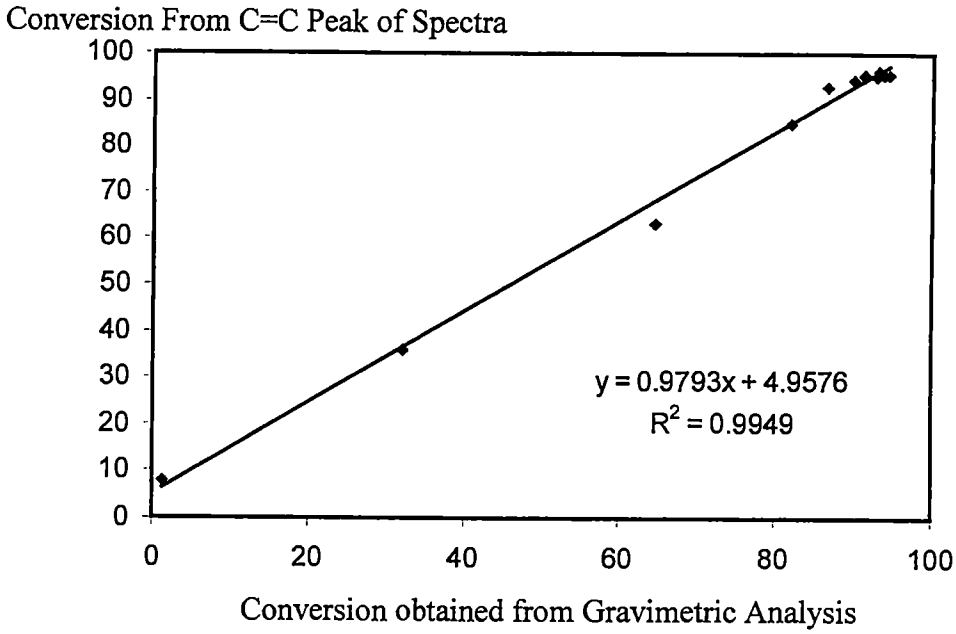


Figure 6.25: Univariate least squares fit for prediction residual monomer content based on intensity changes

This univariate model was used to predict the monomer conversion with time for another reaction carried out under similar reaction conditions. This is an important utilization of Raman spectroscopic tool for process monitoring, as it would be able to detect whether the reaction being monitored follows the projected path. Thus, it would be possible to determine the conversion of monomers at various time points during the reaction; it would also be of importance in end point determination of a batch reaction. In industry, judging the end point of a batch reaction is a tricky process, since the process might not be equipped with on-line real time monitoring instrumentation. Thus, in order to get the residual monomer content below the specifications, the reaction batch time is increased. Such a monitoring tool would also be of use in determination of faulty batches.

Another reaction carried out under similar experimental conditions was used to test the validity of this univariate model. For this reaction, samples were withdrawn during the progress of the reaction and analyzed for the monomer conversion. The real time Raman spectra were also recorded. In order to apply the univariate model to this data, the spectra in the 1600 to 1680 cm^{-1} region were considered and the C=C peak intensity was normalized using the intensity of the first spectrum at t=0 as the beginning of the reaction. The univariate model in equation 6.4 was applied to the spectral data to predict the monomer conversion with time. The resulting prediction of the monomer conversion is plotted in figure 6.26. It shows the predicted conversion during the progress of the reaction plotted with the actual gravimetric conversion

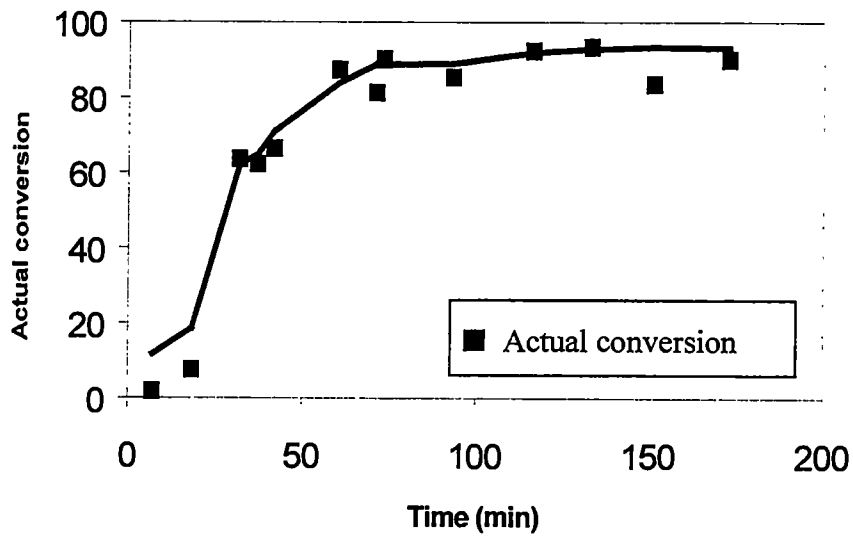


Figure 6.26: Comparison of the measured and predicted monomer conversion with time during emulsion copolymerization of 2-EHA with AA

obtained from the samples that were collected and analyzed. Figure 6.27 shows the comparison and goodness of prediction for the predicted and actual measured value of the conversion. The univariate model error of prediction was 3.49 % based on total monomer content. It can be seen from these figures that the univariate analysis simplifies the mathematical treatment of the data as compared to the multivariate analysis, as in section 6.4.1.

6.4.3 Monitoring difference in rates for 2-EHA/AA emulsion copolymerization reactions at different starting monomer ratios

In this section, emulsion polymerization reactions were carried out at varying starting monomer ratios. In-line Raman spectroscopy was applied as the monitoring tool for observing the rates of reactions. A copolymerization model has been proposed for 2-EHA and AA. According to this model (70) the monomer polymerization occurs in the droplets. This model was developed for the emulsion polymerization reaction carried out at surfactant concentration below the critical micellar concentration (CMC). As the starting monomer ratio is changed, the final properties of the resulting random copolymer change with respect to its tacky nature and its use as pressure sensitive adhesives. Poly(2-EHA) gives a soft tacky film that adheres to almost any surface. The addition of high T_g AA changes the tack of the resulting film even at small concentrations of the functional monomer AA. The T_g of the resulting copolymer can be calculated using equation (6.6):

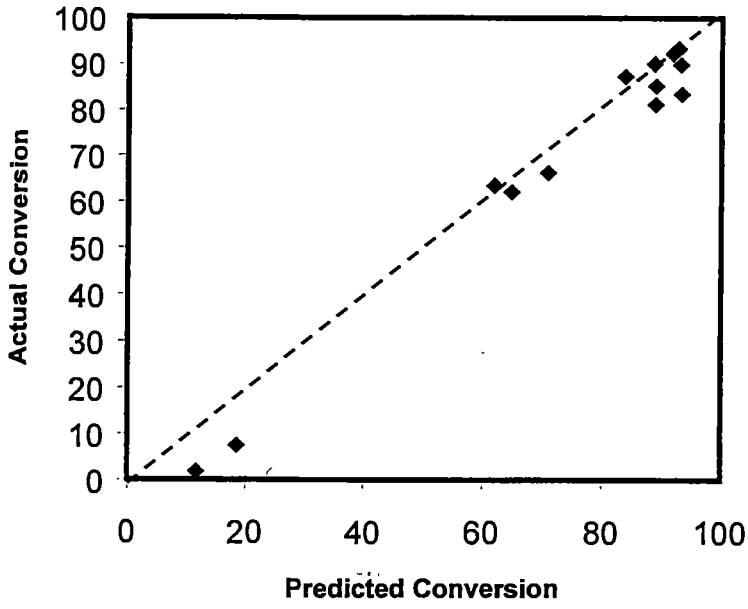


Figure 6.27: Comparison of the measured and predicted monomer conversion during emulsion copolymerization of 2-EHA with AA

$$T_g = \frac{\left[M_a(\alpha_a / W_a) T_{g,a} + M_b(\alpha_b / W_b) T_{g,b} \right]}{\left[M_a(\alpha_a / W_a) + M_b(\alpha_b / W_b) \right]} \quad \ldots(6.6)$$

where, W = Molecular weight of the monomer,

M = Weight fraction of the monomer,

α = Number of flexible bonds contributed to the polymer chain by the monomer, (α=2 for vinyl polymerizations)

a and b = comonomers participating in the reaction.

Data shown in Table 6.5 shows the relative speed of polymerization based on the k_p / k_t value for each monomer. It can be noted that compared to the EHA, the carboxylic monomers are slower as given by the k_p / k_t values. Thus, 2-EHA reacts faster as compared to AA. Table 6.5 also lists the partition of AA between the organic and aqueous phases for emulsion prepared with 10% by weight of organic phase. It indicates that majority is in aqueous phase. Moreover, the true concentration of acid in the monomer droplets is quite low and considerably less than the recipe ratio. Table 6.5 also gives the copolymerization reactivity ratio of the base monomer and the carboxyl monomer as calculated by *Q and e* scheme (14). The reactivity ratios indicate the relative tendency of a monomer to homopolymerize against its tendency to copolymerize. Thus, AA has slightly higher tendency to homopolymerize. However, due to the low solubility of 2-EHA in water, bulk of the 2-EHA is present in the form

Table 6.5: Physical properties of 2-EHA and AA

1. k_p/k_t values of monomers

Monomer	k_p/k_t **x** 10^6
2-EHA	917 (60 ^{0}C)
AA	250 (23 ^{0}C)

[Source: Polymer Handbook, J. Brandrup, E. H. Immergut, J. Wiley and Sons Inc. NewYork, 1989]

2. Partition of AA at 10% oil phase

(95 EHA/5 AA)	**AA**
Organic	4.5 %
Aqueous	95.5 %
(80 EHA/20 AA)	
Organic	8.0 %
Aqueous	92 %

3. Relative rates of copolymerization (Q and e calculations)

M1/M2	***r1***	***r2***
EHA/AA	0.93	1.08

[Source: Loncar, F. Ph.D. Dissertation, Lehigh University, 1985]

of monomer droplets and most of the AA is present in the aqueous phase owing to its higher solubility in the aqueous phase.

Considering these facts, emulsion polymerization reactions were carried out on the 2-EHA/AA system at different initial monomer ratios. The reactions used the recipe as in table 6.6. The monomer ratios as shown in table 6.7 were used for carrying out the reactions. During all the reactions, samples were withdrawn and analyzed for residual monomer content. From the data presented in detail in sections 6.4.1 and 6.4.2 it was observed that there is a small difference in the rates of reactions with change in temperature. In this section, the application of Raman spectroscopy to monitor those small differences in rate will be explored. In-line monitoring of the emulsion copolymerization reactions was carried out using filter based immersion probe. The spectra were collected for 15 seconds and average of 2 spectra recorded. The mathematical treatment of the spectra is similar to that detailed in the section 6.4.2. The spectral region in the C=C peak area was selected and was normalized using the C=O peak intensity. This is an internal standardization method, and removes any bias that might be present within the data set. The C=C peak was also scaled such that all the normalized peaks spanned across the 0 to 100% conversion range. The normalized and scaled spectra are shown in figure 6.28.

Table 6.6: Reaction recipe for emulsion polymerization of 2-EHA and AA

Ingredient	**Parts by weight**	**Weight**
2-Ethylhexyl acrylate	90	68.85 gm
Acrylic acid	10	7.65 gm
n-dodecyl mercaptan	0.2	0.15 gm
Water	900	688.50 gm
Emulsifier	1.0	0.765 gm
Potassium persulfate	0.3	0.23 gm
Total	~1000	766.15 gm

Table 6.7: Ratios of initial monomer concentration

2-EHA	AA
95.0	5.0
92.5	7.5
90.0	10.0
87.5	12.5
85.0	15.0

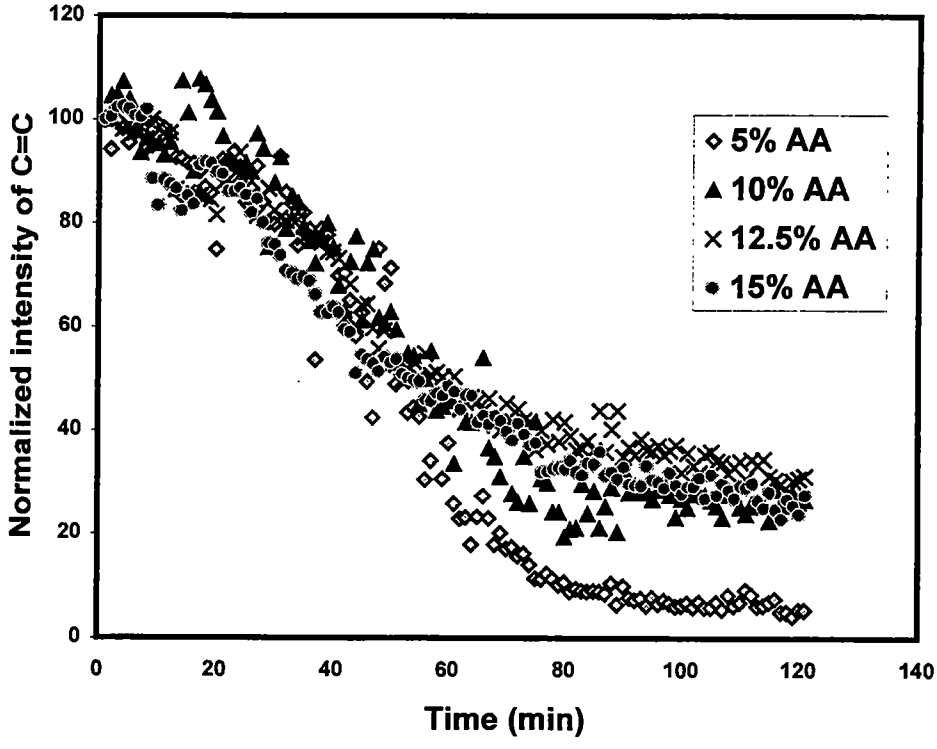


Figure 6.28: Monomer concentration profiles during the reactions with different concentrations of AA

Observations and Conclusions:

From the reaction profiles shown in figure 6.28, it can be seen that the reactions could be monitored for the whole duration of the reaction. The characteristics of the monomers 2-EHA and AA listed in Table 6.5 suggested that as the amount of AA in the reaction mixture increases, the propagation phase of the polymerization would proceed slower owing to the lower k_p/k_t value for AA. As the initiation for emulsion polymerization reactions begins in the aqueous phase, the initiation is faster as the concentration of AA increases. However, the rate of propagation is slower due to higher termination in case of AA. Therefore, the reaction attains the final conversion at a slower pace. Figure 6.29 shows the conversion vs. time results for the emulsion polymerization of 2-EHA and AA at 60 ^{0}C for varying monomer ratios. There is a very subtle change in the reaction rate with concentration of AA.

In figure 6.28, normalized C=C peak for reaction with 5% AA shows a span from 100% normalized intensity to about 5% of the initial value at the end of the reaction. However, the other reactions reach saturation at a higher value of normalized intensity. It is known that as the concentration of AA in the reaction mixture increases the tack of the resulting polymer increases. It was also experimentally found that the possibility of polymer globule sticking to the immersion Raman probe increased with increase in AA. Thus, towards the end of the polymerization period, the probe does not *see* the actual residual monomers in the emulsified reaction mixture. However, the

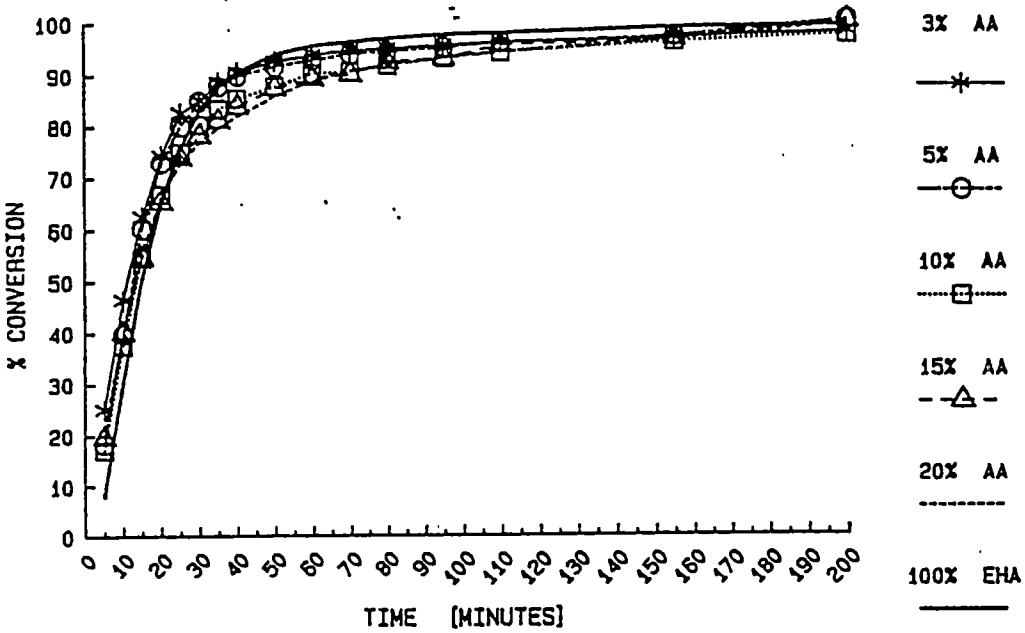


Figure 6.29: Monomer concentration profiles during the polymerization of 2-EHA reactions with different concentrations of AA (70)

probe *sees* some of the monomer trapped in the polymer globule that is attached to the tip of the Raman probe.

6.4.4 Individual comonomer monitoring for 2-EHA and AA polymerization reactions using in-line Raman spectroscopy

Knowledge of the individual concentration of the two comonomers at any time during the reaction is important so that the depletion of each monomer can be followed separately. This is important in determining the reaction profile of each of the monomers and thus gives an idea about the properties of the resultant polymer. In this section, the attempts to determine the individual comonomer concentration during the reaction run are explained in detail. There are two important aspects to consider: ability of Raman spectroscopy to monitor the monomers separately, and the development of a primary method for the individual analysis of the monomers. A primary method was developed for the determination of 2-EHA from the reaction samples using Gas Chromatography. Gravimetric analysis could not be used for this determination due to its inability in determining the concentration of each monomer in the reaction sample. Gravimetric analysis measures the weight lost upon heating. Thus, when samples are heated, and the weight lost is measured, it accounts for the water and monomers present in the sample. Therefore, gravimetric analysis only determines the total concentration of the residual monomers in the sample without differentiating between them. Hence, it could not be used for this analysis where individual determination is the objective.

6.4.4.1 Differentiation of 2-EHA and AA from Raman spectra of neat samples and emulsions

The aim of these experiments is to determine if Raman spectroscopy can be used to determine the individual monomer concentration in known 2-Ethylhexyl acrylate (2-EHA)/ Acrylic acid (AA) neat mixtures. Five mixtures with known concentrations of 2-EHA and AA, as in table 6.8, were prepared.

Raman spectra were recorded using Kaiser Optical Systems HoloProbe Raman spectrometer using 785 nm laser. Spectra were collected for 15 seconds with 2 accumulations. The spectra are as shown in figure 6.30 and figure 6.31 shows the 1600-1750 Raman shift (cm^{-1}) region. The peaks at 1640 cm^{-1} and 1730 cm^{-1} are due to C=C, and C=O present in the monomers respectively. In figure 6.31 it can be seen that there is a small shoulder on the right side of C=C peak at about 1660 cm^{-1} and it increases as the amount of AA in the mixture increases.

The spectra obtained during in-line reaction monitoring are shown in figure 6.32. These spectra were recorded from the beginning of the reaction until the end of the batch time. There is a significant decrease in the overall spectral intensity as compared to the spectra in figure 6.30. This is due to the fact that in the reaction mixture, the monomers amount only to about 10% by weight of the total amount. Hence, the Raman peak due to the monomer is lower in intensity as compared to that in the spectra of neat samples. In figure 6.33, the peak at 1640 cm^{-1} appears as a single

Table 6.8: Compositions of neat mixtures of 2-EHA and AA

Sample Number	2-EHA (wt %)	AA (wt %)
1	0	100
2	25	75
3	50	50
4	75	25
5	100	0

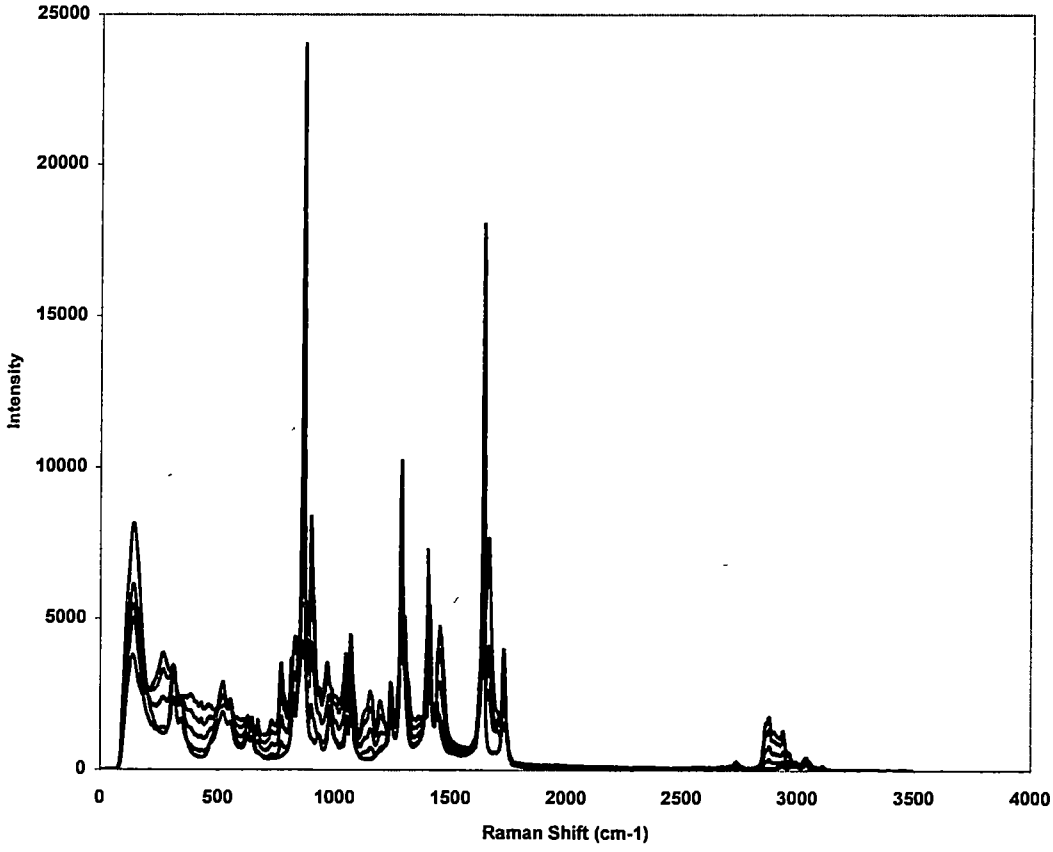


Figure 6.30: Raman spectra of neat mixtures of 2-EHA and AA in a set of five samples of varying AA content.

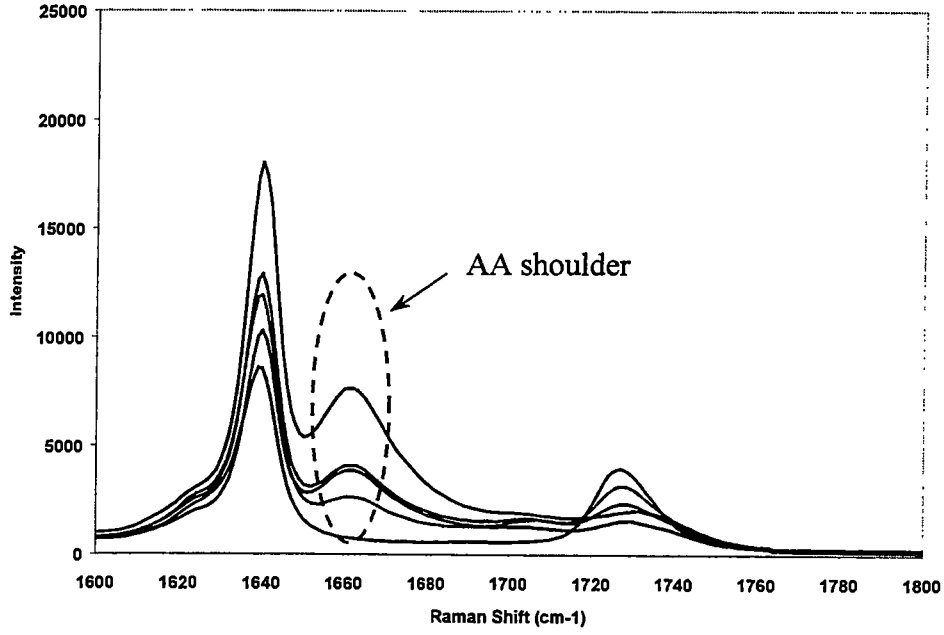


Figure 6.31: Raman spectra of neat 2-EHA/AA mixtures in 1600 to 1800 Raman shift region (C=C and C=O region)

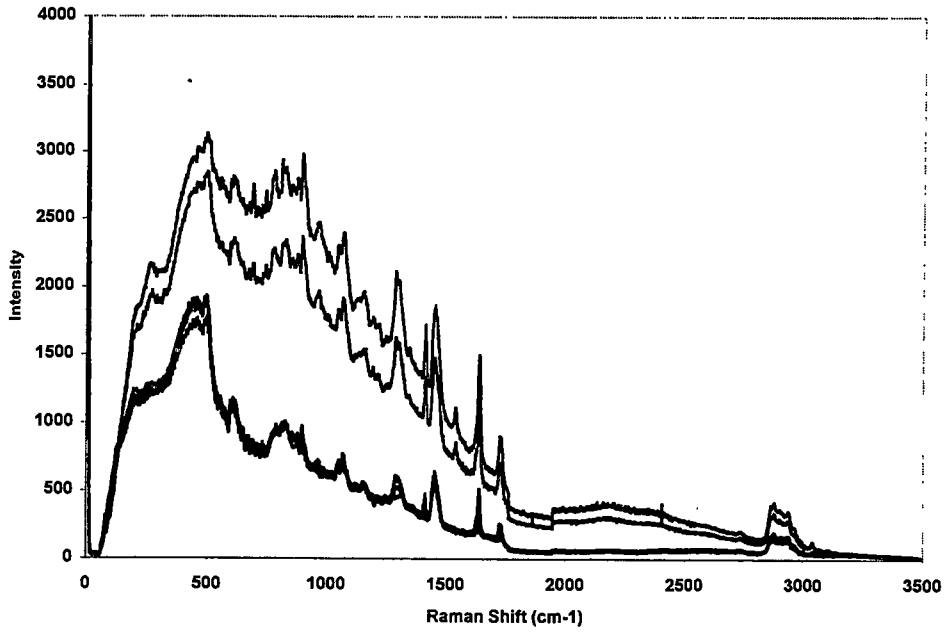


Figure 6.32: In-Line Raman spectra obtained during emulsion polymerization of 2-EHA/AA

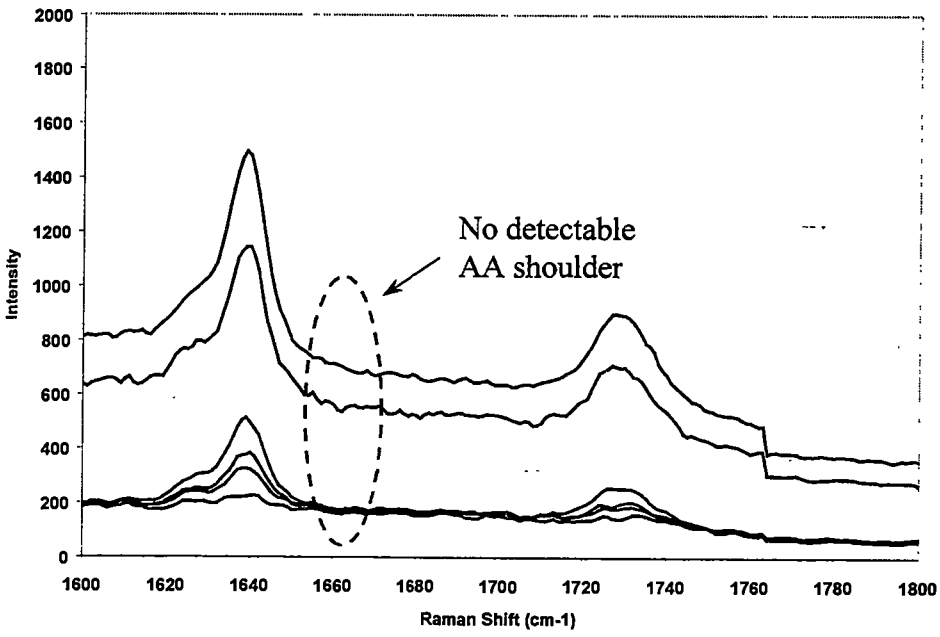


Figure 6.33: In-line Raman spectra during emulsion polymerization in the C=C and C=O region

peak without any shoulder. It gives an idea about the total absolute amount of (C=C) moieties present in the reaction mixture. Hence, this peak can be used to give an idea of the total residual monomer content in the reaction mixture at any given time. The shoulder seen in the spectra of neat mixtures is not seen here. This could be due to the fact that the shoulder at 1660 cm^{-1} is buried in the higher noise level in the spectrum.

Results and Discussion:

In order to determine whether the spectra convey information about both the comonomers, the spectra were analyzed using pattern recognition techniques as described in detail in chapter 4. The spectra were subjected to principal component analysis (PCA) in the region of 1600 to 1750 cm^{-1}. Table 6.9(A) lists the variance explained by each of the principal components for neat samples and table 6.9(B) lists that from the PCA of emulsion spectra. For the spectra of pure mixture samples, the resulting loadings as shown in figure 6.34 were obtained. It can be observed from table 6.9(A) that the second PC explains about 5% of the data variance. Therefore, it can be said that the second PC accounts for the information about amount of AA in the neat samples. Figure 6.35 shows the loadings for the PCA carried out on spectra from in-line monitoring of emulsions. From table 6.9(B) and figure 6.35, it is observed that about 99% of the information in the data is explained by the first PC. Hence, distinction between the 2-EHA and AA is not seen in the in-line Raman spectra of the reaction mixture. From figure 6.35 it can be clearly seen that PC1 has shape similar to the spectra and PC2 can be attributed to noise in the region of interest in the spectra.

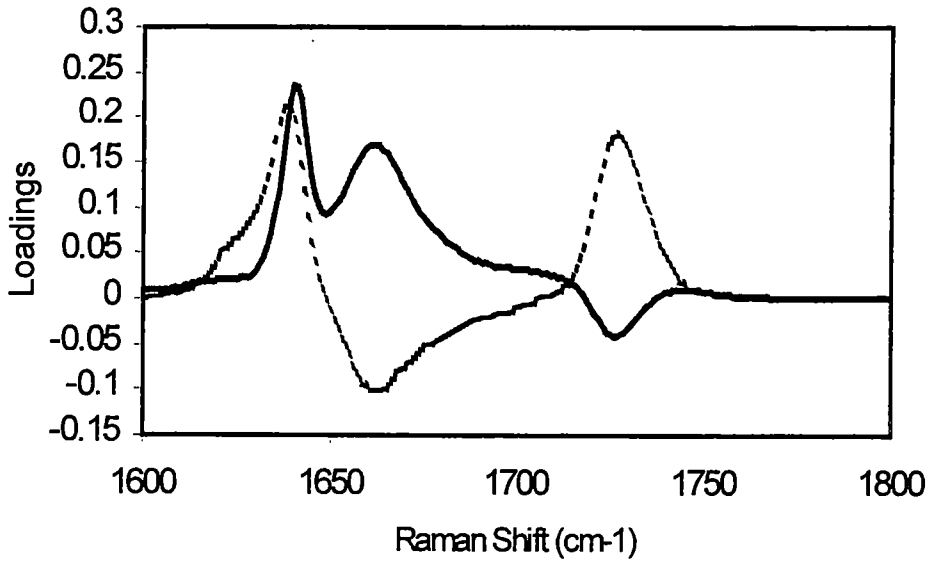


Figure 6.34: First and second loadings obtained from PCA performed on Raman spectra of neat 2-EHA and AA samples.

Table 6.9: Variance explained by each principal component for PCA performed on the spectra obtained from neat samples and emulsion

A) Neat 2-EHA and AA samples:

PC	Variance %	Cumulative %
1	93.70	93.70
2	5.59	99.29
3	0.70	99.99

B) Emulsion polymerization:

PC	Variance %	Cumulative %
1	99.03	99.03
2	0.76	99.79
3	0.13	99.92

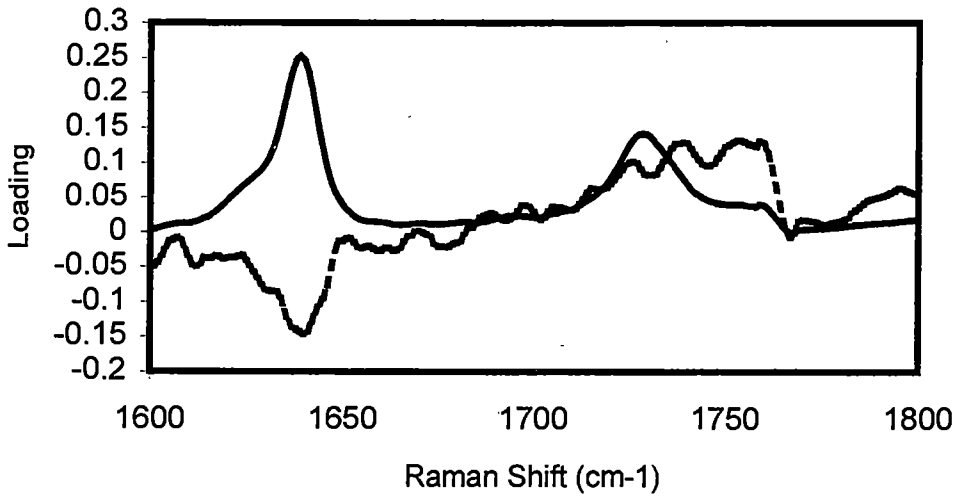


Figure 6.35: First and second loadings obtained from PCA performed on in-line Raman spectra of emulsions

CHAPTER 7
IN-LINE MONITORING OF POLYMER PROCESSING OPERATIONS USING RAMAN SPECTROSCOPY

7.1 Introduction

Polymer processing operations form a major class of operations in the polymer industry. These operations include extrusion, molding processes of polymer to produce useful articles. Monitoring the polymer processing operations is of importance as it directly results in reduced waste during production thus increasing profitability of the manufacturing process. In-line monitoring of polymer processing operations has been demonstrated previously using spectroscopic techniques such as near infrared (NIR) spectroscopy and UV-Visible spectroscopy (28,37,71-73). In this research, the applicability of in-line monitoring to extrusion processes using Raman spectroscopy will be demonstrated. The polymer systems studied include ethylene vinyl acetate (EVA), polypropylene (PP) and polyethylene. EVA samples with varying VA content and melt indices were studied. For the polypropylene samples, the information obtained from Raman spectra was correlated to the complex viscosity of the samples. In the PE sample set, varying octene content in the samples was investigated using polarized Raman spectroscopy.

7.1 Experimental set up

A single screw extruder (C. W. Brabender) was used to obtain molten polymer from particulate polymer pellets. The feed hopper was continuously purged with nitrogen gas in order to minimize any possible moisture absorption from the surroundings. The molten polymer was pumped using a gear pump at uniform mass flow rate of about 0.5 Kg/hr to a flow cell at a temperature of about 200 ^{0}C. Figure 7.1 shows schematic of the extrusion process. A schematic of the cell is shown in figure 7.2 (74). The flow cell provides a flow channel of rectangular cross section that is 20 mm wide and 9.5 mm high. The extruder die head has a circular opening of 3/8" diameter. A transition piece is present between the die head and the flow cell. This transition piece ensures that the complete area is free from any "dead-flow" polymer zones, where the polymer might accumulate and degrade. In-line monitoring is carried out using single sided scattering type Raman probe. The probe is fit into housing whose internal dimensions match that of the standard industry pressure transducer dimensions. Ring shaped spacers are mounted on the neck of the housing such that the pathlength could be varied. The thickest spacer makes the housing flush with the walls of the flow channel and by reducing the thickness of the spacer, the pathlength can be varied between 1 to 9.5 mm. A pressure restrictor attached to the flow cell can be used to vary the pressure of the flowing polymer. This valve also prevents molten polymers of low viscosity from draining. Thus, it also ensures that the optical measurement volume is not empty.

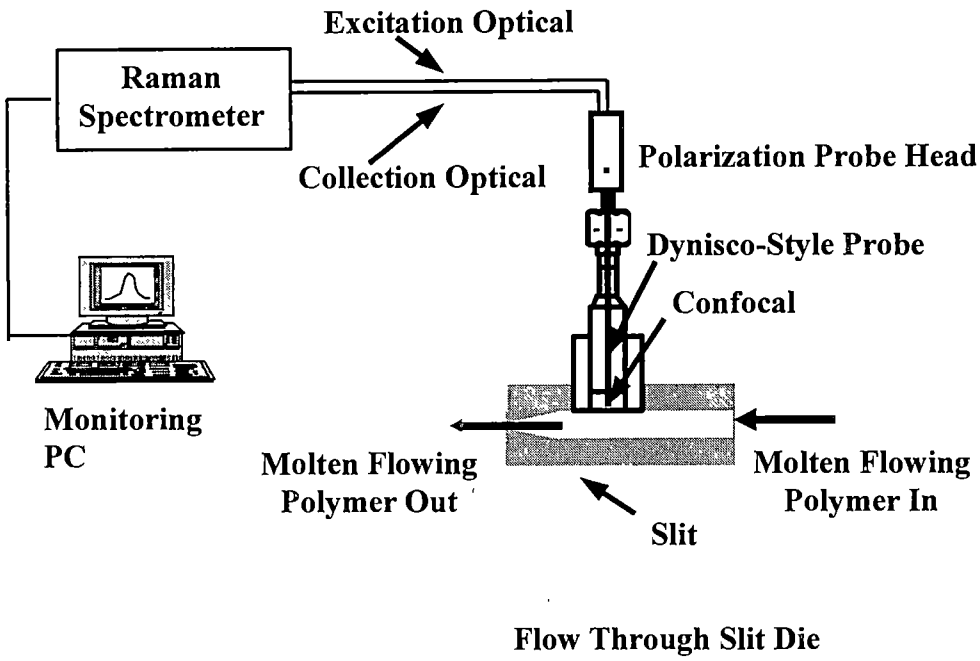


Figure 7.1: Schematic of extruder and in-line monitoring using Raman spectroscopy

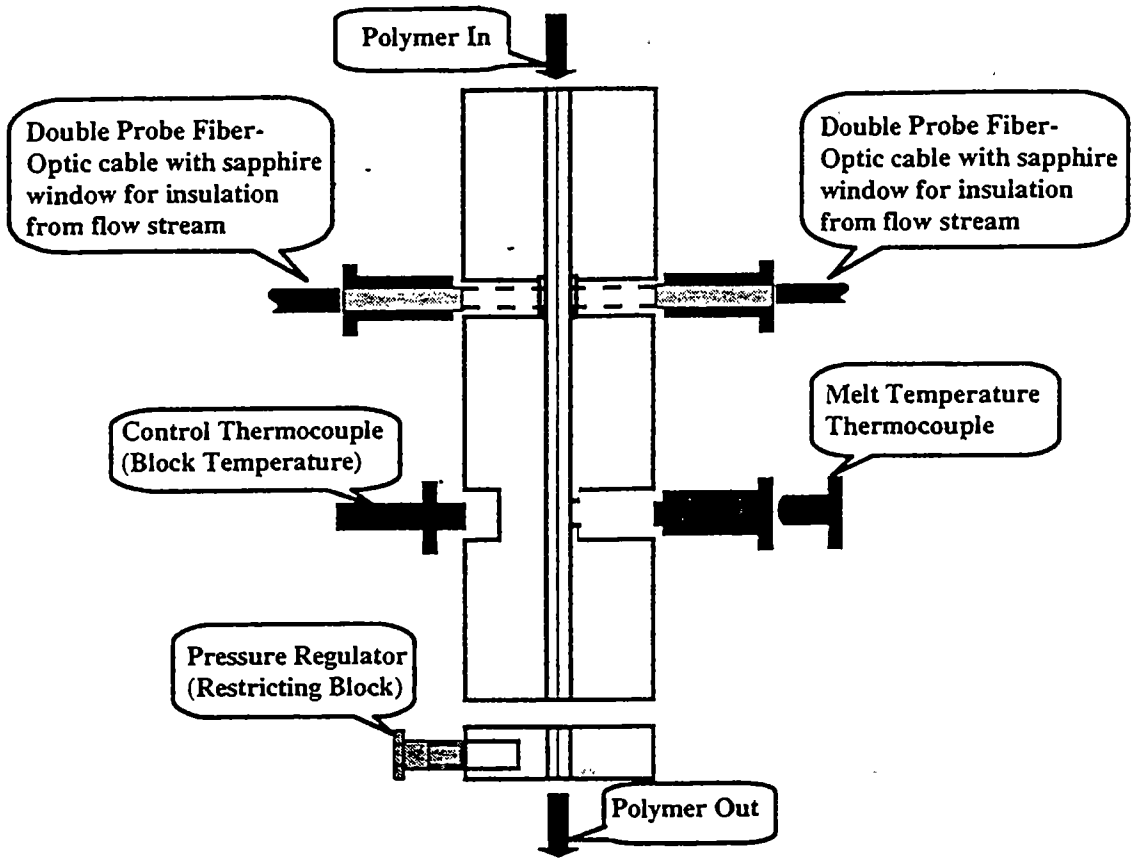


Figure 7.2: Schematic of the extruder flow cell

7.2 In-line monitoring of ethylene vinyl acetate (EVA) copolymers

Poly(ethylene vinyl acetate) copolymers are obtained by copolymerization of ethylene and vinyl acetate under high pressure. The incorporation of vinyl acetate (VA) reduces the crystallinity thus improving the flexibility, clarity, and impact strength of the polymer. These resins are widely used as adhesives, films and also for injection molding, blow molding, and many extrusion processes. Their applications include use as hot melt adhesives, coatings and textile products (75). The VA monomer is usually randomly distributed in the polymer chain and brings polarity to the chain. As polarity increases, there is a shift in the chemical resistance of the material. The structure of EVA polymer is shown in figure 7.3. Different EVA grades can also be distinguished based on their molecular weight. As the molecular weight increases, the melt viscosity also increases. Melt Index (MI) is an industrial parameter that is used to characterize the melt viscosity of the polymer.

In-line real time monitoring of processes is important for its numerous advantages over conventional off-line monitoring techniques. Off-line monitoring techniques do not yield instantaneous results and thus can not be used to identify varying product quality. In-line process monitoring techniques yield almost instantaneous results regarding the monitored parameter. Thus, result in reduced waste and lower process cost. In-line monitoring of % VA content in EVA copolymers have been previously carried out using near infra-red (NIR) technique (27). Raman spectroscopy has been evolving as a complimentary spectroscopic

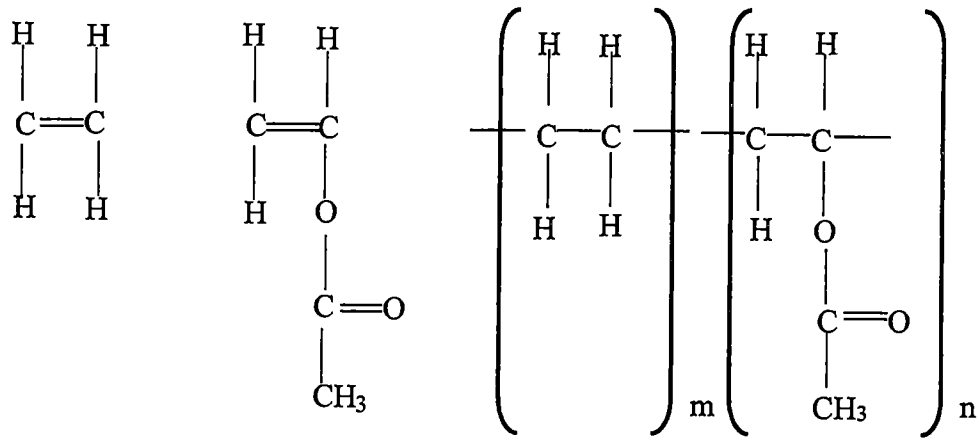


Figure 7.3: Chemical structures of ethylene, vinyl acetate and ethylene vinyl acetate (EVA) copolymer

method to NIR spectroscopy. Raman spectroscopy offers distinct advantages over conventional NIR spectroscopy (76). Raman spectroscopy is a scattering technique, whereas NIR spectroscopy is a transmission technique. Hence, a single sided probe can be used for acquiring Raman spectra from molten polymer samples. It can also be used to investigate pellets, films, or bulk samples without much sample preparation. Raman spectra consist of sharp fundamental peaks as against broad overtone bands in NIR spectroscopy.

In this research, in-line spectra were collected using a single sided Dynisco® style probe during the extrusion process. The probe has confocal optics built into it. Details of the Dynisco style Raman probe are depicted in figure 7.4. The probe is essentially made of two barrels, in which the outer barrel is fixed and the inner barrel is movable. The inner barrel has a lens attached to its tip and the outer barrel has a window at its tip. The light travels in the form of a collimated beam and encounters the lens at the tip of the inner barrel. As the inner barrel is moved relative to the outer barrel, the distance of the focus varies relative to the outside window of the outer barrel. Thus, the focus of the excitation laser beam could be adjusted in order to achieve the maximum possible intensity of the collected Raman spectra. The probe head has two built in polarizers, one each on the excitation and the collection light path. The probe was adjusted such that the maximum intensity was obtained in the polarization in which the excitation and collection polarizers were parallel to each other. This is referred to as the plane polarization. Spectra were also recorded in

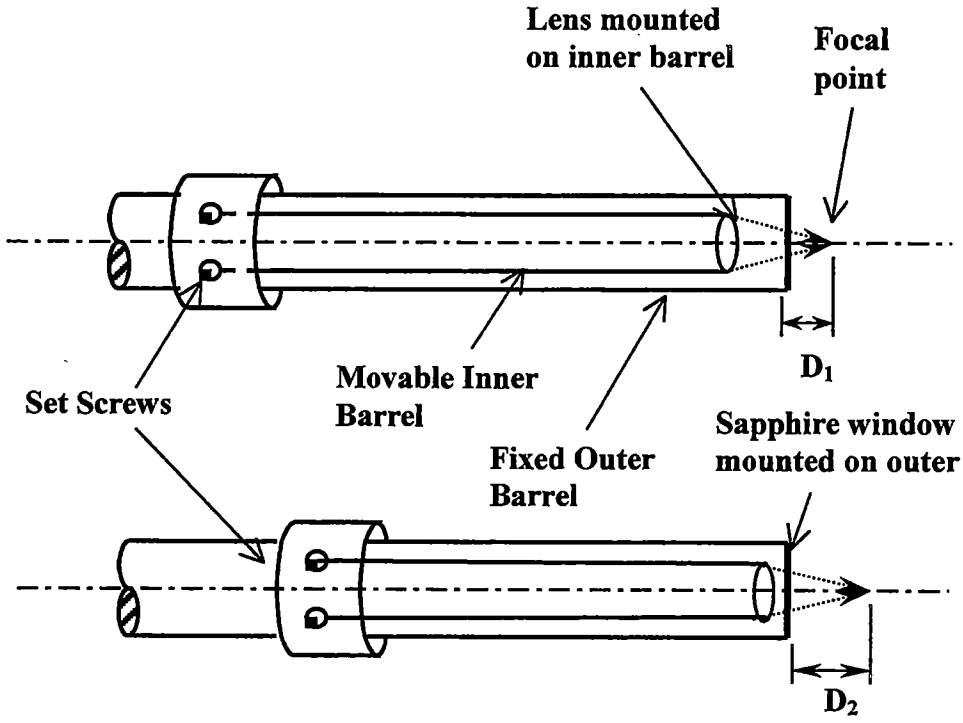


Figure 7.4: Dynisco style Raman probe with movable inner barrel and fixed outer barrel. D = Focal distance from the window ($D_1 < D_2$)

orientation where the excitation and collection polarizers were adjusted perpendicular to each other, referred to as the cross polarization. Details of polarized Raman spectroscopy and the nomenclature were discussed in chapter 2. In-line Raman spectra were recorded using a Kaiser Optical Systems Inc. HoloProbe® Raman spectrometer. The spectra were collected using a 785 nm laser with 300 mW power. Use of laser wavelength in the near infrared region reduces the possibility of sample fluorescence.

7.2.1 Monitoring of VA content in EVA samples

For this study, EVA random copolymer samples from two different sources were used. These two sets are referred here as set I and II. These sets provide a wide range of samples with varying VA content and MI values. Table 7.1 shows the VA content of the samples in set I and II. Processing temperatures were set as shown in Table 7.2 for the six zones in the extruder. The spacer used was 5 mm in thickness. Spectra were collected using the Dynisco® style probe described in detail before. The spectra were recorded for 15 seconds and two collections were averaged. For each sample, 5 spectra were recorded in the plane polarized and cross polarized orientation each. These spectra were averaged and used for mathematical analysis. The flow rate of the extruded polymer through the flow cell was kept constant at (7.5 $\pm$ 0.5) g/min. For samples with very high melt index (MI > 100 g/10 min) it was found difficult to maintain the flow rate exactly in this range. For these samples the

Table 7.1: EVA sample set

Set 1

Sample	VA Content
1	0
2	9.08
3	12.12
4	12.04
5	15.18
6	9.11
7	17.91
8	19.06
9	24.89
10	25.22
11	28.49
12	27.84
13	28.59
14	28.37
15	32.05
16	35.57

Set 2

Sample	VA Content
17	21.01
18	34.8
19	34.95
20	26.87
21	18.72
22	18.62

Table 7.2: Processing temperatures for EVA

Zone	Temperature (^{0}C)
1	190
2	195
3	200
4	210
5	210
6	210

flow rate was maintained in the range (7.5 $\pm$ 1.5) g/min. Since the flow rate is maintained constant, a constant shear rate at wall will be experienced by all the samples. These conditions influence orientation of the molten polymer chain based on its molecular weight.

Figure 7.5 shows overlaid spectra of PE (EVA with 0% VA) and EVA with 35.57% VA (sample 16 from Set I). This figure was used to identify the peaks in Raman spectra attributed to the vinyl acetate in EVA random copolymer. Raman spectrum in 2000-5000 cm^{-1} region of EVA copolymers is characterized by bands at 1740, 1461, 1439, 1416, 1298, 1126, 1063, 629 cm^{-1} due to C=O stretching, CH_2 scissoring, CH_2 scissoring, CH_2 wagging, CH_2 twisting, C-C stretching, C-C stretching, and O-C=O deformation modes, respectively. It can be clearly seen from figure 7.5 that the bands at 1740 and 629 cm^{-1} arise due to VA. Figure 7.6 shows overlaid Raman spectra of the sample 16 in set I in plane and cross polarized orientation. The Raman spectrum from a species arises due to change in the polarizability of the molecule upon incident light. Polarizability of a molecule is the ease with which the electron cloud of the molecule can be distorted. Thus, the plane and cross polarized spectra show presence of the same bands, however, with varying intensity. The overall intensity of the Raman spectrum is higher in the plane polarized orientation as compared to the cross polarized orientation. In the cross polarized geometry of data collection, the collection polarizer is perpendicular to the

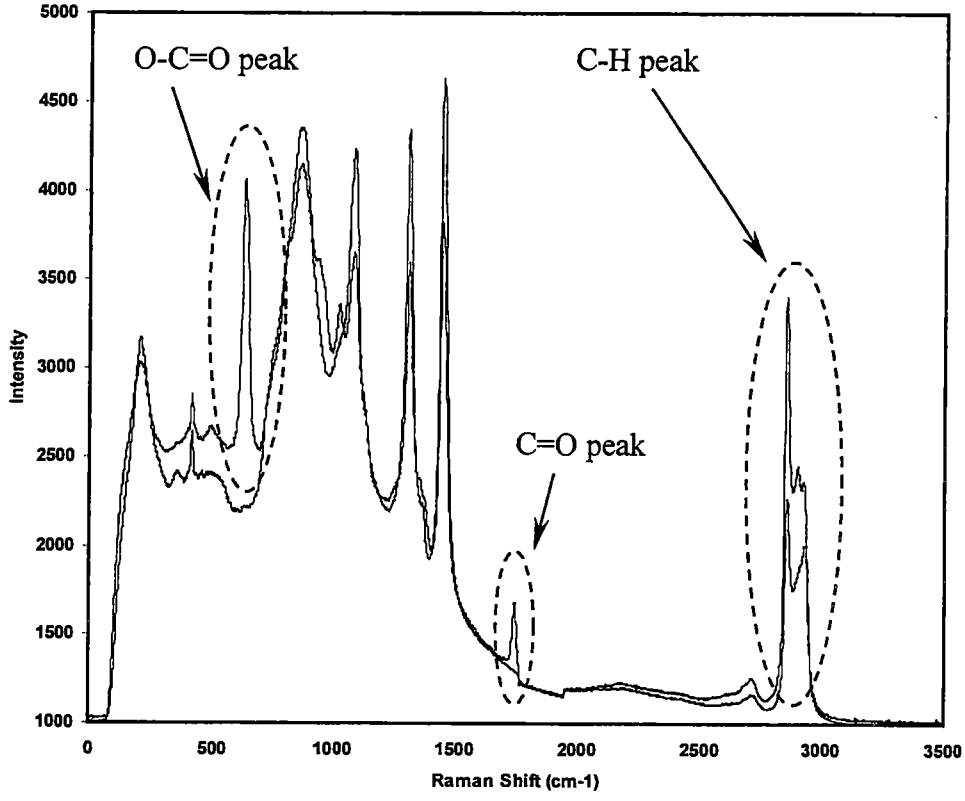


Figure 7.5: Overlaid Raman spectra of PE and EVA with 35.57% VA in plane polarized orientation

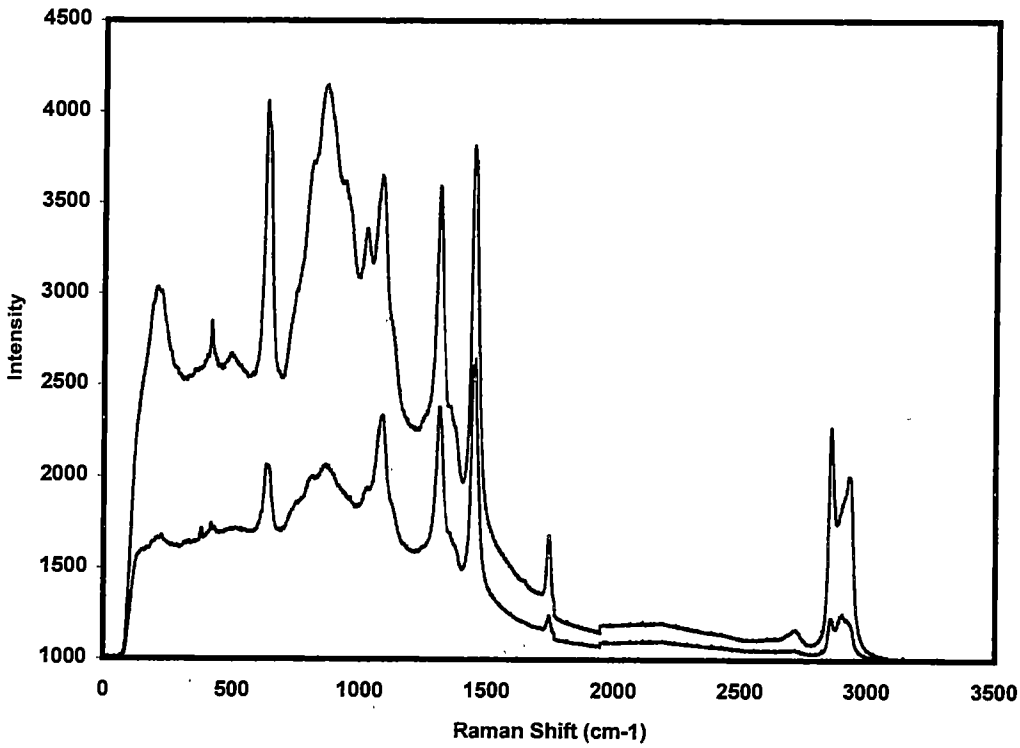


Figure 7.6: Overlaid Raman spectra of sample 16 in set I in plane and cross polarized orientation

excitation polarizer. Hence, intensity of the cross polarized spectrum is lesser than the plane polarized spectrum.

Mathematical Analysis:

The spectra for plane and cross polarized samples were averaged and arranged in the form of two individual matrices. This matrix was subjected to PCA, a pattern recognition technique. PCA was carried out in order to make a qualitative model that discriminates between the samples according to their VA content and PLS was used to make a quantitative model that predicts the VA content in EVA samples. PCA was performed on the baseline corrected and mean centered Raman spectra in 1710 to 1760 cm^{-1}. This peak is due to the presence of C=O in the VA group. Figure 7.7 shows the baseline corrected C=O peak in 1710 to 1760 cm^{-1} region. It can be clearly seen that the intensity of the peak increases with increasing amount of VA in the sample. Figure 7.8 shows the score plot of factor 1 against factor 2. This plot shows the relative weightage of each sample on PC1 and PC2. A score plot was plotted using the mean centered data without any pretreatment, however, the data with multiplicative scatter correction (MSC) pretreatment gave slightly better results, and the results are presented in figure 7.8. This treatment is an approach to compensation for scattering by solids. Each sample spectrum is regressed against an ideal spectrum to yield a slope and intercept. The sample spectrum is then corrected at each wavelength by subtracting the intercept and then dividing by the slope. It can be seen from figure 7.8 that the samples in set I and II

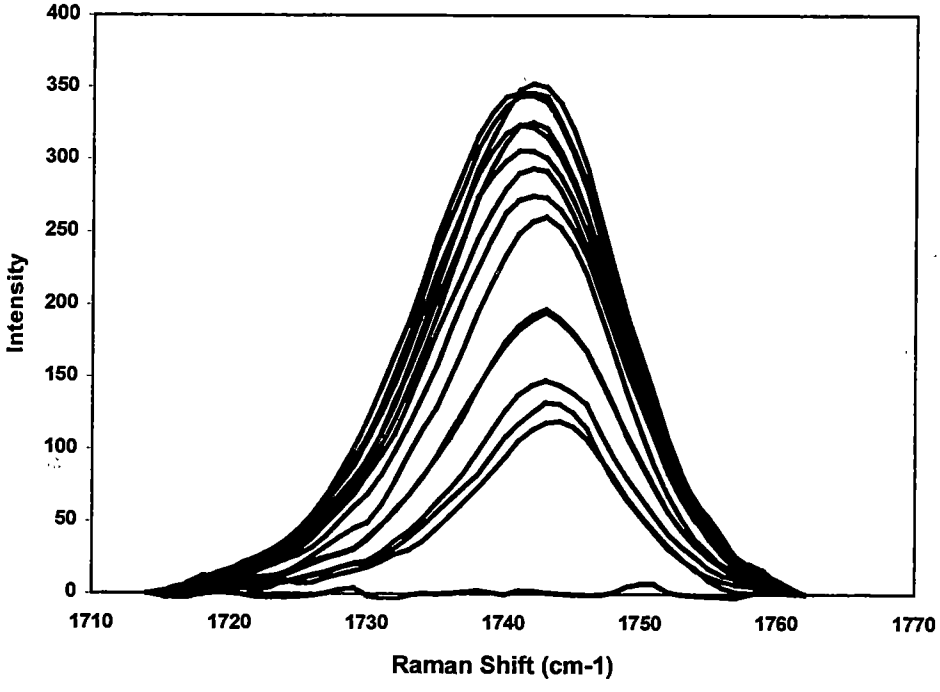


Figure 7.7: Baseline corrected spectra in the C=O peak region (1710 to 1760 cm^{-1}), showing increasing band intensity with increasing VA content in EVA samples

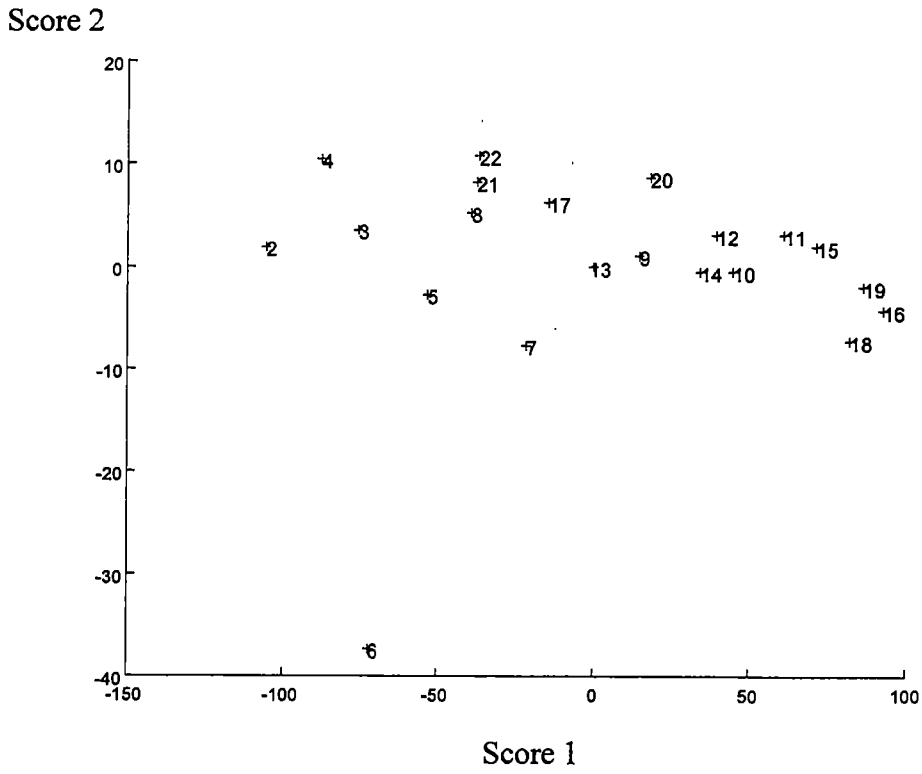


Figure 7.8: Score plot for PC1 and PC2 for the EVA samples in set I and II

are arranged according to increasing VA content. Thus, the VA content of samples appears as the primary information in PC1. This analysis was performed on all samples in set I and II, except sample 1 from set I, as its response was that of an outlier. The incorporation of VA in the EVA samples reduces its crystallinity (77). It has been suggested before that the score on factor 2 appeared as a result of the crystallinity. From figure 7.8, it can be observed that the score on factor 2 decreases with the increasing VA content, with an exception of sample 6. Sample 6, with VA content 9.11%, has an exceptionally high score on PC2. Results in figure 7.8 also show a trend, where the score on factor 2 decreases with the increase in the VA content of the samples. Thus crystallinity or MI effects appear as a secondary information in the Raman spectra in the region under consideration.

In order to correlate the amount of VA in the EVA samples, linear least squares and PLS analysis was carried out on all the samples in set I and II. The spectral region in the 1710 to 1760 cm^{-1} region was used for building a chemometric model. Figure 7.9 shows the maximum intensity of the baseline corrected peak in figure 7.8 plotted against the known VA content in EVA samples. Linear regression gives a good fit between the baseline corrected intensity of the C=O peak and the known VA content of the EVA samples. The correlation coefficient, r^2, which is a measure of goodness of fit, is 83%. The PLS regression model was built using cross validation method as described in chapter 4 on regression methods. Figure 7.10 shows the standard error of validation (SEV) that is used to decide the number of

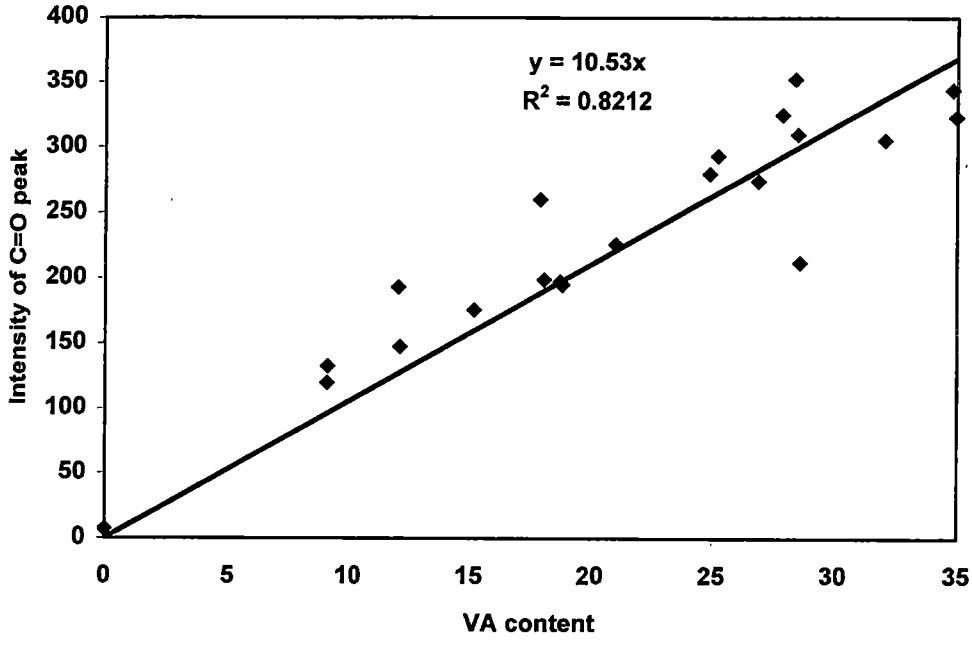


Figure 7.9: Linear regression fit for intensity of C=O peak with known VA content in EVA samples

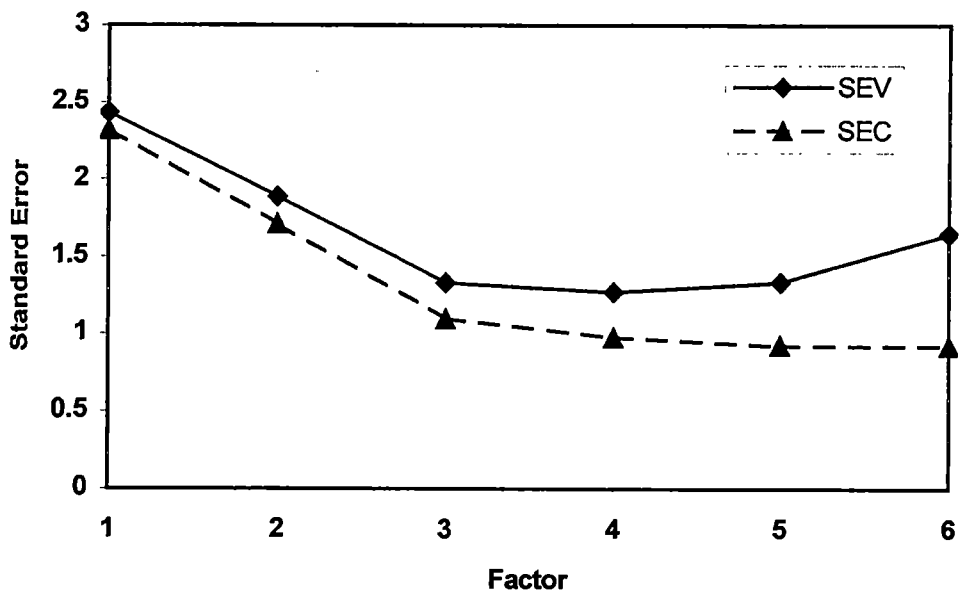


Figure 7.10: Comparison of measured and predicted values of VA content of samples from set I and II

factors. Three factors were chosen for building the prediction model as the SEV is lowest at three factors, at 1.32. Figure 7.11 shows the prediction of samples in set I and II using leave a sample (LAS) cross validation method. Prediction of VA content in EVA samples has been previously carried out using the region of C-O bending in C=O group in VA (78).

Results and Discussion:

These experiments have described the use of dispersive Raman spectroscopy in monitoring and predicting the VA content of EVA samples. The chemometric techniques such as PCA and PLS were applied to the spectroscopic data for determining the possible outlier samples and predicting the VA content, respectively. Twenty-two EVA samples from set I and II could be discriminated based on their VA content. The scores plot was used to identify the possible outliers. Sample 6 appeared as an outlier as seen from the scores plot. However, the prediction of sample 6 using PLS analysis did not reveal this anomaly. The meaning of first and second factor were also deduced using this data. It was found that the VA content of a sample reflected as the score on the first factor and the crystallinity of the EVA samples reflected as the score on the second factor. The PCA analysis was carried out using the multiplicative scatter technique, which corrects for the background and/or scattering effect during spectral acquisition. A calibration model was made using linear least squares fit and PLS technique. The linear least square technique served as a primary data analysis tool for developing basic understanding of the data

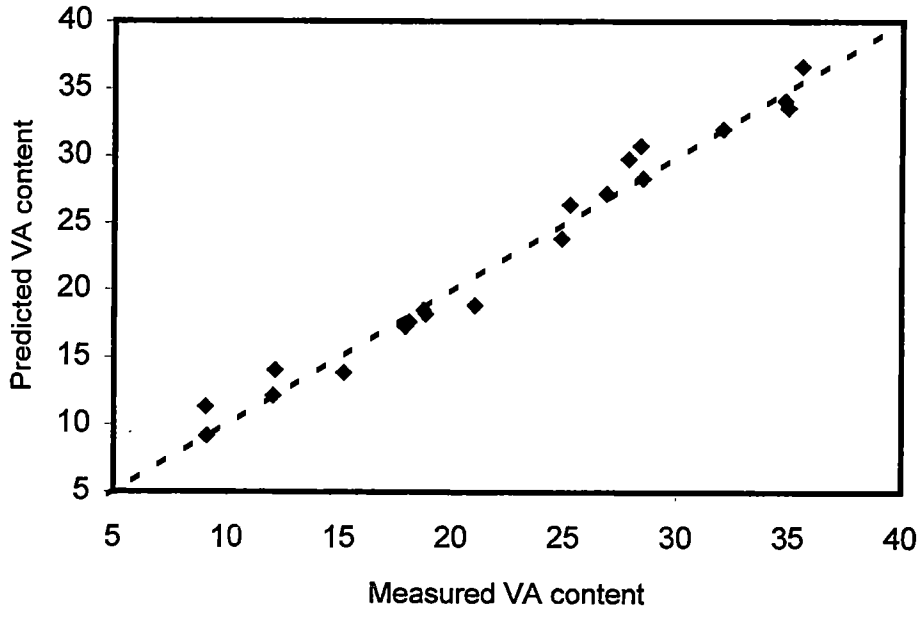


Figure 7.11: Comparison of measured and predicted values of VA content of samples from set I and II

and correlation of the variables with the VA content. PLS model was developed using leave-a-sample cross validation technique for the prediction of VA content. The standard error of validation for the samples in set I and II was 1.32, with three factors used for the model.

The application of Raman spectroscopy to monitoring extrusion processes in real time has been demonstrated. The development of rugged fiber optic probes that can withstand the temperatures in the extruder flow cell is of crucial importance to this application. Raman spectroscopy contains information about the structure and chemical composition of polymer species due to a number of sharp and well-resolved bands. In-line fiber-optic Raman spectroscopy coupled with multivariate statistical analysis provides capability of monitoring the copolymer composition in EVA samples.

7.2.2 Monitoring rheological properties in EVA

EVA copolymers find industrial applications as hot melt adhesives. Hot melt adhesives are thermoplastic materials that can be heated to form a melt and then applied as a liquid to an adherend. The bond is formed when the hot melt adhesive resolidifies. The formulation of hot melt adhesives involves providing the best possible properties over a wide range of temperatures (79). EVA can be manufactured in a wide range of molecular weights and in a variety of compositions.

As the molecular weight increases, the melt viscosity also increases. Melt Index (MI) is an industrial parameter that is used to characterize the melt viscosity of the polymer. The ASTM melt index test (ASTM D-1238) (80) gives the flowability of the plastic resins in the melt form and is measured in units of g/10 min. Melt index is used as an approximate measure of the average molecular weight of the polymer. Often, a general relationship between the melt index (MI) and the molecular weight ($\overline{M}_W$) is given by equation (7.1).

$$\log_{10}(MI) = k_1 - k_2 \log_{10}(\overline{M}_W) \qquad \ldots(7.1)$$

where, MI = Melt index of the polymer,

$\overline{M}_W$ = Average molecular weight,

K_1 and K_2 = constants.

Thus, for EVA copolymers with similar weight average molecular weight, $\overline{M}_W$, the polymer with narrower molecular weight distribution (MWD) will flow faster.

A schematic of the melt index apparatus, called Melt indexer, is shown in figure 7.12. The variables for the MI measurements are the temperature and the input load on the piston. The standard values of these variables change as the polymer under study varies. For PE based resins and their copolymers, the common operating condition involves 190 ^{0}C and 2.16 kg of load on the piston (81).

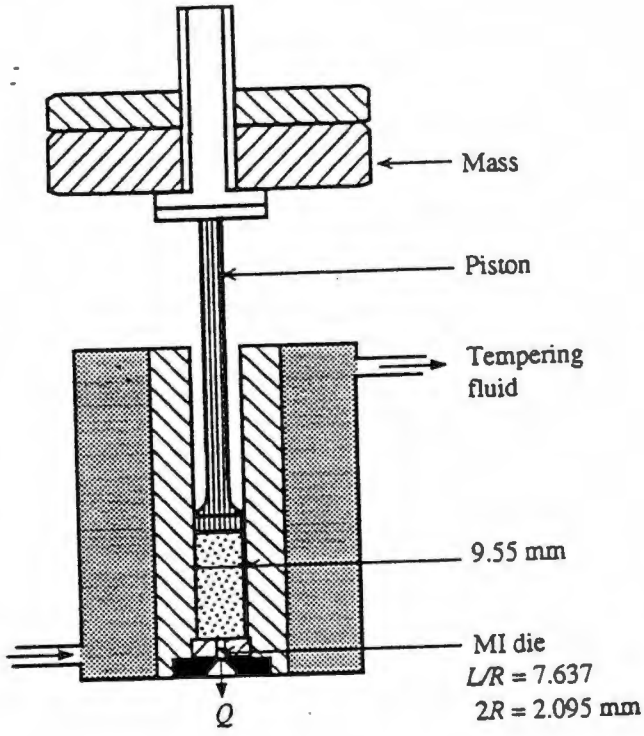


Figure 7.12: Schematic of ASTM standardized melt index (MI) measurement apparatus
[Source: Macosko, C. W. in "Rheology - Principles, Measurements and Applications" (John Wiley & Sons, Inc., New York, 1987)]

The EVA copolymer samples were obtained from independent sources. The sample sets are shown in Table 7.3. Set I comprise of 16 samples from one manufacturer, set II comprises of 6 samples. The EVA samples were extruded under conditions described in detail in section 7.3.1. The flow rate of the samples was maintained constant at 7.5 g/min. However, for samples with very high melt index (MI > 100 g/10 min) it was found difficult to maintain the flow rate exactly in this range. For these samples the flow rate was maintained in the range 7.5 ± 1.5 g/min. Since the flow rate is maintained constant, a constant shear rate at wall will be experienced by all the samples. These conditions influence orientation of the molten polymer chain based on its molecular weight. Hence, the intensity of the Raman spectra can be used to obtain rheological information about the polymer. When a polymer experiences stress, changes in the vibrations take place. These changes result in orientation in the molecules. Therefore, it is possible to build a relationship between the Raman spectra and rheological properties of molecules. In this research, the Raman spectra were collected in plane and cross polarized orientation. Variations in the rheological properties affect the overall spectra obtained from the polymer. However, the Raman peaks in which the rheological effects appear strongly show larger changes than other peaks. The C-H stretching bands appear in the region 2850-2930 cm^{-1} (Raman shift). These bands show a strong orientation effect, as seen in figure 7.13. The intensity in the plane polarized orientation is much greater than the intensity in the cross polarized orientation. The plane polarized spectra were used for mathematical analysis.

Table 7.3: EVA sample set for MI correlation

Set 1

Sample	Melt Index
1	1.89
2	6.45
3	7.79
4	0.34
5	7.84
6	1.92
7	0.64
8	6.92
9	17.54
10	370
11	6.07
12	143
13	368
14	23.68
15	37.8
16	0.77

Set 2

Sample	Melt Index
1	2.86
2	27.09
3	26.63
4	6.26
5	25.36
6	40.74

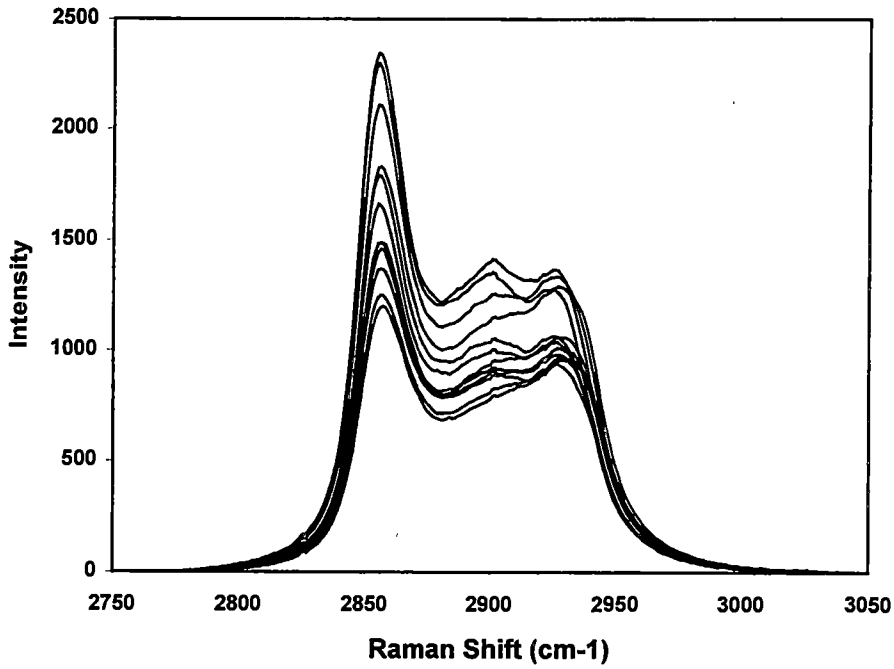


Figure 7.13: Raman spectra of EVA samples in calibration set (2750-3050 cm^{-1} region) used to correlate the MI values of EVA samples

Availability of EVA samples from three independent sources allowed the use of calibration model to predict the MI values for the samples in the prediction set. The EVA samples from set I were used as the calibration set due to the wide range of MI. The samples from set II were used as the prediction set. A logarithmic relationship was proposed based on the equation (7.1) between the Raman intensity and the MI of EVA samples. Leave-a-sample (LAS) cross validation technique was used to build a calibration model between the plane polarized spectra as the **X** matrix and *ln*(MI) values of the samples as the dependent variable. Hierarchical Cluster analysis (HCA) was used as a pattern recognition technique to observe the natural clustering tendency of the samples. Details of HCA analysis were described in detail in chapter 4. The results of the HCA analysis carried out on samples in the calibration set are shown in figure 7.14. Two main clusters based on the melt index values of the samples are observed. In cluster 1, in the upper part of the figure 7.14, the samples with MI values less than 10 are seen clustered. Whereas, in cluster 2, in the lower part of figure 7.14, we observed samples with relatively higher MI and VA values. It can also be observed that the samples in cluster 1 all have higher % VA values. Samples 16 and 11 have high % VA content but are observed to fall in cluster 1 due to their lower MI values. This clearly demonstrates that clustering is observed according to MI value. Within a cluster, the samples with similar % VA values are arranged in subclusters. The results of HCA showed that the samples 10,12, and 13 are clustered in cluster 2. The samples 10 and 13 have similar MI value that is

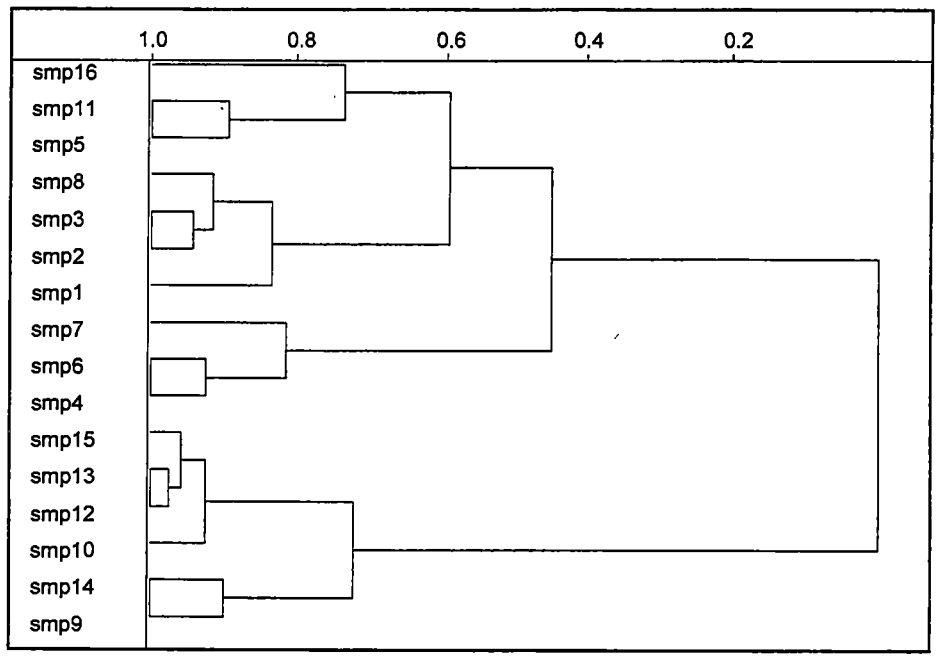


Figure 7.14: Hierarchical Cluster Analysis of EVA samples in the calibration set

considerably higher than the other samples. The samples in the prediction set have MI values that are close to the samples clustered in cluster 1 in HCA. Hence, the calibration model made on samples in cluster 1 was used to build the prediction model. Based on the results of HCA, the PLS analysis of this region was carried out to correlate the *ln*(MI) value with Raman spectra.

The PLS calibration model was made using leave -a -sample (LAS) cross validation method. The variance explained by the principal components is given in table 7.4. Figure 7.15 shows the standard error of validation for the calibration model based on the cross validation method. The minimum error of 0.47 in *ln*(MI)was obtained with 5 factors. This calibration model was used to predict the values of *ln*(MI) for sets II and III. The results of prediction using LAS method are shown in figure 7.16. A comparison of the measured and predicted *ln*(MI) values for the prediction set is shown in table 7.5. A comparison of the goodness of prediction for the VA content of the EVA samples with the MI values showed that the VA prediction results had lower standard error of prediction as compared to the *ln*(MI) prediction. This could be due to the fact that difference in VA concentration in the EVA samples appears as a primary effect in the Raman spectra. Therefore, the calibration and the prediction of VA content were less sensitive to the small changes in the experimental conditions. Melt index of the polymer is a rheological property that manifests itself as a secondary effect in the Raman spectra. Melt index was monitored using the C-H stretching band in the Raman spectra. The polymer

Table 7.4: PCA variance results of 2750-3050 cm^{-1} region

Factor	% Variance	Cumulative % Variance
1	95.10	95.10
2	4.18	99.28
3	0.61	99.89
4	0.06	99.95
5	0.02	99.97
6	0.01	99.98
7	0.01	99.98

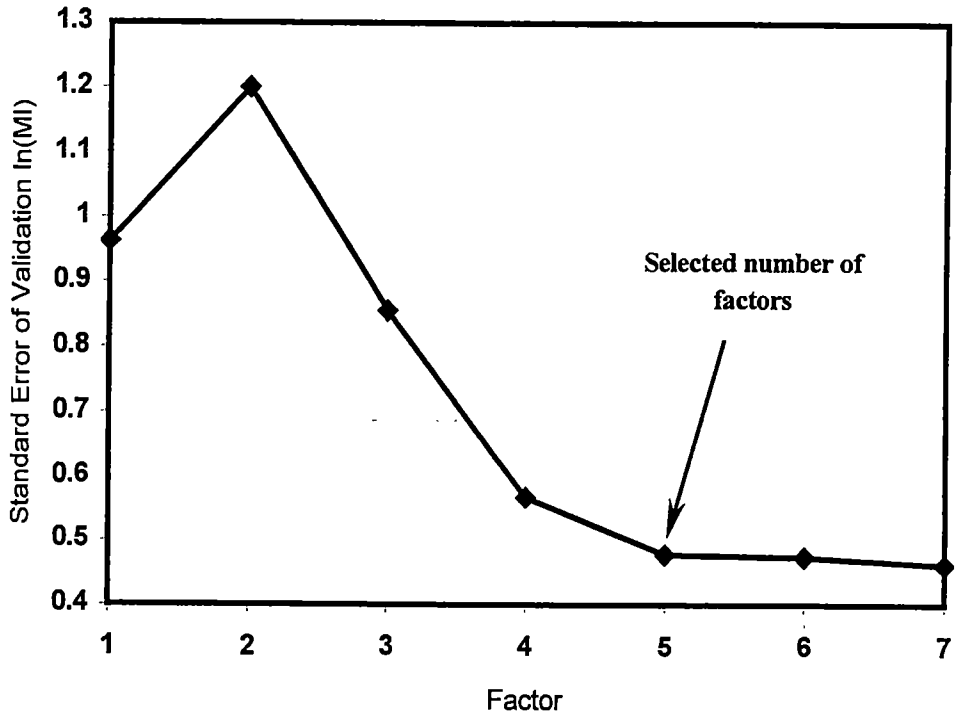


Figure 7.15: Plot of standard error of validation vs. number of factors for PLS regression of Raman spectral intensity with melt index

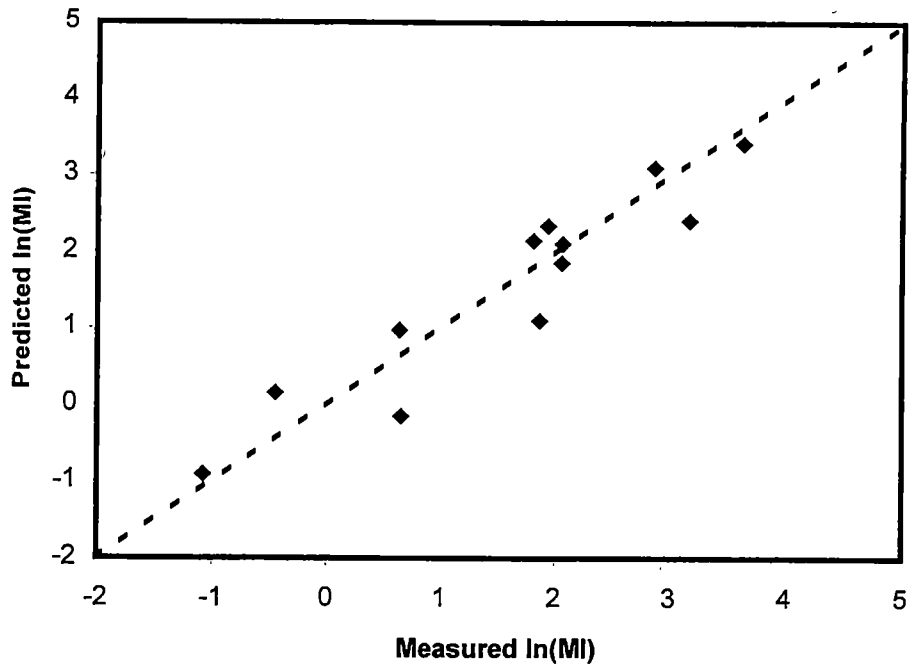


Figure 7.16: Measured vs. predicted *ln*(MI) values for EVA samples

Table 7.5: Comparison of the measured and predicted *ln*(MI) values of the prediction set

ln(MI) Measured	**ln(MI) Predicted**
3.282	3.2303
1.0508	2.1318
3.2993	3.8174
3.1485	3.5464
3.2332	3.6937

molecules orient as the flow through the slit dies progresses. The molecules experience different shear rate at different positions in the flow. The polymer at the slit die wall experiences highest shear. Thus, the degree of orientation varies as the distance from the die wall changes. This causes a difference in the C-H peak in the Raman spectra. Hence, the melt index effects are less pronounced as compared to the VA effects in the Raman spectra.

7.3 Correlation of complex viscosity with the Raman spectra in polypropylene samples

Polymeric materials exhibit a time dependent behavior when subjected to stress. When a load is applied to a polymer, instantaneous deformation takes place. When the load is removed, part of the deformation is recovered instantaneously, more is recovered with time, and in some materials there is a permanent set. This time dependent response is called viscoelasticity. Complex (or dynamic) viscosity, $|\eta^*(\omega)|$ is a material function that takes into account the effect of sinusoidal stress applied to the polymer sample. The response of the material is analyzed by decomposing it into the in-phase and out-of-phase component of response. The response is also a function of the polymer molecular weight parameters, such as $\overline{M}_w$ and molecular weight distribution (MWD). Complex viscosity is a widely used parameter in industry. Hence, it is of importance to correlate it with Raman spectra information in order to get a quantitative model.

In this section, in-line polarized Raman spectra of polypropylene (PP) samples were recorded in molten conditions. The information obtained from the spectra is correlated with the complex viscosity data for the samples. The complex viscosity measurements were performed using a Rheometrics® Dynamic Stress Rheometer. A schematic of this apparatus is shown in figure 7.17. The PP samples were compression molded using a hot press and made into the form of small disks of 25 mm diameter. A 25 mm diameter cone and plate viscometer with a gap angle of 0.1 radians was used for these measurements. Constant amplitude, sinusoidal shear stress at 200 Pa was applied to the molten samples and the rheological response was recorded over a range of angular frequencies. The storage modulus, G'(ω), loss modulus G"(ω) and $|\eta^*(\omega)|$ as a function of ω were measured from these experiments. Figure 7.18 illustrates typical behavior of G'(ω), G"(ω) and $|\eta^*(\omega)|$ with ω. Figure 7.19 illustrates the complex viscosity response of the PP samples in angular frequency range of 0.01 to 100 rad/sec. In correlating the $|\eta^*(\omega)|$ response to the Raman spectra of the PP samples, a separate methodology as compared to the correlation of MI was developed based on earlier studies (74). The $|\eta^*(\omega)|$ values are varying with ω. Hence, the **Y** matrix to be correlated to **X** matrix, is no longer a single column, but a matrix. In developing a PLS model for such data sets, either PLS1 or PLS2 procedure could be used. PLS1 treats each column of the dependent matrix **Y** as independent of each other and are independently regressed against the

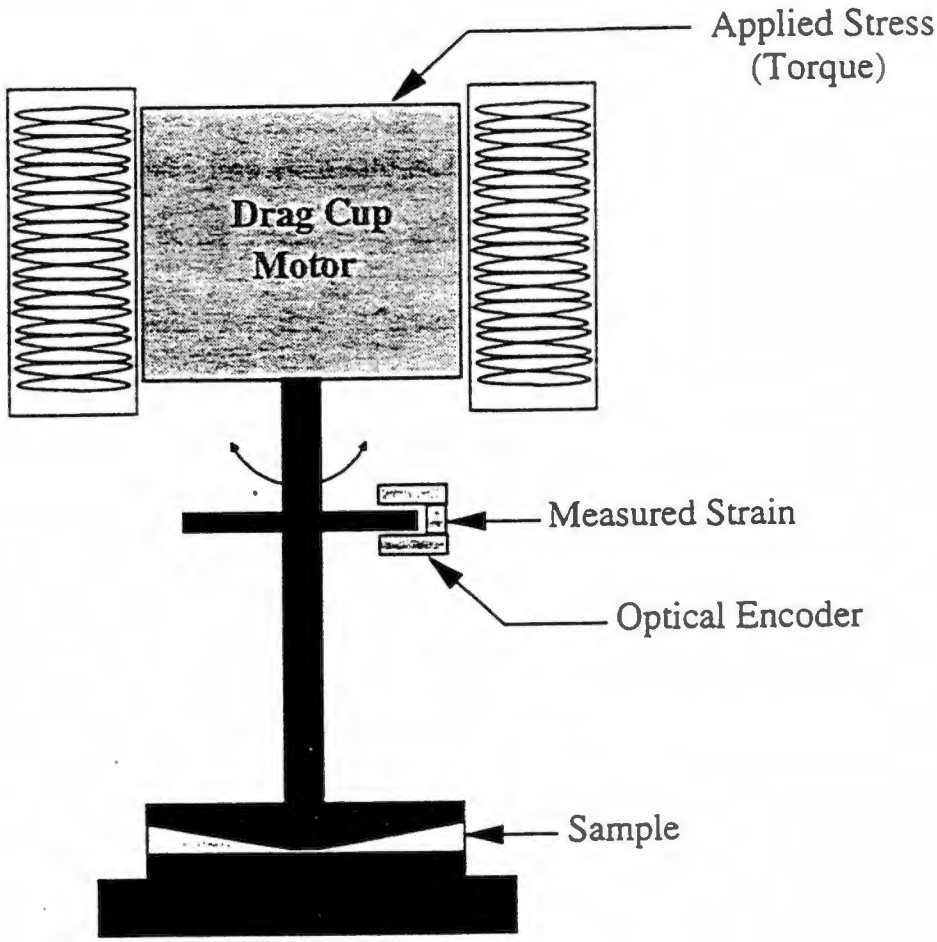


Figure 7.17: Schematic representation of experimental setup for rheological measurements using Rheometrics Dynamic Stress Rheometer.

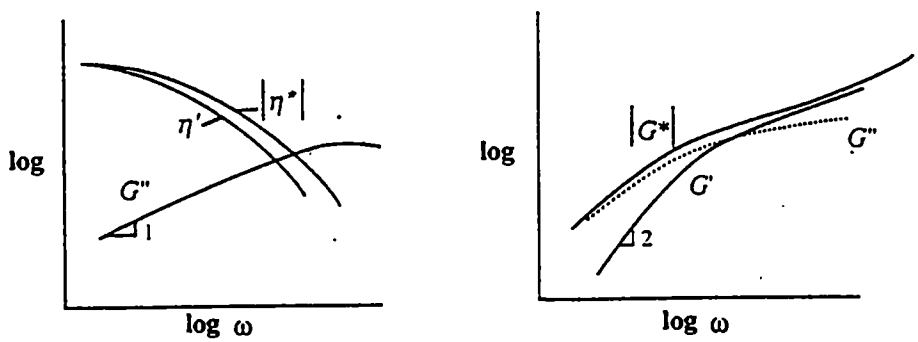


Figure 7.18: Typical behavior of G'(ω), G"(ω) and $|\eta^*(\omega)|$ as a function of ω.

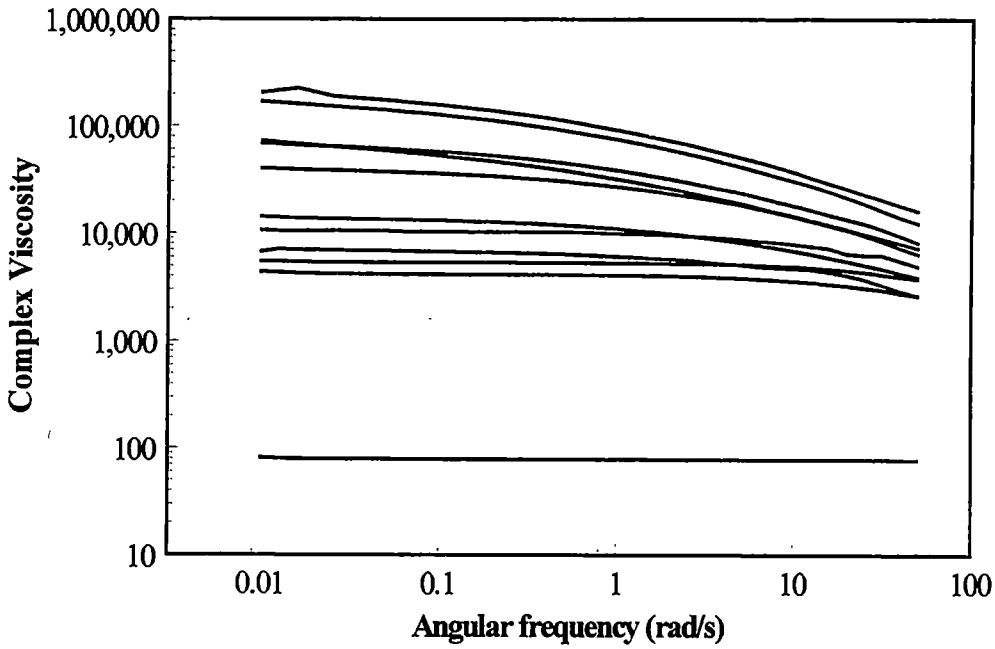


Figure 7.19: Complex viscosity response for PP samples over angular frequency range of 0.01 to 100 rad/sec, measured at 220^{0}C.

information in the **X** matrix. Hence, if there are n columns in the **Y** matrix, n independent PLS models are generated. In PLS2 technique, the whole **Y** matrix of n columns is treated as one matrix and is regressed against the **X** data (82). PLS2 involves extensive calculations as it requires evaluating the SVD of a large covariance matrix. If the columns of the **Y** matrix, that is the response variables in **Y** matrix, are highly intercorrelated, then the **Y** matrix can be decomposed into a small number of principal components. The variables would be highly correlated if there were only a few process variables that affected the **Y** variables. The sample 4 in the PP set has a complex viscosity response vastly different as compared to the other samples. Hence, the mathematical analysis was performed without sample 4. Therefore, PCA was carried out on the **Y** data. Table 7.6 shows the variance explained by each of the principal components. The first PC explains 99.98% of the variance in the data. Hence, the use of the first PC is justified for building a correlation between the Raman spectra of PP samples in molten state and $\ln(|\eta^*(\omega)|)$.

The Raman spectra were collected in 2 different polarization states, the plane and cross polarized state. The representative spectra are shown in figure 7.20. The spectral region in 2850-3000 cm^{-1} that corresponds to the symmetric and anti-symmetric CH_2 and CH_3 bands in the polymer was used as the **X** matrix for regression. The peak of interest was baseline corrected using a two-point baseline correction technique. This **X** matrix was regressed against the first score vector

Table 7.6 Variance explained by the principal components of the **Y** matrix

Number	% Variance explained	Cumulative % Variance
1	99.98	99.98
2	0.02	100.00

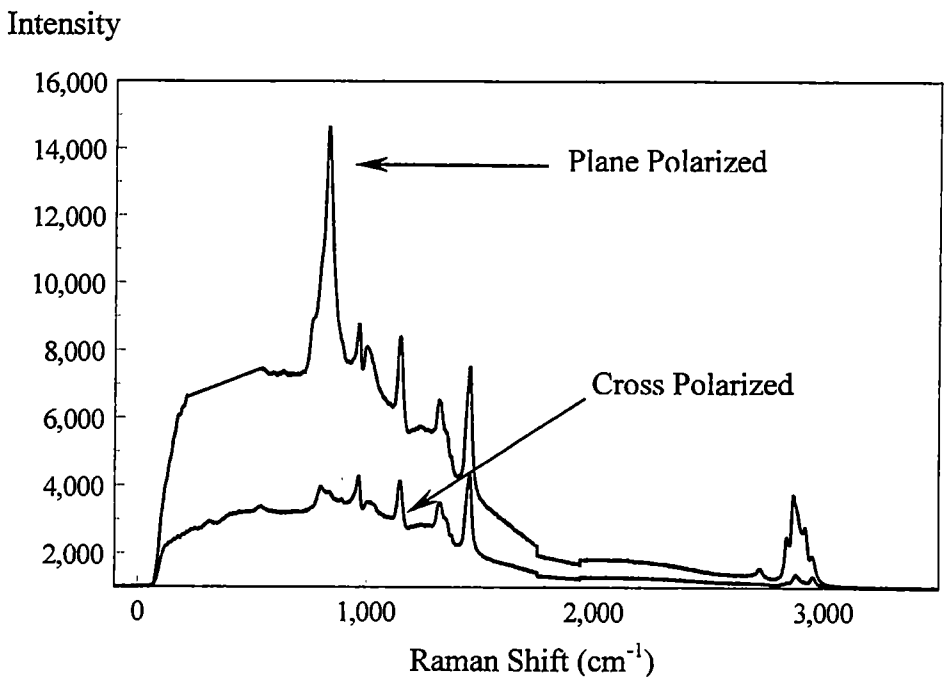


Figure 7.20: Plane and cross polarized Raman spectra of polypropylene samples in molten state, measured at 220^0C.

obtained from the PCA of $\ln(|\eta^*(\omega)|)$ matrix. Figure 7.21 shows the loadings obtained from the PCA of the **Y** matrix plotted against ω, the angular frequency. It shows a trend that is similar to the complex viscosity curves seen in figure 7.19. This graph is representative of the average complex viscosity curve. The score vector is made of magnitudes or vertical shifts that are represented in the data. When these score and loadings vectors are multiplied, the represent the complex viscosity data. This methodology is similar to the shifting and superposition principles used by rheologists (83). Figure 7.22 shows the comparison between the measured and predicted first score values. The prediction of the scores was carried out with minimum error of prediction, 1.5, obtained with four principal components. The data can be reconstructed by multiplication of the predicted score with the loadings that resulted from the PCA of complex viscosity data. The reconstructed data is shown in figure 7.23 overlaid with the actual complex viscosity. The data agrees well with the original data.

7.4 Determination of Octene content in PE samples

Polyethylene (PE) is produced as one of the bulk polymers in most quantities. This versatile polymer is used for a range of uses including use in housewares, film, and injection molded items. Polyethylene was initially produced as a homopolymer of ethylene, but today most of the polyethylenes are produced as copolymers of ethylene with 1 to 10% of α-olefins, such as 1-butene, 4-methylpentene, 1-hexene,

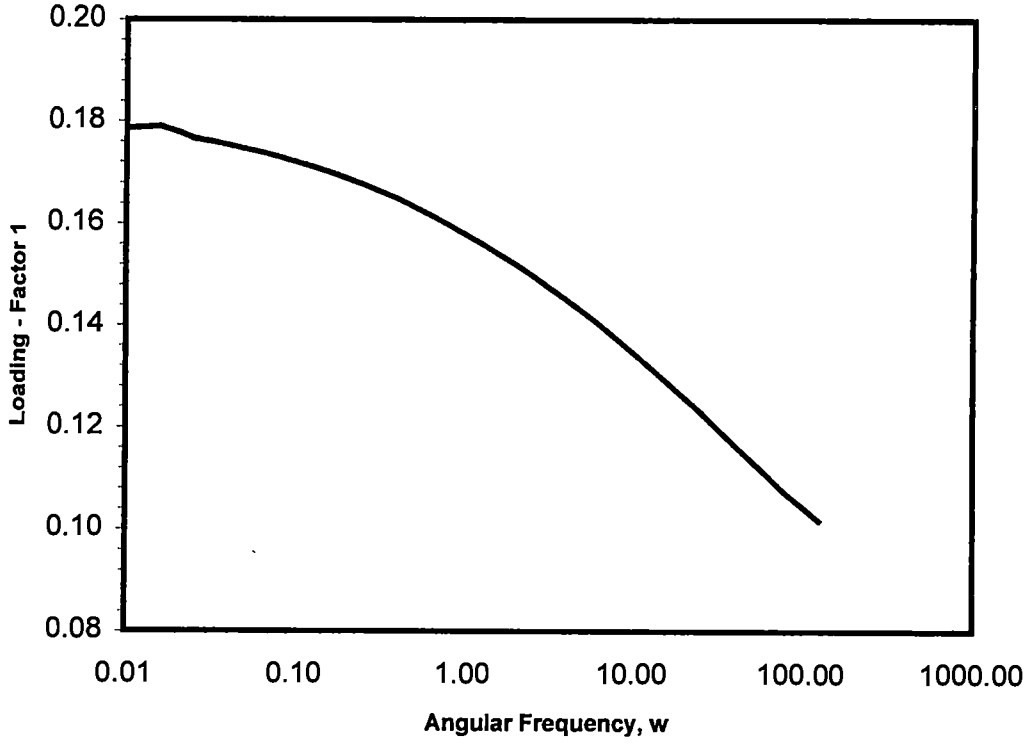


Figure 7.21: The first loadings obtained from the PCA analysis of the complex viscosity data of PP during extrusion

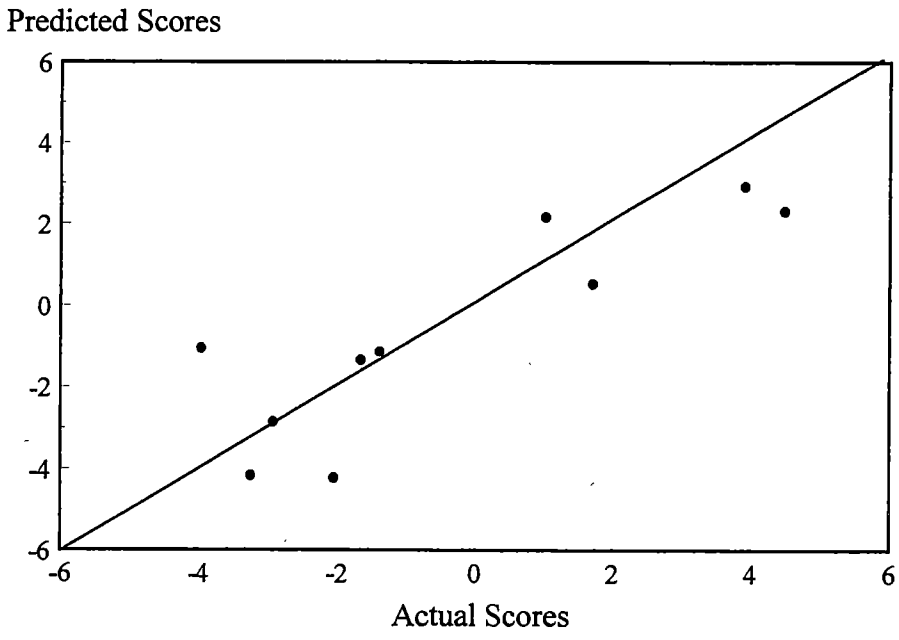


Figure 7.22: Comparison of predicted vs. actual scores for PP samples

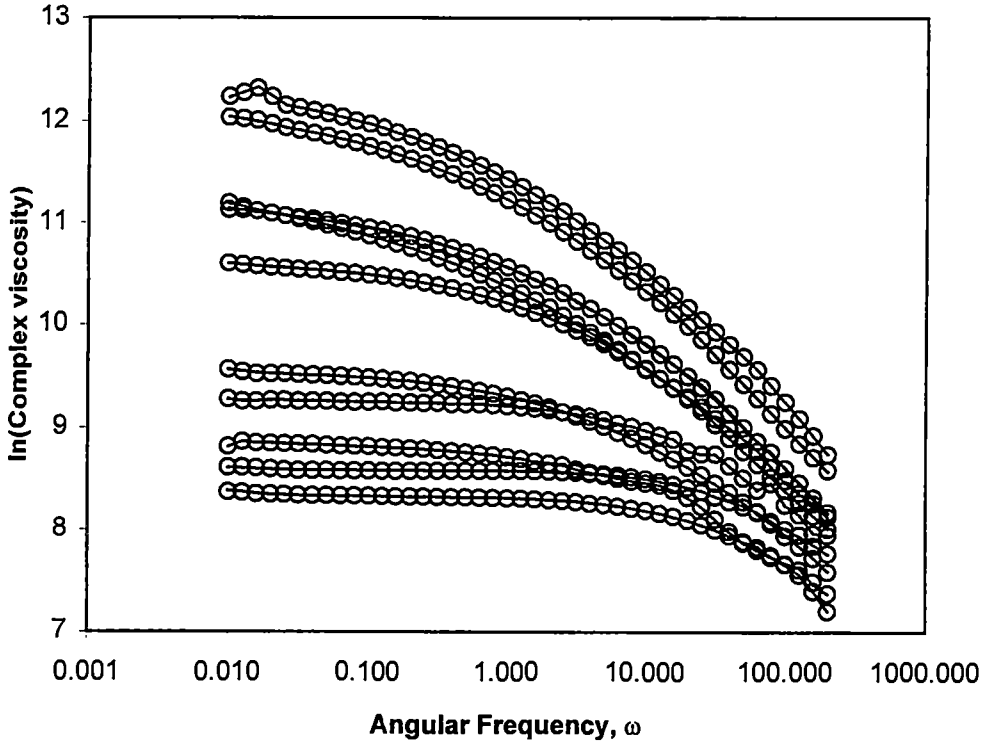


Figure 7.23: Comparison of the measured complex viscosity (Symbol - solid line) and predicted complex viscosity (Symbol - o)

and 1-octene (43,84) The tailoring of PE properties in commercial processes is achieved by controlling the density, molecular weight, molecular weight distribution, or by crosslinking. Successful control of all the reaction parameters enables the manufacturer to produce a family of PE products with considerable differences in physical properties such as softening temperatures, stiffness, hardness, clarity, impact and tear strength. The crystallinity of catalytically produced PE is primarily determined by the amount of comonomer (α-olefin) in ethylene copolymer (85). The amount of comonomer is controlled by varying the relative amounts of ethylene and comonomer in the polymerization reactor. In this study, five PE samples with varying octene content were studied using in-line Raman spectroscopy. This study illustrates the use of Raman spectroscopy in monitoring the octene percentage in the PE samples.

The schematic of the extruder set up is shown in figure 7.1 and the working of the extruder was described in detail in section 7.1. The octene content of the PE with octene copolymer are shown in table 7.7. The extrusion of PE was carried out at 230 ^{0}C. The Raman spectra were collected on-line using the Kaiser Optical Systems HoloProbe Raman spectrometer. The spectra were recorded for 15 seconds and two scans were averaged. Figure 7.24 shows the structure of PE polymer with octene as copolymer. The Raman spectra in the plane and cross polarized state are shown in figure 7.25. The spectra in the region around the C-H stretch band region at 2800 to 3000 cm^{-1} was used to correlate the spectra with the octene content and are shown in

Table 7.7: Details of the PE samples with varying octene copolymer content

Sample	Octene Percentage
1	16.1
2	9.3
3	13.1
4	1.05
5	0

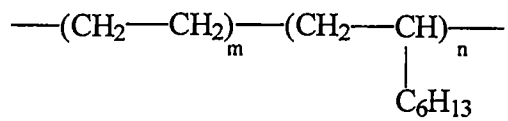


Figure 7.24: Structure of PE polymer with octene copolymer unit.

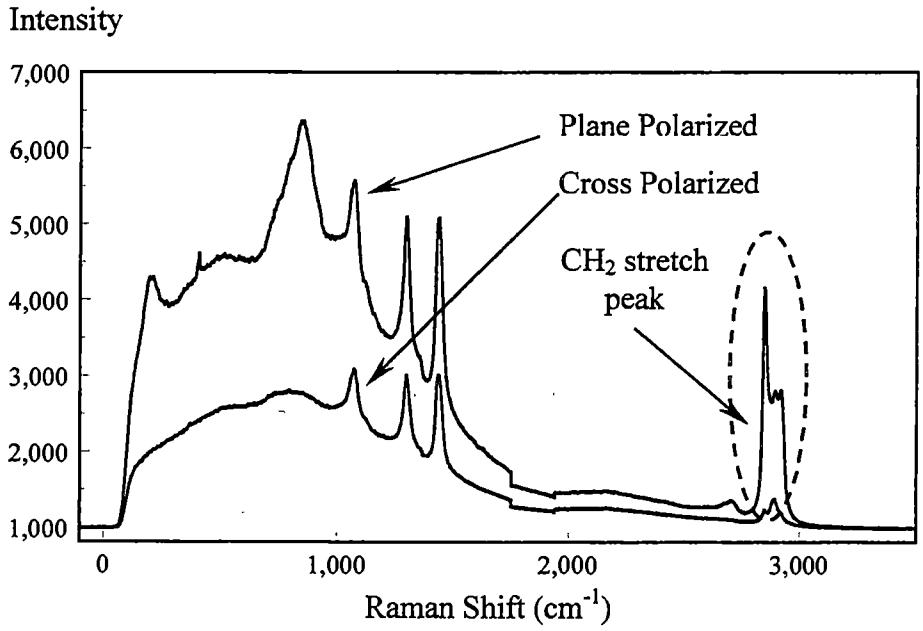


Figure 7.25: Raman spectra of molten PE in plane and cross polarized orientation, measured at 230^0C

figure 7.26. Sample 2 in the set (see table 7.7) was found to exhibit fluorescence. Hence, the response of sample 2 was observed to vary from the other samples in the set. Sample was not included in the analysis. It is seen that the Raman intensity decreases with increasing octene content in PE. As the octene copolymer content increases, the branching and the crosslinking in the chains increases, thus the polymer is less packed. Therefore the number of C-H bands decreases, causing decreased C-H stretch intensity. This fact is confirmed from the results seen in figure 7.25. The maximum intensity of the baseline corrected peak is plotted against the octene content in the PE samples. The trend of increasing intensity with decreasing octene content is evident from figure 7.27. Thus, this study has proved that in-line Raman spectroscopy on molten polymer can be used to determine the copolymer content in PE polymer samples. In a similar study by Strobl *et al.* (86), the crystallinity of PE was correlated with the intensity in Raman spectroscopy. As the copolymer content is varied, the branching in the polymer increases and thus the melting range of the polymers expands. Raman spectroscopy has been used to derive additional quantitative information about this process.

7.5 Results and Discussion

The use of Raman spectroscopy in monitoring rheological properties of polymers in molten state has been demonstrated. The melt index of EVA samples was successfully monitored using in-line near real time polarized Raman

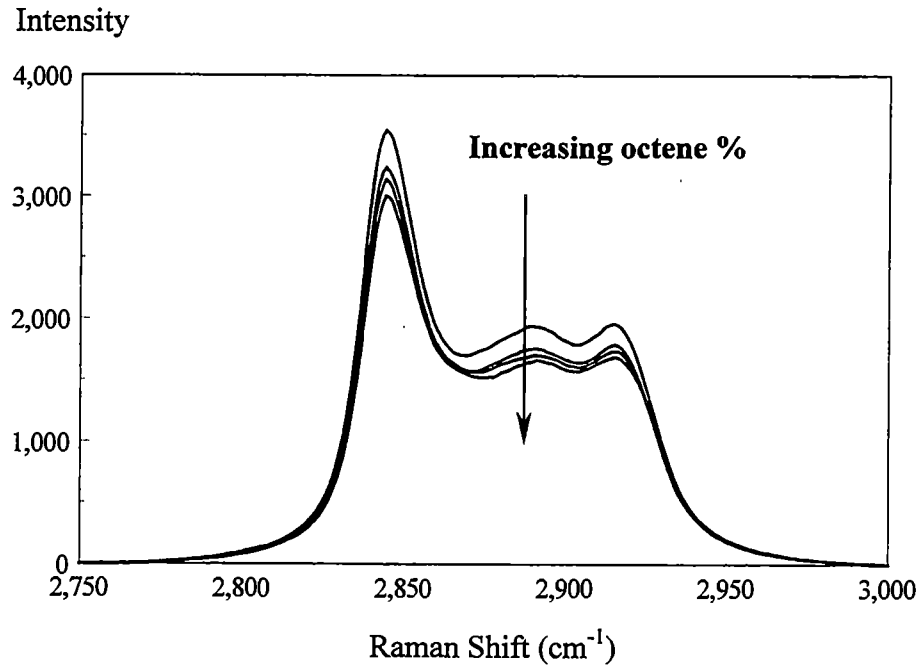


Figure 7.26: Baseline corrected Raman spectra of molten PE in 2750 to 3000 cm^{-1} region depicting the CH_2 and CH_3 stretching peak. The intensity of the peak decreases with increasing octene copolymer content.

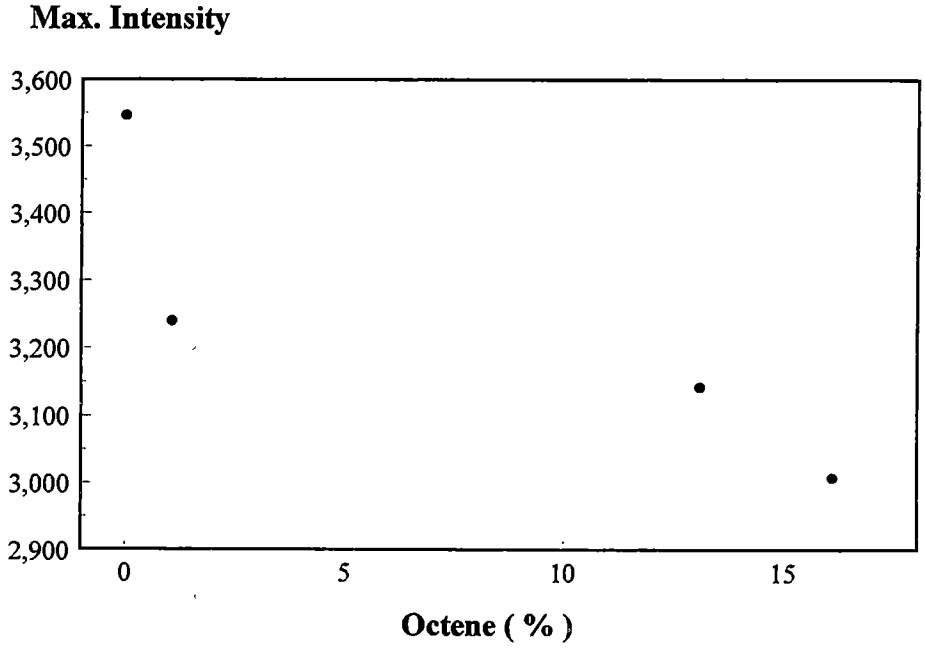


Figure 7.27: Normalized maximum intensity of the C-H stretching band plotted vs. octene content in the PE samples

spectroscopy. The C-H stretching peak around 2700-3000 cm^{-1} was used to correlate the melt index with the intensity observed in Raman spectra. The melt index for EVA samples and the complex viscosity for the molten PP samples was successfully correlated with the polarized Raman spectra. For the EVA samples, the variation in VA content is the principal variation as seen by Raman effects. The variation in MI is captured as a secondary effect as seen by the HCA in figure 7.14. HCA classified the sample set into two main categories. The experiments that were carried out at a constant flow rate of the samples gave better prediction results than the previous experimentation. The ability to capture the melt index reproducibly the system needed to be driven to a state where the spectroscopic instrumentation was able to capture the changes in orientation that resulted in the molten flowing polymer due to the variation in the melt index of the samples. The changes in the orientation of the macromolecular chains occur according to its viscosity. For the correlation of the complex viscosity of molten PP samples, molecular properties of the samples were not known. However, based on the chemometric analysis the samples could be distinguished from one another according to their rheological properties. The sample 4 in PP set had completely different range of complex viscosity as seen in figure 7.19. This sample was not considered in the PCA and PLS models. The correlation of the octene copolymer content in the PE samples was demonstrated with the use of Raman spectroscopy. The data set consisted of five samples. During experimentation, it was found that one of the samples fluoresced. Hence, the data set was reduced to four samples. This data is very limited in order to make chemometric

models for the prediction of the octene content with varying Raman intensity. However, as seen in figures 7.25 and 7.26, an inverse trend is observed between the Raman intensity and the octene content in PE samples. The calibration models considered here are not universal by any means. The data and the effective calibration would change with changes in the experimental conditions. However, a methodology for calibration and prediction of data obtained from in-line monitoring of the laboratory extruder set up has been presented.

CHAPTER 8

CONCLUSIONS AND FUTURE WORK

This research has focused on the development of in-line monitoring methodology for polymer processes. Two industrially important processes were studied, batch emulsion polymerization and polymer extrusion. The residual monomer concentration in emulsion polymerization was correlated with the information in the Raman spectra. The copolymer concentration (VA) in EVA copolymer was studied during extrusion of molten polymers along with the rheological information. The experimental studies demonstrated that Raman spectroscopic techniques along with the use of powerful chemometric methods could be utilized for extracting important information about the processes regarding estimation of residual monomer conversion and estimation of rheological properties of polymers.

A systematic study of emulsion polymerization reactions showed that the effect of temperature on rate of the reaction could be monitored using Raman spectroscopy. In reality, for batch emulsion polymerization reactions several variables in the reaction environment affect the rate of reaction. These variables include temperature and monomer concentration (for copolymerization), emulsifier concentration and initiator concentration. Effect of temperature can be seen as a pronounced effect on the rate of monomer conversion. Ability to monitor the profiles of monomer consumption gives qualitative and quantitative information that can be

used in conjunction with regression techniques to yield calibration models. Variation in the comonomer ratio for copolymerization reactions yields latex with specifically tailored properties for various applications. The ability of Raman spectroscopy to monitor the subtle changes in the rate of consumption of monomer with varying initial concentration of monomers is a significant contribution towards the development of monitoring techniques for emulsion polymerization on industrial scale. The use of regression techniques, univariate and multivariate, resulted in a calibration models. The use of calibration models in predicting the comonomer conversion was demonstrated for polymerization reaction carried out under similar experimental conditions. Thus, Raman spectroscopy coupled with chemometric tools shows the potential as a method for in-line monitoring of industrial reactions. Application of Raman spectroscopy would result in an economic advantage over other in-line/on-line monitoring techniques such as on-line gas chromatography, on-line densimetry, due to lower maintenance cost. This coupled with the rugged Raman spectrometers that could withstand the harsh industrial environments and reliability in use provides a very lucrative alternative for in-line monitoring of emulsion polymerization reactions.

Monitoring the individual consumption of the monomers in a copolymerization reaction was investigated in this research. In order to observe the individual monomer consumption, Raman bands in the spectrum due to reactive species need to be identified. These bands should be distinctly resolved for various comonomers. In this study, it shown that the lack of separate Raman bands for individual monomers that

change with changing monomer concentration proved to be a disadvantage. PCA did not reveal the presence of information in C=C peak about the individual comonomer amount. Hence, the two comonomers could not be distinguished. The use of gravimetric analysis for measuring the monomer conversion could introduce some operator error. Gas chromatography could be used as a more accurate alternative technique.

This research also demonstrated the use of polarized Raman spectroscopy in monitoring the extrusion process for molten polymers. Polarized Raman spectroscopy is useful over more conventional isotropic Raman spectroscopy as it captures information that has strong, physical dependence on the molecular weight parameters of the polymer. The copolymer (VA) content and rheological properties of EVA copolymers were successfully carried out using polarized Raman spectroscopy. The standard error of prediction is one of criteria used to evaluate the correlation model. For the extrusion experiments carried out at constant flow rate through the flow cell of the extruder, the error of prediction showed great improvement. This is due to the fact that when the polymer is extruded at constant flow rate, a constant shear rate at wall is experienced by all the samples. These conditions influenced orientation of the molten polymer chain based on its molecular weight. Polarized Raman spectroscopy combined with chemometric techniques such as HCA, PCA and PLS were used to derive valuable quantitative information about the MWD properties melt index and $|\eta^*(\omega)|$ in molten EVA and PP polymers respectively. In this research, an attempt was

made to understand the physical origin of the rheological effects by identifying the spectral origins of Raman bands that display strong correlation with the changes taking place in the polymer process being monitored.

In-line real time monitoring of processes can be further advanced to incorporate feedback process control. Advances in detector technology for Raman spectroscopy makes it possible to monitor several processes at the same time. Such multi-channel Raman spectrometric monitoring systems are being commercially developed. Thus, in the future, chemometric models and algorithms need to be developed to accommodate such modifications. Further research in Raman immersion probes would be aimed at development of probe window that would not foul when monitoring *sticky* emulsions. For monitoring the rheological properties of molten polymers using polarized Raman spectroscopy, a no-moving parts probehead could be developed. This probehead would be a modified version of the existing probehead with an added polarized beam splitter. This would allow for the two polarization states to be collected simultaneously. Since, the polarization state does not need to be changed manually, operator effects are minimized. Raman spectroscopy of polymers is developing at a fast pace since this technique is non-destructive and provides almost instantaneous analysis results. In the future, Raman spectroscopy would be used as a complimentary technique along with NIR spectroscopy for monitoring processes.

REFERENCES

REFERENCE LIST

1. D. Satas, *Handbook of Pressure Sensitive Adhesive Technology*, (1989).
2. M. Claybourne, T. Massey, *Journal of Raman Spectroscopy* **25**, 123 (1994).
3. Y. Maeda, H. Kitano, *Spectrochimica Acta A* **51**, 2433 (1995).
4. I.R. Lewis, P.R. Griffiths, *Applied Spectroscopy* **50**, 12A (1996).
5. J.L. Koenig, *Applied Scpectroscopy Reviews* **4**, 233 (1971).
6. T.J. Vickers, C.K. Mann, *Analytical Raman Spectroscopy*, J.G. Grasselli and B.J. Bulkin, Eds. (John Wiley & Sons, New York, 1991).
7. T.J. Vickers, C.K. Mann, *The International Society for Optical Engineering* **2367**, 219 (1995).
8. D.A. Long, *Raman Spectroscopy* (McGraw Hill Publishers, New York, 1976).
9. P. Painter, M.M. Coleman, J.L. Koenig, *The Theory Of Vibrational Spectroscopy And Its Applications To Polymeric Materials* (Wiley, NY, 1982).
10. F.A. Cotton, *Chemical Applications of Group Theory* (Wiley-Interscience Publication, 1990).
11. J.G. Grasselli, B.J. Bulkin, *Analytical Raman Spectroscopy* (John Wiley and Sons, 1991).
12. B. Chase, *Applied Spectroscopy* **48**, 14A (1994).
13. E. Gantner, S. Dieter, *Fresenius Journal of Analytical Chemistry* **338**, 2 (1990).
14. G. Odian, *Principles of Polymerization* (John Wiley & Sons, 1981).
15. G. Poehlein, *Encyclopedia of Polymer Science and engineering*, (John Wiley and Sons, NY, 1996).
16. W.D. Harkins, *Journal of American Chemical Society* **69**, 1428 (1947).
17. W.V. Smith, R.W. Ewart, *Journal of Chemical Physics* **16**, 592 (1948).

18. P. Lovel, M.S. El-Aasser, *Emulsion Polymerization and Emulsion Polymers* (John Wiley and Sons, England, 1997).

19. P.W. Atkins, *Physical Chemistry* (Oxford University Press, 1990).

20. D.E. Irish, H. Chen, *Applied Spectroscopy* **25**, 1 (1971).

21. L.A. Lyon, *et al*, *Analytical Chemistry* **70**, 341 (1998).

22. P.J. Hendra, G. Ellis, D.J. Cutler, *Journal of Raman Spectroscopy* **19**, 413 (1988).

23. C.K. Chong, *Vibrational Spectroscopy* **3**, 35 (1992).

24. C.H. Jones, *Spectrochimica Acta* **47**, 1313 (1991).

25. H.G.M. Edwards, A.F. Johnson, I.R. Lewis, *Journal of Raman Spectroscopy* **24**, 475 (1993).

26. G. Ellis, M. Claybourn, S.E. Richards, *Spectrochimica Acta* **46A**, 227 (1990).

27. J.F. Aust, K.S. Booksh, M.L. Myrick, *Applied Spectroscopy* **51**, 247 (1997).

28. B.H. Stuart, *Spectrochimica Acta* **53**, 111 (1997).

29. P. Marteau, *Vibrational Spectroscopy* **9**, 101 (1995).

30. S. Damoun, R. Papin, et al, *Journal Raman Spectroscopy* **23**, 385 (1992).

31. C.W. Wang, T.J. Vickers, J.B. Schlenoff, *Applied Spectroscopy* **46**, 1729 (1992).

32. G. Poehlein, *Polymer International* **30**, 243 (1993).

33. L. Noel, E. Brouwer, *Journal of Applied Polymer Science* **57**, 245 (1995).

34. M. Alonso, F. Recasens, L. Puigjaner, *Chemical Engineering Science* **41**, 1039 (1986).

35. S. Canegallo, M. Apostolo, G. Storti, M. Morbidelli, *Journal of Applied Polymer Science* **57**, 1333 (1995).

36. J. Clarkson, S.M. Mason, K.P.J. Williams, *Spectrochimica Acta* **47A**, 1345 (1991).

37. E. Gulari, K. McKeigue, K.Y.S. Ng, *Macromolecules* **17**, 1822 (1984).

38. C. Wang, T.J. Vickers, J.B. Schlenoff, C.K. Mann, *Applied Spectroscopy* **46**, 1729 (1992).

39. G. Horlick, *Applied Spectroscopy* **22**, 617 (1968).

40. T. Mayo, S. Reegan, *Proceedings of Symposium on Adhesion and Cohesion.* P. Weiss, Ed. 209-217 (1962).

41. E.G. Chatzi, O. Kammona, C. Kiparissides, *Journal of Applied Polymer Science* **63**, 799 (1997).

42. E.G. Chatzi, O. Kammona, *Macromolecular Chemical Physics* **198**, 2409 (1997).

43. M. Shimoyama, H. Maeda, *Vibrational Spectroscopy* **14**, 253 (1997).

44. B.K. Lavine, *Analytical Chemistry* **70**, 209 (1998).

45. A. Khettry, M.G. Hansen, *Polymer Engineering and Science* **36**, 1232 (1996).

46. S. Vedula, M.G. Hansen, *Journal of Applied Polymer Science* **68**, 873 (1998).

47. M.G. Hansen, S. Vedula, *Journal of Applied Polymer Science* **68**, 859 (1998).

48. T. Rohe, *Journal of Near Infrared Spectroscopy* **6**, 325 (1998).

49. H.L. McPeters, S.O. Williams, *Process Control and Quality* **3**, 75 (1992).

50. Infometrix Inc. (P. O. Box 1528, Woodinville, WA98072-1528, 1998).

51. K.R. Beebe, R.J. Pell, M.B. Seasholtz, *Chemometrics: A Practical Guide* (John Wiley & Sons Inc., 1998).

52. J.E. Jackson, *S.J.Qual Tech* **13**, (1981).

53. M.B. Seasholtz, B.R. Kowalski, *Journal of Chemometrics* **6**, 103 (1992).

54. M.J. Piovoso, K.A. Kosanovich, *The Use of Multivariate Statistics in Process Control* (CRC Press, 1996).

55. K. Esbensen, S. Schonkopf, T. Midtgaard, *Multivariate Analysis in Practice* (Wennbergs Trykkeri AS, 1994).

56. P.H. Garthwaite, *Journal of the American Statistical Association* **89**, 122 (1994).

57. J.M. Asua, *Polymeric Dispersions: Principles and Appkications* (Kluwer Academic, 1996).

58. R. Gaufres, P. Huguet, Y. Arab, *Journal of Raman Spectroscopy* **26**, 243 (1995).

59. Kaiser Optical Systems Inc., 371 Parkland Plaza, Ann Arbor, MI 48103.

60. A. Al-Khanbashi, M.G. Hansen, E.A. Wachter, *Applied Scpectroscopy* **50**, 1089 (1996).

61. A. Al-Khanbashi, In-Line Monitoring of Batch Emulsion Polymerization using Fiber Optic Raman Spectroscopy (1996), Ph. D. Dissertation, University of Tennessee, Knoxville.

62. A. Al-Khanbashi, M.S. Dhamdhere, M.G. Hansen, *Applied Spectroscopy Reviews* **33**, 115 (1998).

63. M. Litt, V. Stannett, *Journal of Polymer Science* **8**, 3607 (1970).

64. R. Patsiga, M. Litt, V. Stannett, *Journal of Physical chemistry* **64**, 801 (1960).

65. Visionex Inc., 430 Tenth Street NW, Suite N205, Atlanta, GA 30318.

66. J.W. Vanderhoff, *Science and Technology of Polymer Colloids* (Martinus Nijhoff Publishers, The Hagues, 1983).

67. M.J. Roberts, A.A. Garrison, S.W. Kercel, E.C. Muly, *Process Control and Quality* **1**, 281 (1991).

68. V. Vangani, A.K. Rakshit, *Journal of Applied Polymer Science* **60**, 1005 (1996).

69. T.W. Wang, S. Vedula, A. Khettry, *The Proceedings of the Conference on Process Control -V* (1996).

70. F. Loncar, Analysis, kinetics and alkali-swellability of carboxylated latexes (acrylic acid, 2-ethylhexyl acrylate, methacrylic acid, copolymerization) (1985), Ph. D. Dissertation, Lehigh university.

71. R.E. Schirmer, *ISA Transactions* **28**, 65 (1989).

72. D. Fisher, T. Bayer, K.J. Eichhorn, M. Otto, *Fresenius Journal of Analytical Chemistry* **359**, 74 (1997).

73. T. Rohe, W. Becker, S. Kolle, N. Eisenreich, P. Eyerer, *Talanta* **50**, 283 (1999).

74. S. Vedula, Fiber Optic Spectroscopy: Applications to Polymer Process Monitoring (1997), Ph. D. Dissertation, University of Tennessee, Knoxville.

75. G.R. Landvatter, *Modern Plastics Encyclopedia* (McGraw Hill Publishers, NY, 1994).

76. A. Khettry, In-Line Monitoring of Polymeric Processes(1995), University of Tennessee, Knoxville.

77. R.E. Duncan, *Modern Platics Encyclopedia* (McGraw Hill Publishers, 1988).

78. J. Li, In-Line Monitoring of Polymer Processing using Fiber Optic Spectroscopy (1999), Ph. D. Dissertation, University of Tennessee, Knoxville:

79. A. Pocius, *Ullmann's Encyclopedia of Industrial Chemistry* **1**, 445 (1985).

80. ASTM Standards, D 1238 (1986).

81. C.W. Macosko, *Rheology, Principles, Measurements and Applications* (VCH Publishers, 1994).

82. H. Martens, T. Naes, *Multivariate Calibration* (John Wiley & Sons, England, 1989).

83. J. Ferry, *Viscoelastic Properties of Polymers* (John wiley & Sons, New York, 1961).

84. H. Ulrich, *Introduction to Industrial Polymers* (Hanser Publishers, Munich, 1993).

85. B.H. Stuart, *Vibrational Spectroscopy* **10**, 79 (1996).

86. G. Strobl, W. Hagedorn, *Journal of Polymer Science* **16**, 1181 (1978).

VITA

Mrunalini Shireesh Dhamdhere was born in Pune, India on July 15, 1974. She attended high school at Wamanrao Muranjan High School in Mumbai, India. She joined the University Department of Chemical Technology (UDCT) in July 1991 and received baccalaureate degree in Chemical Engineering in May 1995. She worked at the Reliance Industries Ltd. in India until June 1996, after which she joined the University of Tennessee, Knoxville in August 1996. She received the Doctor of Philosophy degree in Chemical Engineering in May 2000.